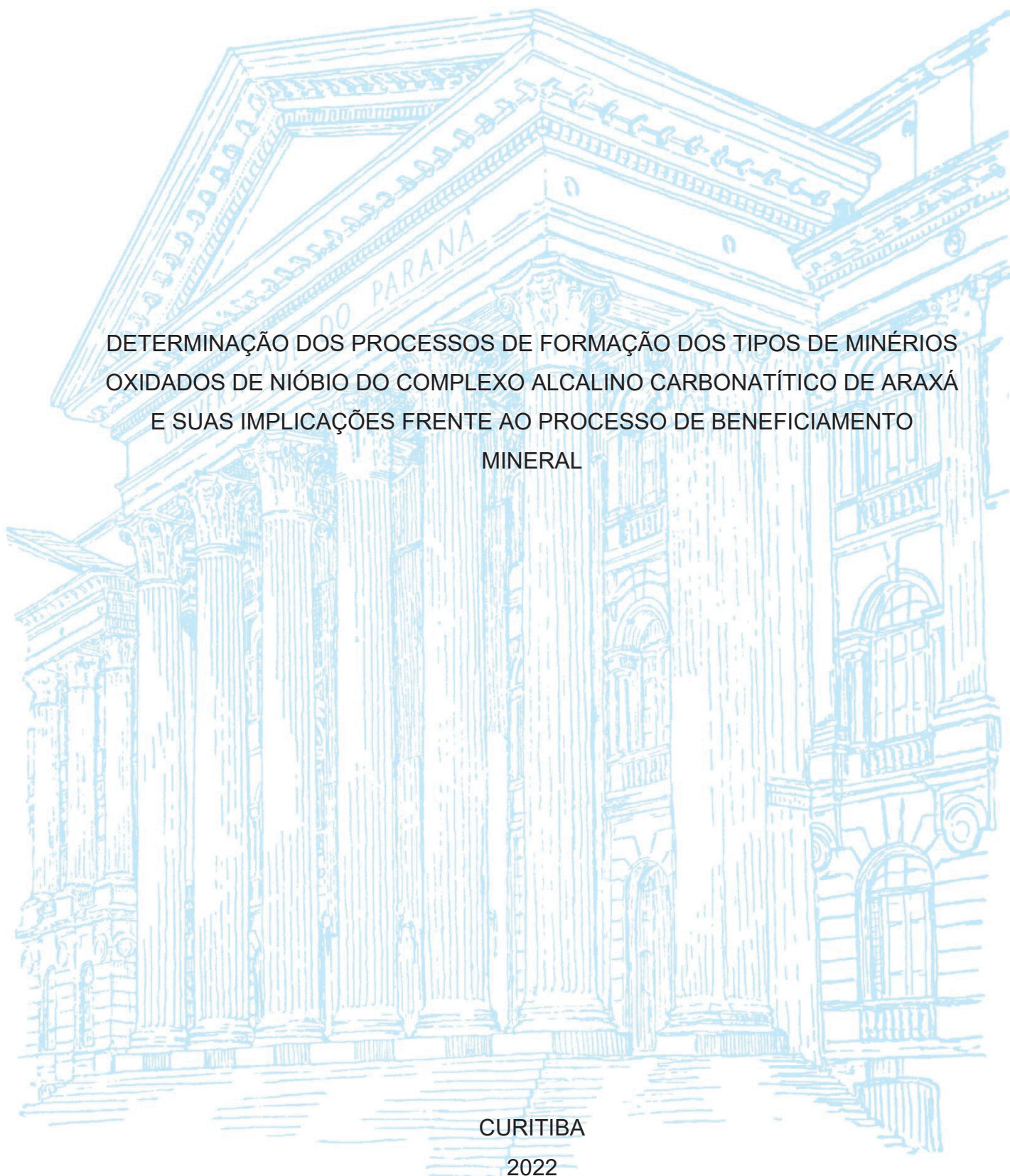UNIVERSIDADE FEDERAL DO PARANÁ

JOSÉ MARQUES BRAGA JÚNIOR

DETERMINAÇÃO DOS PROCESSOS DE FORMAÇÃO DOS TIPOS DE MINÉRIOS OXIDADOS DE NIÓBIO DO COMPLEXO ALCALINO CARBONATÍTICO DE ARAXÁ E SUAS IMPLICAÇÕES FRENTE AO PROCESSO DE BENEFICIAMENTO MINERAL

CURITIBA

2022

JOSÉ MARQUES BRAGA JÚNIOR

DETERMINAÇÃO DOS PROCESSOS DE FORMAÇÃO DOS TIPOS DE MINÉRIOS OXIDADOS DE NIÓBIO DO COMPLEXO ALCALINO CARBONATÍTICO DE ARAXÁ E SUAS IMPLICAÇÕES FRENTE AO PROCESSO DE BENEFICIAMENTO MINERAL

Tese de doutorado apresentada ao Programa de Pós-graduação em Geologia da Universidade Federal do Paraná, setor de Ciências da Terra, como parte dos requisitos necessários à obtenção do título de Doutor em Geologia.

Orientador: João Carlos Biondi

CURITIBA
2022

TERMO DE APROVAÇÃO

Os membros da Banca Examinadora designada pelo Colegiado do Programa de Pós-Graduação GEOLOGIA da Universidade Federal do Paraná foram convocados para realizar a arguição da tese de Doutorado de **JOSÉ MARQUES BRAGA JUNIOR** intitulada: **DETERMINAÇÃO DOS PROCESSOS DE FORMAÇÃO DOS TIPOS DE MINÉRIOS OXIDADOS DE NIÓBIO DO COMPLEXO ALCALINO CARBONATÍTICO DE ARAXÁ E SUAS IMPLICAÇÕES FRENTE AO PROCESSO DE BENEFICIAMENTO MINERAL**, sob orientação do Prof. Dr. JOÃO CARLOS BIONDI, que após terem inquirido o aluno e realizada a avaliação do trabalho, são de parecer pela sua APROVAÇÃO no rito de defesa.

A outorga do título de doutor está sujeita à homologação pelo colegiado, ao atendimento de todas as indicações e correções solicitadas pela banca e ao pleno atendimento das demandas regimentais do Programa de Pós-Graduação.

CURITIBA, 08 de Dezembro de 2022.

Assinatura Eletrônica
08/12/2022 17:00:43.0
JOÃO CARLOS BIONDI
Presidente da Banca Examinadora

Assinatura Eletrônica
12/12/2022 07:32:12.0
LUCIANO NUNES CAPPONI
Avaliador Externo (COMPANHIA BRASILEIRA DE METALURGIA E MINERAçãO)

Assinatura Eletrônica
08/12/2022 18:13:19.0
BÁRBARA TRZASKOS
Avaliador Interno (UNIVERSIDADE FEDERAL DO PARANÁ)

Assinatura Eletrônica
12/12/2022 12:19:25.0
CARLA BERTUCCELLI GRASSO DE MEDEIROS
Avaliador Externo (THE MOSAIC COMPANY)

Assinatura Eletrônica
09/12/2022 08:26:29.0
EDUARDO CHEMAS HINDI
Avaliador Externo (UNIVERSIDADE FEDERAL DO PARANÁ)

Dedicatória

Dedico este trabalho ao Professor João Carlos Biondi que me inspirou e me motivou a conhecer uma geologia fascinante.

AGRADECIMENTOS

"Mantenha-se forte diante do fracasso e livre diante do sucesso."

Jean Cocteau

RESUMO

O Complexo Alcalino Carbonatítico de Araxá apresenta depósitos relevantes de Nb, P, Ba, ETR e Fe, com minérios regolíticos e saprolíticos formados pelo intemperismo de rochas com flogopita e magnetita-apatitito, cortadas por vênulas de carbonatitos. Os minérios são classificados em ocre, marrom e laranja, conforme o grau de intemperismo. Hidroxicalciopirocloro e hidrokenopirocloro são os principais minerais de Nb nos minérios ocre e marrom, enquanto hidrokenopirocloro predomina no laranja. Fluorapatita, barita, monazita e rabdofanita são os minerais predominantes de fosfato, Ba e ETR, respectivamente. Os corpos minerais são estratiformes e horizontais, originados pelo fluxo de água meteórica, formando-se sequencialmente: ocre, marrom e laranja. O intemperismo residualmente concentrou minerais de Nb, P e Fe, enquanto barita, monazita e rabdofanita são autigênicas. Essa dinâmica resultou em espessamento e disseminação lateral, radial e centrífuga dos corpos mineralizados, cobertos por sedimentos lacustres. Testes geometalúrgicos identificaram minérios de nióbio com recuperações metalúrgicas inferiores a 50% na área de transição ao redor do corpo mineralizado principal. Minerais contaminantes e características morfológicas e texturais explicam a ausência ou baixas recuperações metalúrgicas de nióbio nessas áreas. Os minérios do halo sul apresentam baixas recuperações devido à presença de minerais contaminantes, como os argilominerais no minério laranja e a dolomita e vermiculita nos minérios marrom e ocre. No halo norte, a correlação do baixo desempenho geometalúrgico é atribuída à presença de contaminantes no minério ocre e a outros minerais contendo nióbio nos minérios marrom e laranja, indicado principalmente pela correlação entre U_3O_8 e Nb_2O_5.

Palavras-chave: Minério supergênico; pirocloro; minerais contaminantes; minerais portadores de nióbio.

ABSTRACT

The Alkaline Carbonatitic Complex of Araxá contains significant deposits of Nb, P, Ba, REE, and Fe, with regolithic and saprolitic ores formed by the weathering of rocks composed of phlogopite and magnetite-apatite, intersected by carbonatite veinlets. The ores are classified as ochre, brown, and orange according to the degree of weathering. Hydroxycalciopyrochlore and hydrokenopyrochlore are the main Nb minerals in ochre and brown ores, while hydrokenopyrochlore predominates in orange ores. Fluorapatite, barite, monazite, and rhabdophane are the primary minerals of phosphate, Ba, and REE, respectively. The stratiform and horizontal mineral bodies originated by meteoric water flow, forming sequentially: ochre, brown, and orange. Weathering processes residually concentrated Nb, P, and Fe minerals, while barite, monazite, and rhabdophane are authigenic. This dynamic resulted in the thickening and lateral, radial, and centrifugal dissemination of the mineralized bodies covered by lacustrine sediments. Geometallurgical tests identified niobium ores with metallurgical recoveries lower than 50% in the transition area around the main mineralized body. Contaminant minerals and morphological and textural characteristics explain the niobium's absence or low metallurgical recoveries of Nb in these areas. The ores of the southern halo exhibit low recoveries due to the presence of contaminant minerals, such as clay minerals in the orange ore and dolomite and vermiculite in the brown and ochre ores. In the northern halo, low geometallurgical performance is attributed to contaminants in the ochre ore and other niobium-bearing minerals in the brown and orange ores, indicated primarily by the correlation between U_3O_8 and Nb_2O_5.

Keywords: supergenic ore; metallurgical recovery; pyrochlore; contaminating minerals; Nb-bearing minerals

LISTA DE FIGURAS

Artigo 2

LISTA DE TABELAS

LISTA DE ABREVIAÇÕES

Unidades

%	Percentagem
3D	Tridimensional (plano X, Y, Z)
cm	Centímetros
E	Dimensão espacial correspondente ao leste
g/cm³	Gramas por centímetro cúbico
kg	Quilogramas
km	Quilômetros
km²	Quilômetros quadrados
kT	Mil toneladas
m	Metros
m²	Metros quadrados
m³	Metros cúbicos
Ma	Milhões de anos
mg/L	Miligrama por litro
mm	Milímetros
N	Dimensão espacial correspondente ao norte
NE	Dimensão espacial correspondente ao nordeste
NW	Dimensão espacial correspondente ao noroeste
pH	Potencial hidrogeniônico. (Escala numérica utilizada para especificar a acidez ou basicidade de uma solução aquosa)
ppm	Parte por milhão
S	Dimensão espacial correspondente ao sul
SE	Dimensão espacial correspondente ao sudeste
SW	Dimensão espacial correspondente ao sudoeste
t	Toneladas
W	Dimensão espacial correspondente ao oeste

Laboratório

AAS	Espectrometria de Adsorção Atômica
ALS	ALS Limited. (Laboratório de Análises Químicas)
ICP	Plasma por acoplamento indutivo (método analítico)
LA-ICP-MS	Laser Ablation Inductively Coupled Plasma Mass Spectrometry
SGS	Société Générale de Surveillance. (Laboratório de Análises Químicas)
XRD / DRX	Difração de Raio-X (Análise mineral)
XRF / FRX	Fluorescencia de Raio-X. (Métodos analítico)

Fórmulas e elementos químicos

Al_2O_3	Óxido de alumínio (alumina)

Ba	Elemento químico bário
Ba^{2+}	Íon de bário
BaO	Óxido de bário
BaSO$_4$	Sulfato de bário (barita)
CaO	Óxido de cálcio
ETR / RRE	Elemento terras raras
Fe	Ferro
Fe	Elemento químico ferro
Fe$_2$O$_3$	Óxido de ferro
FeNb	Liga de ferro-nióbio
HCO$_3^-$	Íon bicarbonato
LOI	Perda por calcinação
MgO	Óxido de magnésio
MR / RM	Recuperação Metalúrgica em massa do Nb$_2$O$_5$
Nb	Elemento químico nióbio
Nb$_2$O$_5$	Óxido de nióbio
Ni	Níquel
OTR / REO	Óxidos de terras raras
P	Elemento químico fósforo
P$_2$O$_5$	Óxido de fósforo
S	Elemento químico enxofre
SO$_2$	Dióxido de enxofre (gás)
SO$_4^{2+}$	Íon sulfato
Sr	Elemento químico estrôncio
TiO$_2$	Óxido de titânio
U$_3$O$_8$	Óxido de urânio

Sondagem

AC	Sondagem Air core
DDH	Sondagem Rotativa Diamantada
HQ	Diâmetros de sondagem (63,5mm)
NQ	Diâmetros de sondagem (47,6mm)
RC	Circulação reversa (Método de sondagem)

Mina e Planejamento de Lavra

Cut Off	Teor de corte
ROM	Minério *insitu* (sem alteração)

Geral

CACA	Complexo Alcalino Carbonatítico Araxá
CACB	Complexo Alcalino Carbonatítico do Barreiro

CBMM	Companhia Brasileira de Metalurgia e Mineração
CODEMIG	Companhia de Desenvolvimento Econômico de Minas Gerais
COMIPA	Companhia Mineradora do Pirocloro de Araxá
CPRM	Companhia de Pesquisa de Recursos Minerais
LCT	Laboratório de caracterização tecnológica
UFPR	Universidade Federal do Paraná
UNESP	Universidade Estadual Paulista
USP	Universidade de São Paulo

1 INTRODUÇÃO

Os complexos alcalino-carbonatíticos constituem importantes depósitos de minerais metálicos de filiação magmática. São estruturas geológicas presentes em todos os continentes, tendo sido formadas majoritariamente no período que compreende o Proterozóico até o Cenozóico.

Os carbonatitos são feições essencialmente continentais, sempre associadas às zonas de grandes rifts, situando-se preferencialmente nas zonas de inflexão das placas continentais, nas bordas dos megafraturamentos. A mesma posição é ocupada pelas províncias alcalinas que, no entanto, são menos restritivas ao ambiente tectônico onde se situam (Biondi, 1986).

Os Complexos Alcalinos Carbonatíticos presentes no Brasil, Angola, região sudoeste da África e Uruguai ocorrem preferencialmente segundo lineamentos que coincidem com falhas transformantes centradas no polo de rotação cretáceo para a América do Sul (Marsh, 1973; Rodrigues, 1970 apud Biondi, 1986).

Os principais depósitos minerais associados aos Complexos Alcalinos Carbonatíticos são consequência de processos de concentração secundária ativo sobre as rochas ígneas. A concentração residual e a lateritização foram os principais agentes mineralizadores na formação dos diversos depósitos dessa natureza, como o depósito de Nb de Araxá (Souza e Castro, 1962 apud Biondi, 1986).

O Complexo Alcalino Carbonatítico Araxá (CACA), também conhecido na literatura como Complexo Alcalino Carbonatítico do Barreiro (CACB), está inserido na Província Ígnea do Alto Paranaíba (Almeida, 1983; Brod et al., 2004), que se desenvolveu sobre o setor meridional da Faixa de Dobramentos Brasília, com alinhamento NW-SE, coincidente com o Arco do Alto Paranaíba.

A Província Ígnea do Alto Paranaíba (Almeida, 1983; Brod et al, 2004) está localizada na borda nordeste da Bacia do Paraná, apresentando alinhamento NW-SE, coincidente com o Arco do Alto Paranaíba, desenvolvido sobre o setor meridional da Faixa de Dobramentos Brasília. Esta, por sua vez, está edificada na borda oeste do Cráton do São Francisco e se estende por mais de 1.000 km na direção norte/sul, pelos estados de Minas Gerais, Goiás, Distrito Federal e Tocantins (Almeida, 1967) (Figura 1).
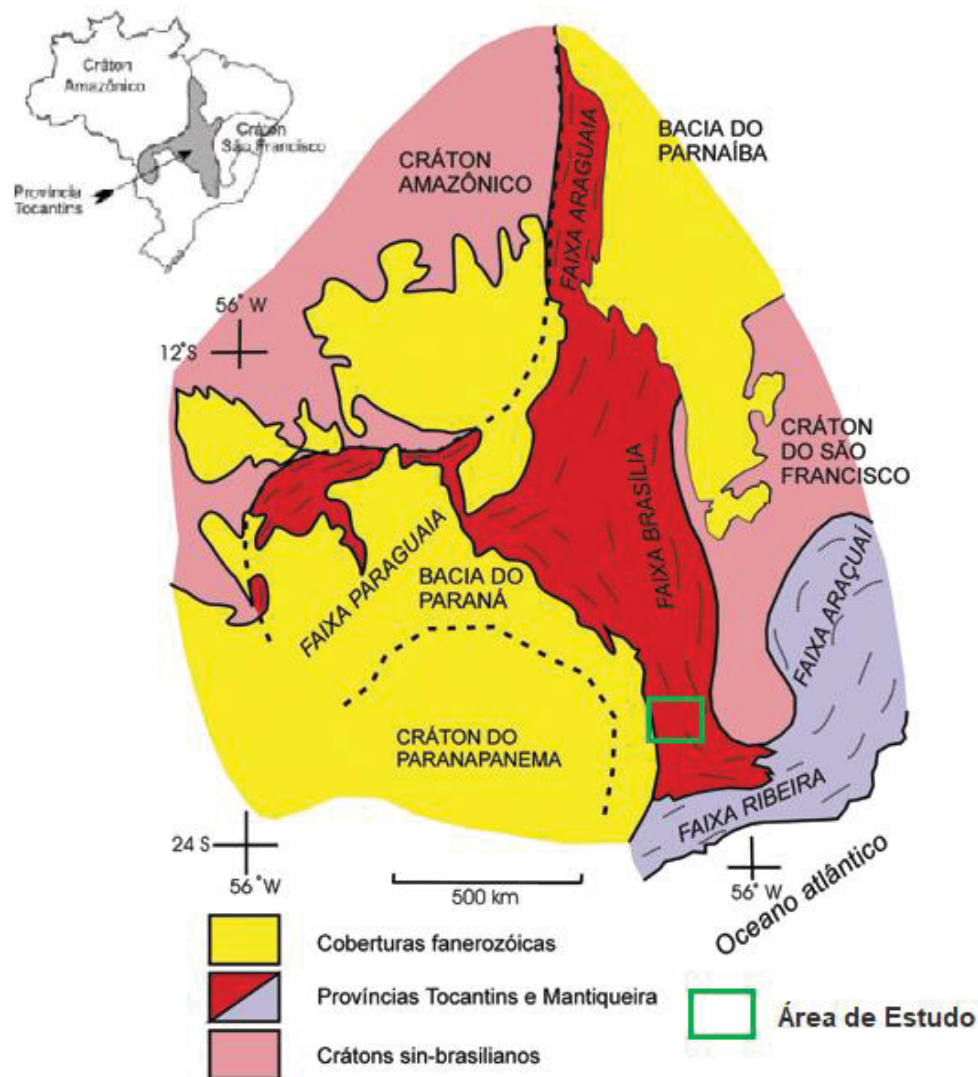
Figura 1- Compartimentação Tectônica do Brasil Central com destaque para Província Tocantins e suas Faixas de Dobramentos.

As unidades geológicas que ocorrem na região foram interpretadas no Programa de Mapeamento Geológico do Estado de Minas Gerais, 2015, descritas em ordem cronológica, da mais nova, para a mais antiga (Figura 2), a seguir:

a) Coberturas Detrítico-lateríticas: depósitos sedimentares variados (alúvios, colúvios e elúvios), associados a variações do nível de base no pleistoceno. A partir do processo de pedogênese podem apresentar laterização incipiente.

b) Complexo Alcalino Carbonatítico Araxá: Complexo ígneo de idade variando entre 76 e 97 Ma (magmatismo policíclico), formado a partir de sucessivos eventos magmáticos de rochas ultrabásicas duníticas e peridotíticas e posterior intrusão do magma carbonático (Brod et al., 2004). Atualmente, o CACA se encontra fortemente pedogeneizado – culminando em um manto de alteração superior à 100 m.

c) Complexo Alcalino Carbonatítico de Tapira: Este Complexo ígneo possui idades que variam entre 85 e 87 Ma (Sonoki & Garda, 1988). Segundo Brod

et al. (2004) é constituído por clinopiroxenitos e bebedouritos com menores quantidades de carbonatitos, foscoritos, dunitos, flogopititos e sienitos.

d) Complexos Alcalinos de Salitre I, II e III e Serra Negra: São Complexos de forma ovalada que possuem raios de ordem quilométrica, onde são observadas rochas intrusivas (Salitre I e Serra Negra). Já em Salitre II, observa-se piroxenitos, localmente com rochas da série foscorítica associadas, na porção sul do corpo (Brod et al., 2004); também foram encontradas amostras bastantes intemperizadas de rochas vulcânicas piroclásticas.

e) Grupo Bambuí: Ocupa a porção norte da área e é intrudido pelos Complexos Alcalinos de Salitre e Serra Negra. De idade neoproterozóica (540 Ma), a Formação Serra da Saudade é composta por siltitos e arenitos finos predominantes, com folhelhos e lentes carbonáticas subordinadas.

f) Grupo Ibiá (Formação Rio Verde): metassedimentos detríticos, metamorfizados em fácies xisto verde baixo (zona da clorita) no neoproterozóico (900 a 600 Ma), compostos predominantemente de muscovitamuscovita-clorita-quartzo xisto, clorita-quartzo xisto, muscovita-quartzo xisto e clorita-muscovita-quartzo xisto. De maneira geral, possuem foliação sub-horizontal, entretanto, nas proximidades da Serra da Bocaina a foliação é preferencialmente sub-vertical (Seer, 1999).

g) Grupo Araxá: composto predominantemente por micaxistos e quartzitos formados entre 900 e 600 Ma, com intercalações de anfibolitos metamorfizados em fácies epidoto-anfibolito. Como minerais acessórios podem ocorrer granada, rutilo, zircão, turmalina e estaurolita, além de cianita (Seer, 1999).

h) Grupo Canastra: este Grupo, consiste em quartzitos diversos de idade neoproterozóica (900 a 600 Ma), por vezes milonitizados, e variações localizadas de hematita filito, muscovita, biotita, cloritóide, clorita, quartzo xisto, com albita, estabilizados em fácies xisto verde médio (Seer, 1999).

Fonte: Modificado do mapa geológico obtido no site da CPRM (2015).
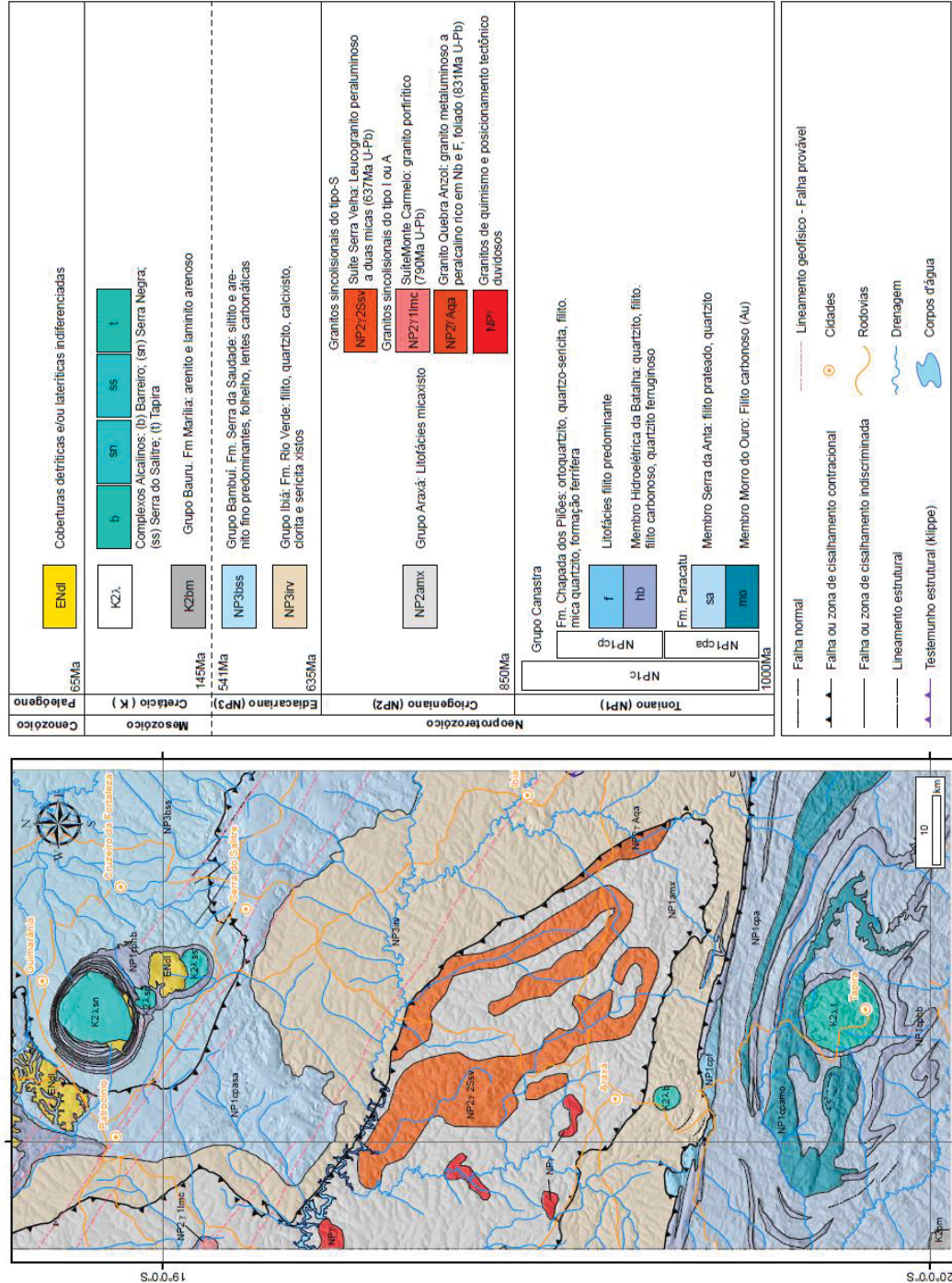
Figura 2- Mapa geológico regional com os principais domínios e feições geológicas.

Sob o ponto de vista tectônico, a região de Araxá está estruturada em uma dobra sinformal regional, denominada Sinforma de Araxá. Esta estrutura regional tem seus flancos principais nos setores nordeste e sudoeste e sua linha de charneira apresenta direção aproximada N70W, com caimento suave para NW. Em seu flanco sul, está localizada a Zona de Cisalhamento da Bocaina que consiste em um sistema de falhas transcorrentes sinistrais (Seer, 1999).

A tectonoestratigrafia da região compreende três escamas tectônicas alóctones (Figura 3), separadas por zonas de cisalhamento que configuram falhas de empurrão. Na escama inferior, ocorrem as litologias do Grupo Canastra, constituída de xistos e quartzitos e quartzitos micáceos, que, por sua vez, cavalga o Grupo Bambuí, que caracteriza uma cobertura cratônica autóctone. A escama tectônica intermediária reúne as litologias do Grupo Ibiá, formada por xistos e quartzitos subordinados, nas quais o Complexo Araxá estaria encaixado. Empurrada sobre esta ocorre a escama tectônica superior que é constituída pelas rochas do Grupo Araxá, que fica ao norte da área estudada.

Fonte: Seer (1999).
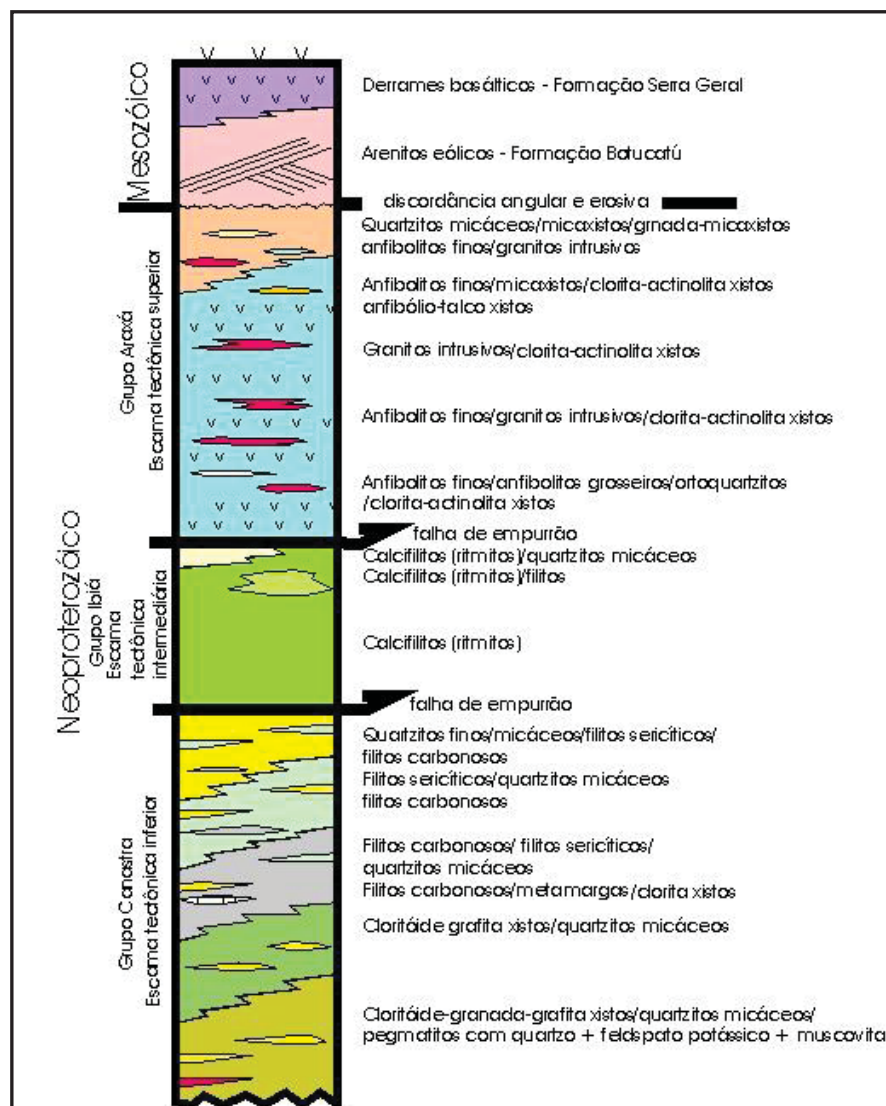
Figura 3- Tectonoestratigrafia da Sinforma de Araxá.

Introdução

O comportamento estrutural do CACA é identificado facilmente por conta da estruturação dômica assumida pelas rochas encaixantes do Grupo Ibiá, resultante dos efeitos dos eventos magmáticos. Estes são observados com maior magnitude nas rochas quartzíticas, nas quais são verificados os resultados da fenitização e do intenso fraturamento, determinado por meio da ocorrência de juntas e falhas (Viana et al., 1998). O mapa da Figura 4, proposto por Grossi Sad e Torres (1971), mostra o posicionamento das principais falhas observadas nos domínios do anel quartzítico. Estas se posicionam de forma radial, basicamente na metade norte no Complexo e apresentam mergulho subvertical. Com relação ao fraturamento, Moraes et al. (2008) afirmam que o quartzito se apresenta intensamente fraturado nas proximidades do contato e que, por seu comportamento reológico, é mais fraturado do que o xisto.

Fonte: Grossi Sad e Torres (1971) in: Viana et al. (1998)
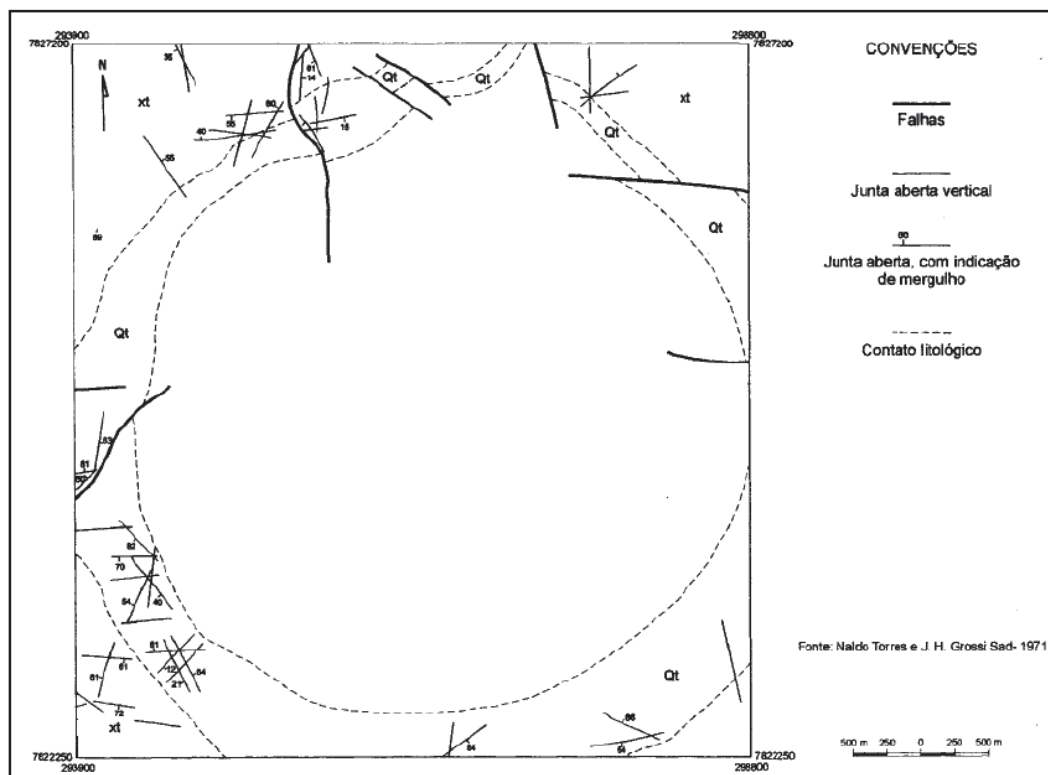
Figura 4- Mapa de falhas e fraturas do Complexo Araxá.

O CACA está encaixado em rochas quartzíticas com intercalações de xistos (Grupo Canastra), seguindo-se uma unidade composta por muscovita-xistos e clorita muscovita-xistos com intercalações de quartzitos (Formação Rio Verde). A unidade predominantemente quartzítica está em contato com o Complexo, formando um anel completo em torno das rochas magmáticas. A espessura da unidade quartzítica varia entre 100 e 600 m (Grossi Sad e Torres, 1971) e ambas as unidades apresentam suas litologias afetadas, com intenso fraturamento, recristalização, e mostrando os efeitos metassomáticos da intrusão.

A forma do Complexo Araxá é aproximadamente circular, com diâmetro interno de aproximadamente 4,5 km, formando uma estrutura dômica em cujo interior ocorrem as mineralizações de Nb_2O_5 (pirocloro), P_2O_5 (apatita), OTR – Óxido de Terras Raras (monazita) e $BaSO_4$ (Barita). A Figura 5 é composta por 5 secções verticais orientadas

Introdução

em SW-NE (ver mapa de localização da secção na figura 1 do artigo 1). As quais representam: (A) Perfil litológico e pedológico; (B) Distribuição dos teores Nb_2O_5; (C) Distribuição dos teores de P_2O_5; (D) Distribuição dos teores de BaO; (E) Distribuição dos teores de OTR. As distribuições dos teores foram obtidas pela interpolação dos dados amostrais do banco de dados de longo prazo da CBMM.

Fonte: Autoria própria
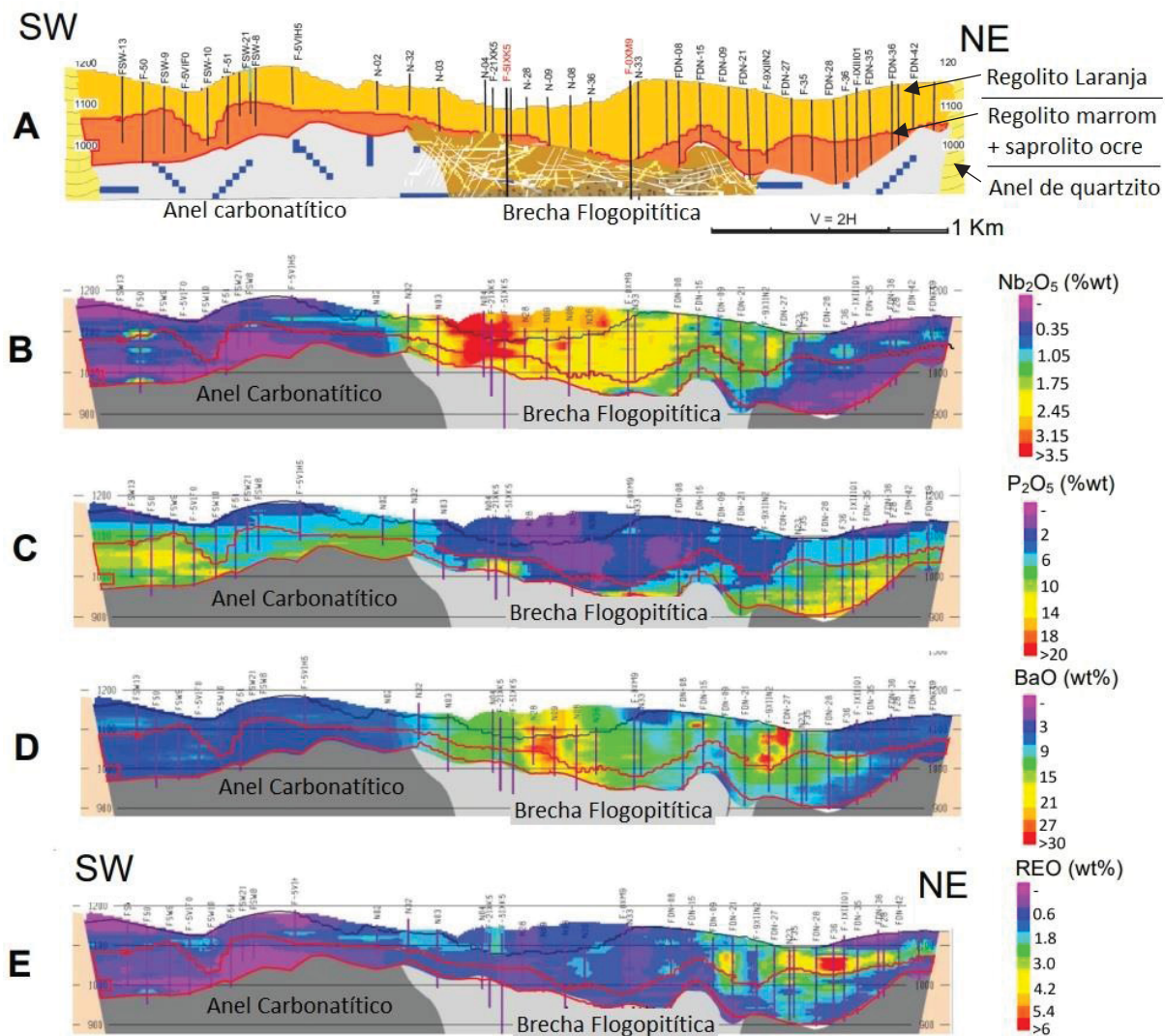
Figura 5- Perfis mostrando: (A) Perfil geológico e pedológico; (B) Distribuição dos teores Nb_2O_5; (C) Distribuição dos teores de P_2O_5; (D) Distribuição dos teores de BaO; (E) Distribuição dos teores de OTR em secções SW-NE no Complexo Araxá.

Nas unidades encaixantes nota-se a presença, em proporções variáveis, de anfibólio sódico, K-feldspato, apatita, dolomita, calcita, albita e piroxênio, introduzidos possivelmente por metassomatismo. Os efeitos da fenitização estão presentes em afastamentos variáveis, tendo sido observados, na parte leste, até 2,5 km de distância da borda externa do Complexo Araxá. A distribuição dos minerais introduzidos pelo metassomatismo é em geral irregular e, aparentemente, com algum controle por fraturas.

Segundo Barbosa et al. 1970, as rochas encaixantes do CACA são cortadas por inúmeros diques com disposição radial e concêntrica. Esses diques têm em geral

pequena espessura, e na superfície estão muito intemperizados, tornando muito difícil a sua identificação. Em furos de sondagens, nas encaixantes a leste do Complexo, foram encontrados diques de sovito, apatita-sovito e de rochas kamafugíticas, algumas contendo olivina, flogopita, magnetita, apatita, perovsquita e carbonatos, e outras, contendo flogopita, olivina perovskita, magnetita, aegirina, melanita e apatita.

Nas encaixantes, preferencialmente relacionadas a quartzitos e a fraturamentos, ocorrem corpos de rocha silexítica, com formas irregulares, em geral alongados, de coloração marrom escura, compostos por calcedônia e quartzo, contendo também magnetita, barita, e por vezes, apatita. Também são encontrados alguns corpos de silexito no interior do Complexo, como "floats" no manto de intemperização, e ainda na rocha fresca. É provável que esses corpos sejam provenientes da assimilação das encaixantes pelas rochas magmáticas durante a formação do Complexo Araxá.

Afloramentos de rocha no interior do Complexo podem ser observados no fundo da cava do F4, na cava da mina do Barreiro (Mosaic) e no fundo de um pequeno lago na porção NW, nesse último local, a rocha corresponde a um beforsito de granulação grosseira. Na parte central do Complexo, aproximadamente na área ocupada pela cava da CBMM, ocorrem flogopititos recortados por diques e vênulas de carbonatito e magnetita-apatititos mineralizadas com nióbio, fósforo, bário, ferro e, localmente, com Elementos Terras Raras (ETR). Os depósitos de fosfato, localmente com ETR e Nb, lavrados pela MOSAIC, o da cava F4 e o da ITAFOS ocorrem em um anel de carbonatitos que envolve o núcleo flogopitico que contém a mineralização principal de Nb.

No interior do Complexo, as rochas foram intensamente intemperizadas tendo-se formado o chamado manto de intemperização, composto por regolitos e saprolitos. A espessura deste manto varia desde alguns metros até cerca de 200 m. Na parte NW do Complexo, a espessura desse manto é menor, da ordem de 40 a 60 m, enquanto na porção central, onde ocorre a mineralização de Nb, essa espessura é em média de 160 m.

A formação desse espesso manto de intemperização está relacionada a condições especiais, como a presença de um anel quartzítico ao redor de todo o Complexo, dificultando a erosão do material do interior do Complexo, um clima favorável durante um longo período de tempo, a presença de falhas no interior do Complexo, com movimento vertical de blocos, e ainda, a composição mineralógica peculiar dessas rochas, contendo carbonatos abundantes e ainda, quantidades regulares de pirita, cuja alteração pode liberar ácido sulfúrico, que auxilia na lixiviação dos carbonatos. Além disso, a formação dos lagos de cratera no interior do Complexo, propiciou a deposição de sedimentos argilosos sobre os regolitos, contribuindo para preservação deles, dificultando o processo erosivo.

O processo de supergênese teve grande importância para elevar os teores de Nb nos minérios regolíticos e saprolíticos, ocorrendo principalmente por concentração residual. O manto de intemperismo contém os depósitos minerais de Araxá que vêm sendo atualmente explorados. O depósito de nióbio está na parte central do Complexo, tendo sido formado a partir do intemperismo de brecha flogopitica mineralizada em Nb. Nas partes NW e SE encontram-se os depósitos de fosfato (apatita).

O solo argiloso, formado a partir da deposição dos sedimentos nos lagos de cratera dentro do Complexo, cobre praticamente todo interior do Complexo, podendo

ser individualizado em dois horizontes, um de coloração vermelha escuro, com espessura variando entre 0 e 10 m, com abundante caulinita, gibbsita, goethita e limonita. O outro horizonte encontra-se posicionado imediatamente abaixo do horizonte anterior, o qual possui coloração amarelo claro, com espessura variando de 0 a 40 m, contendo muita caulinita e pouca gibbsita. Abaixo desses solos argilosos ocorre o regolito laranja, com cor que varia de laranja a marrom claro e contém magnetita, goethita, barita, hidrokenopiroclro, monazita, gorceixita e quantidades menores de quartzo, ilmenita, rutilo/anatásio e zircão. O pirocloro está distribuído de forma aproximadamente uniforme nesse horizonte. Abaixo do regolito laranja ocorre o regolito marrom, nesse horizonte a monazita e gorceixita são menos frequentes do que no regolito laranja, e a apatita aparece como principal mineral de fosforo. Segue-se um horizonte de rochas alteradas (saprolito ocre), contendo carbonatos e filossilicatos, com espessura de alguns metros e então, a rocha fresca.

No Complexo Araxá ocorrem depósitos importantes de pirocloro (Nb) e apatita (P), secundados por depósitos de barita (Ba), monazita com Elementos Terras Raras (ETR) e minerais de (Fe), tais como magnetita e hematita, além das suas fontes de água sulfurosa, com 420 mg/L de SO_4^2, 0.12 mg/L de Ba^{2+} e 3400 mg/L de HCO_3^- (Barroso, 2011), atualmente exploradas comercialmente nas termas do Hotel Tauá. O minério de nióbio é lavrado desde os anos 1970 pela Companhia Mineradora do Pirocloro de Araxá (COMIPA), em nome da Companhia Brasileira de Metalurgia e Mineração (CBMM) e da Companhia de Desenvolvimento Econômico de Minas Gerais (CODEMIG). Atualmente a MOSAIC Fertilizantes lavra o minério de fosfato na metade oeste do Complexo.

Devido ao comportamento distinto durante os ensaios geometalúrgicos com amostras de sondagem dos minérios de Nb do Complexo, percebeu-se que há saprolitos e regolitos mineralizados em nióbio cujas propriedades são intermediárias entre as dos minérios formados sobre o anel carbonatítico e sobre o núcleo flogopitítico. Esse novo tipo de minério forma um halo de transição que envolve o corpo principal da mineralização de Nb situado no centro do Complexo. Igual aos minérios formados sobre os flogopititos do núcleo ou sobre os carbonatitos que circundam o núcleo, o halo de transição também contém minérios ocre, marrom e laranja, porém suas composições químicas e as propriedades de seus minerais são distintas das dos minérios do núcleo habitualmente lavrados desde os anos setenta. Esse corpo mineralizado foi denominado por "halo de transição", ou simplesmente "halo".

A variável Recuperação Metalúrgica de nióbio (RM) representa a quantidade de nióbio no minério que é aproveitada industrialmente através do processamento mineral adotado. É expressa pela relação entre o nióbio recuperado no concentrado (produto) e o nióbio no minério que alimentou esse processo. As principais etapas do processo de beneficiamento e tratamento do mix do minério de nióbio de Araxá consistem em: britagem primária e secundária, separação magnética, classificação, condicionamento, flotação, espessamento e filtragem. Em 2018 a CBMM começou com um novo processo para recuperar o nióbio da fração ultrafina, passando a recuperar mais metal e gerar menos resíduo. O produto da usina de concentração é um concentrado de nióbio, utilizado exclusivamente pela CBMM como insumo nas fases subsequentes de produção: dessulfuração, desfosforação, metalurgia, química para obtenção de óxidos, e forno de feixe de elétrons para obtenção do nióbio metálico. Os produtos são: ferro-nióbio standard, óxidos de nióbio, nióbio metálico e nióbio-zircônio, além de ligas especiais: ferro-nióbio e níquel-nióbio. A barita e a magnetita são subprodutos do processo de produção do nióbio.

Introdução

1.1 Justificativa

A CBMM é a maior produtora mundial de nióbio, tendo produzido em 2018 cerca de 94 kT de FeNb equivalente. Os recursos de Nb manufaturados pela CBMM são extraídos exclusivamente pela COMIPA da mina de Araxá, localizada no estado de Minas Gerais – Brasil. Em algum momento o minério intemperizado lavrado atualmente pela CBMM começara a mudar para o minério "transicional" que, por sua vez, mudará para o minério primário, magmático. Os estudos desenvolvidos permitirão conhecer e antecipar a preparação dos procedimentos industriais a serem adotados pela Empresa quando essas mudanças começarem a acontecer.

Existem poucos trabalhos científicos sobre depósitos supergênicos de Nb. O Complexo Araxá, por conter a maior concentração conhecida de Nb, a maior mina de nióbio e a associação de concentrações importantes de Nb, ETR, Ba, Fe e P em um mesmo local, provavelmente é o melhor ambiente geológico para desenvolver esses estudos científicos com sucesso.

Além disso, a CBMM tem elevado sua capacidade produtiva ano após ano para atender a demanda crescente de consumo de FeNb. Diante desse cenário de aumento produtivo, faz-se necessário caracterizar apropriadamente os diferentes tipos de minério que compõem os recursos minerais da empresa, principalmente os que apresentam baixo rendimento geometalúrgico comparado ao presente processo de beneficiamento mineral. Essa necessidade se justifica pela dificuldade em produzir concentrados de pirocloro a partir de minérios com características químicas e mineralógicas distintas do minério explorado atualmente, contribuindo assim com os planos de crescimento produtivo da empresa. Além disso, conhecer as características dos minérios secundários de Nb, além de ser economicamente relevante, amplia e aprimora o entendimento dos processos de formação dos minérios intempéricos de Complexos Alcalino Carbonatíticos como os de Araxá.

1.2 Objetivos

Com esse projeto objetiva-se conhecer as principais características dos minérios oxidados de nióbio encontrados no CACA, possibilitando a compreensão de sua gênese e evolução. Além do estudo da mineralização de Nb, também foram consideradas as mineralizações de P, Ba, ETR e Fe.

Este trabalho tem como principais objetivos:

(1) Caracterizar química e mineralogicamente os minérios saprolítico e regolítico dos depósitos minerais contidos no Complexo Araxá, incluindo os minérios formados sobre a núcleo flogopitítico e o anel carbonatítico;

(2) Definir a geometria e a distribuição espacial dos corpos mineralizados desses depósitos;

(3) Propor um modelo que explique o processo supergênico para formação dos minérios saprolíticos e regolíticos reconhecidos no CACA;

(4) Conhecer as características químicas, mineralógicas dos minérios reconhecidos nos halos de transição N e S (Fig. 1B e C do artigo 2);

(5) Correlacionar os resultados dos ensaios de concentração por flotação do pirocloro dos minérios regolíticos e saprolíticos dos halos de transição com as caracteristicas químicas e mineralógicas desses minérios. Para isso foram determinadas as composições químicas, mineral e de flotação típicas desses novos tipos de minério de Nb, e essas características foram comparadas com as dos minérios atualmente processados pela CBMM. Adicionalmente está sendo proposto um critério para classificação dos minérios de Nb dos halos de transição.

1.3   Metodologia

Já foram realizadas pela CBMM12 campanhas de sondagens, totalizando 83.933 m, visando reconhecer e estimar os recursos de Nb, P, Ba, Fe e ETR contidos principalmente em regolito e saprolito, os únicos tipos de minérios lavrados em Araxá. Foram retiradas 20.162 amostras dos testemunhos dessas sondagens que, até 2017 foram analisadas somente para os elementos CaO, MgO, Nb_2O_5, P_2O_5, Fe_2O_3, Al_2O_3, SiO_2, TiO_2, REEO e LOI, com o intuito de atender a produção de liga FeNb e demais produtos de nióbio. Nas campanhas realizadas após 2017 foram analisados também Pb, S, Sr, V_2O_5 e todos os ETR. Os dados dessas sondagens foram utilizados para fazer a maior parte dos diagramas do primeiro artigo, além disso, novas 73 amostras de minério foram coletadas e analisadas para óxidos de elementos maiores, elementos menores, traço e ETR, além de serem analisadas por DRX para determinação dos principais constituintes minerais. Toda essa nova base de dados também foi utilizada nas interpretações e discussões do primeiro artigo.

O número total de sondagens, de amostras analisadas e os resultados das análises realizadas na região oeste do Complexo, onde se localiza o maior depósito de fosfato do Complexo, não foi disponibilizado ou publicado pela MOSAIC Fertilizantes. As análises de amostras dessa região, utilizadas nas interpretações feitas no primeiro artigo, limitam-se a 146 amostras analisadas para SiO_2, Al_2O_3, Fe_2O_3, MgO, CaO, TiO_2, P_2O_5, BaO e C, obtidas com a amostragem dos testemunhos de 98 sondagens rasas, divulgadas na tese de Grasso (2015).

Um depósito de ETR, Nb e P_2O_5, situado próximo a margem norte do Complexo, foi avaliado pela ITAFOS (VENMYN RAND). O relatório de pesquisa, elaborado por Clay e Ackroyd (2012), mostra que entre 2011 e 2012, foram feitas 103 sondagens com profundidade média de 80 m, usadas para estimar os recursos dessa área. As amostras provenientes dessas sondagens foram analisadas para La_2O_3, CeO_2, Pr_6O_{11}, Nd_2O_3, Sm_2O_3, Eu_2O_3, Gd_2O_3, Tb_4O_7, Dy_2O_3, Ho_2O_3, Er_2O_3, Tm_2O_3, Yb_2O_3, Lu_2O_3, Y_2O_3, P_2O_5 e Nb_2O_5. Os autores concluíram que o depósito contém recursos medido + indicado que totalizam 6.4 Mt de minério com teores médios de 5,01% LREO, 8,4% de P_2O_5 e 1,02% de Nb_2O_5. Essas informações também foram usadas na elaboração do primeiro artigo.

Para a elaboração do segundo artigo foram selecionadas 246 amostras dos furos FAN2-06 (40), FAS-37 (41), FAS-31 (25), FAN2-12 (27), FAG-42 (24), FAS-35 (37), F-0XM9 (29) e F-5XIJ3 (23). Cada amostra correspondendo a 5 metros de comprimento dos testemunhos de sondagem, as quais foram consideradas para caracterização química por FRX para determinação dos principais óxidos; perda ao fogo por calcinação a 1.000°C (% LOI); os ETR foram determinados por LA-ICP-MS; e a determinação de S total foi feita por células infravermelhas não dispersivas da

amostra submetida a combustão. Essas mesmas amostras também foram submetidas à ensaios laboratoriais, em escala de bancada, para determinação da recuperação metalúrgica de Nb_2O_5 e foram analisadas também por DRX para determinação e semi-quantificação mineral.

A CBMM realizou estudos mineralógicos no laboratório de caracterização mineral da Universidade de São Paulo no período de 2016 a 2019. As informações geradas a partir dessas caracterizações contribuíram para interpretação da origem dos minérios dos halos, bem como para entender o motivo da baixa recuperação apresentada pelos minérios dessas regiões.

2   RESULTADOS E DISCUSSÃO

2.1   **Artigo1** – Geology, geochemistry and mineralogy of regolith and saprolite ore with Nb, P, Ba, REEs (+Fe) in mineral deposits from the Araxá Alkali Carbonatite Complex, Minas Gerais State, Brazil

José Marques Braga Jr.[a*], João Carlos Biondi [b,]

[a] CBMM – Companhia Brasileira de Metalurgia e Mineração, Araxá, Minas Gerais, Brasil

[b] UFPR – Universidade Federal do Paraná, Departamento de Geologia, Curitiba, Paraná, Brasil

* Corresponding author

Tel.: +55 34998163581.

E-mail address: jose.marques@cbmm.com

Abstract

The Araxá Complex, 97 – 76 Ma, holds important Nb, P, Ba, rare earths, and Fe deposits. In the Complex core, regolith and saprolite ores have formed from the weathering of phlogopitic breccia and magnetite apatitites. Phosphate and rare earths ores have formed on carbonatites that surround the core. The ores are ocher (> 2% CaO and MgO), brown (< 2% MgO and > 2% CaO), and orange (< 2% MgO and CaO). In the ocher and brown ores, hydroxycalciopyrochlore and hydrokenopyrochlore were ore minerals. In the orange, hydrokenopyrochlore and Nb-bearing goethite predominate. The phosphorus ore mineral in the ocher and brown ores was fluorapatite. Barite was the only Ba ore mineral. Monazite occurred in the brown and orange ores, whereas gorceixite, rhabdophane, and florencite occurred only in the orange. The 200m-thick orebodies are stratiform and horizontal, formed by meteoric water that flowed vertically and downward, then horizontally, radially, and centrifugally. First, the ocher was generated, which consumed the rock (protore), then the brown (ocher protore), and then the orange (brown protore). The weathering of 100 m of rock formed ~33 m of orange, ~9 m of brown, and ~4 m of ocher ore on the Complex core, and ~35 m of orange, ~7 m of brown, and ~10 m of ocher ore on carbonatite ring. With continual weathering, the Nb, P, and Fe ore minerals were residually concentrated, whereas most barite, monazite, and rhabdophane appeared to be authigenic. Continuous weathering caused the thickening of mineralized bodies and lateral, radial, and centrifugal minerals scattering. Crater lake sediments accumulate on the top surface.

2.1.1 Introduction

The Araxá alkali-carbonatitic Complex is known for its pyrochlore (Nb) + barite (Ba) + magnetite (Fe) ± monazite (LREE), and apatite (P) deposits, as well as its sulfur-rich water sources (near Hotel Tauá) (Fig. 1). Niobium ore has been mined in this Complex since the 1970s by COMIPA (Companhia Mineradora do Pirocloro de Araxá), a joint-venture between CBMM (Companhia Brasileira de Metalurgia e Mineração) and CODEMIG (Companhia de Desenvolvimento Econômico de Minas Gerais). Currently, The Mosaic Company (Mosaic Fertilizantes) mines the phosphate ore in the western half of the Complex (Fig. 1). In 2020, CBMM estimated the remaining Nb resource in the regolithic ore at 896 Mt, i.e., 1.49% Nb_2O_5. In 2017, the estimated resources of the other mineralization types were 770 Mt containing 10.4% P_2O_5, 768 Mt having 20.1% $BaSO_4$, and 352 Mt containing 5.6% REOs (rare earth oxides). Magnetite is a byproduct of pyrochlore and apatite ore processing. Ores with high concentrations of pyrochlore, apatite, barite, and magnetite predominate in the center of the Complex, whereas ores with apatite are mostly found in the western half, at the Mosaic pit, and in pit F4 on the southeastern edge (Fig. 1). It is not evident whether LREE ores occur in a defined geologic-geographical position. Since the beginning of the operation, CBMM has carried out 12 drilling campaigns, totaling 83,933 m, mainly in regolith and saprolite, which have been the only ore types mined in Araxá since the beginning of mining operation. A total of 20,162 samples have been collected from the cores of these drilling campaigns; before 2017, only CaO, MgO, Nb_2O_5, P_2O_5, Fe_2O_3, Al_2O_3, SiO_2, TiO_2, LREOs, and LOI were analyzed in an attempt to meet the requirements for the production of Fe-Nb alloy and other Nb products. In drilling campaigns after 2017, all the oxides and LOI analyzed before 2017, and Pb, S, Sr, V_2O_5, and all REEs were analyzed. Appendix 1 presents a summary of the CBMM database, which was used to plot most diagrams in this study. An additional 73 ore samples were collected to meet the requirements of this study and were analyzed for major element oxides, minor elements, trace elements, and REEs (Appendix 2). Table 1 presents the average compositions of the rocks and ores formed in the core of the Complex on phlogopitic breccia and magnetite apatitites. Table 2 lists the average compositions of the rocks and ores formed on the carbonatites in the ring that surrounds the core.

Resultados e discussão
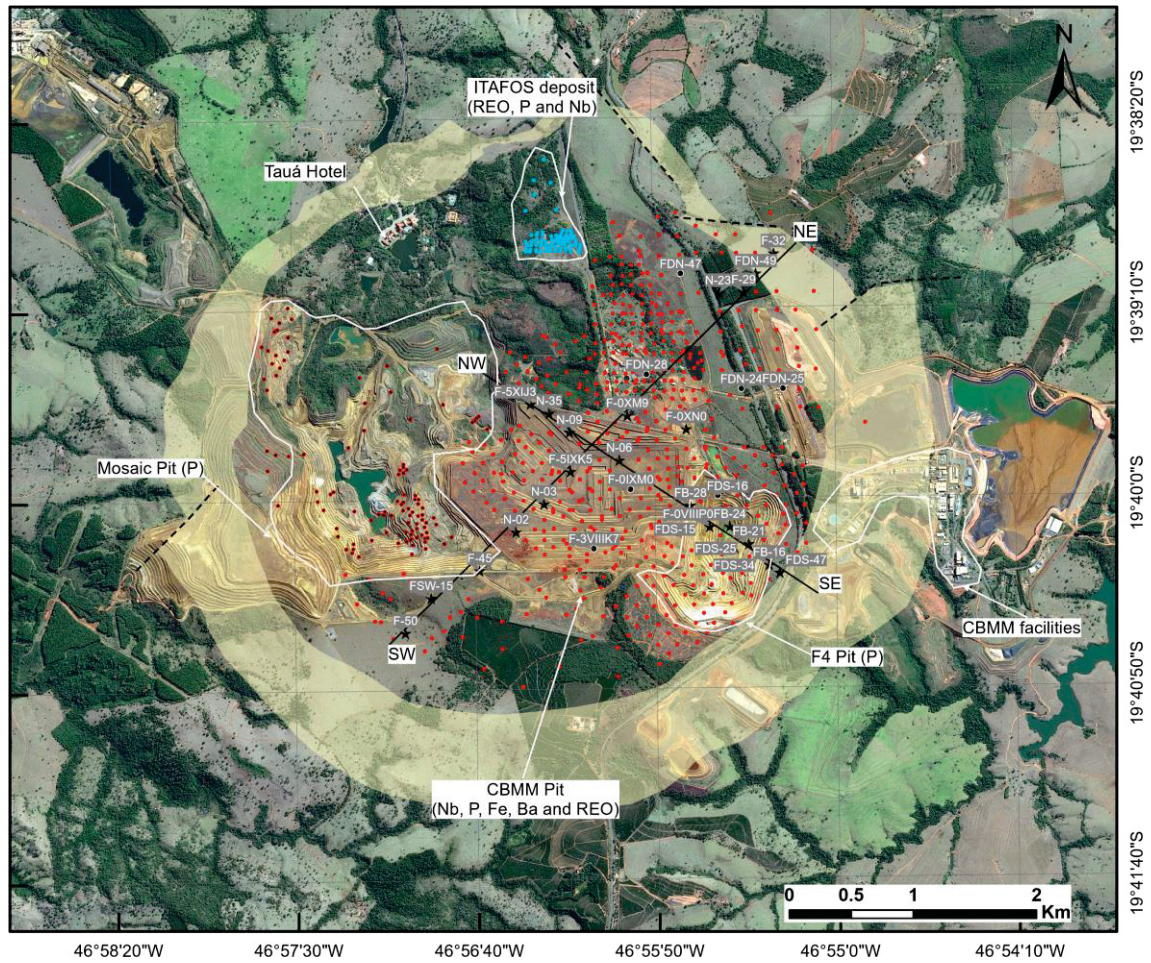
Fig. 1 – Aerial photography of the Araxá alkaline-carbonatitic Complex. The ring of muscovite-quartz schists and phenitized quartzites surrounding the Complex represents the limits of the mineralized bodies containing Nb, P, Ba, REEs, and Fe. The perimeters of the open pits in the main mines operating in the Complex are identified. The drill holes (black spots) are mentioned in this study. The stars represent the drill holes used for the SW–NE and NW –SE profiles.

Resultados e discussão

Table 1- Average compositions of rocks and ores from deposits located on phlogopitic breccia and magnetite apatitites from the core of the Araxá Complex.

Analyte (wt%)	Rock (phlogopitite)		Ocher ore		Brown ore		Orange ore	
	Mean	SD (n= 6)	Mean	SD (n= 6)	Mean	SD (n=6)	Mean	SD (n=6)
Al_2O_3	0.5	0.6	0.8	0.8	1.2	1.0	1.5	1.4
BaO	6	3	8	2	11	4	14	7
CaO	15	3	15	4	15	5	0.20	0.06
Fe_2O_3	14	8	21	6	31	7	47	10
K_2O	1.1	1.1	1.0	0.4	0.10	0.09	0.02	0.01
LOI	20	10	16	6	5.2	0.9	6.8	1.1
MgO	12	5	10	2	0.51	0.23	0.38	0.06
MnO	0.4	0.2	0.5	0.1	0.87	0.1	1.3	0.3
Na_2O	0.08	0.12	0.13	0.14	0.17	0.17	0.10	0.12
Nb_2O_5	0.9	0.6	1.2	0.9	1.6	0.6	2.7	1.0
P_2O_5	3.0	1.6	5	3	10	6	2.2	1.1
S	1.1	0.8	1.4	0.5	2.0	0.9	2.5	1.6
SiO_2	7	6	10	8	8	4	6	3
TiO_2	1.4	1.2	2.1	1.5	3.2	2.03	4	3

Table 2 - Average compositions of rocks and ores from deposits located on carbonatites from the Araxá Complex.

XRF (wt%)	Rock (carbonatite)		Ocher ore		Brown ore		Orange ore		Clayey soil	
	Mean	SD (n=5)	Mean	SD (n=5)	Mean	SD (n=5)	Mean	SD (n=5)	Mean	SD (n=5)
Al_2O_3	1.0	0.5	1.6	0.4	2	8	5	7	24	6
BaO	1.6	1.7	1.9	2.2	1.9	2.1	3.0	2.0	2.2	1.6
CaO	24	7	19	6	12	10	0.6	10.1	0.3	0.2
Fe_2O_3	11	3	16	2	24	13	43	13	32	11
K_2O	0.9	0.3	1.02	0.3	0.35	0.45	0.03	0.45	0.14	0.09
LOI	18	9	11	5	5	7	8	7	12	6
LREO	7	12	5	7	3	7	5	7	4	5
MgO	14	8	9	6	5	8	0.4	7.4	0.2	0.2
MnO	0.4	0.1	0.5	0.2	0.9	0.5	1.4	0.5	0.4	0.4
Na_2O	n.a.	n.a.	n.a.	n.a.	n.a.	n.a.	n.a.	n.a.	n.a.	n.a.
Nb_2O_5	0.3	0.3	0.5	0.4	0.3	0.3	0.6	0.3	0.5	0.3
P_2O_5	4	2	6	5	9	4	4	4	3	3
PbO	0.01	0.01	0.03	0.03	0.05	0.03	0.06	0.03	0.02	0.01
SiO_2	11	5	20	6	24	9	16	9	16	9
S	0.7	0.6	0.9	1.0	1.0	1.5	1.6	1.4	0.4	0.4
TiO_2	1.5	0.5	2.6	0.4	3.4	1.9	6.7	2.0	3.9	0.8

Mosaic has not disclosed all drill holes and the results of analyses carried out in the western region of the Complex, where the largest phosphate deposit is located. The sample analysis from this region used in this study was published by Grasso (2015), with 166 samples analyzed for SiO_2, Al_2O_3, Fe_2O_3, MgO, CaO, TiO_2, P_2O_5, BaO, and C, obtained by sampling cores from 98 shallow drill-holes. A deposit of REEs, Nb, and P_2O_5, located near the northern edge of the Complex (Fig. 1), was evaluated by ITAFOS (VENMYN RAND). The mineral resource estimation report (Clay and Ackroyd, 2012) showed that 103 drill-holes were dug at an average depth of 80 m. Samples were analyzed for La_2O_3, CeO_2, Pr_6O11, Nd_2O_3, Sm_2O_3, Eu_2O_3, Gd_2O_3, Tb_4O_7, Dy_2O_3, Ho_2O_3, Er_2O_3, Tm_2O_3, Yb_2O_3, Lu_2O_3, Y_2O_3, P_2O_5, and Nb_2O_5. The measured + indicated resources totaled 6.4 Mt of ore at average 5.01% LREOs, 8.4% P_2O_5, and 1.02% Nb_2O_5.

In the central region of the Complex, below the CBMM pit (Fig. 1), phlogopitic breccia is cut by dikes and venules of carbonatite and magnetite apatitite mineralized with Nb, P, Ba, Fe, and REEs. Phosphate deposits at the Mosaic and F4 pits, and the ITAFOS deposit, locally containing REEs and Nb (Fig. 1), occur in the carbonatite ring surrounding the core.

The objectives of this study were to (1) chemically and mineralogically characterize the saprolytic and regolithic ores found in the mineral deposits present in the Araxá Complex; (2) define the geometry and spatial distribution of the mineralized bodies in these deposits; (3) understand the mineralizing processes and formation of the main minerals that compose the ores; and (4) propose a model capable of explaining the genesis of these ores and their mineralized bodies.

2.1.2 Geochronology and geotectonic setting

Ulbrich and Gomes (1981) first categorized Brazilian alkaline Complexes that border the Paraná Basin by age and related them to the rift that caused the opening of the Atlantic Ocean between 137 and 134 Ma. More recently, Gomes and Comin-Chiaramonti (2017), with a set of new dates, categorized these Complexes into seven types: (1) one group encompassing Permo–Triassic ages, (~250 Ma); (2) four lower Cretaceous groups with ages of ~139, ~130, ~126, and ~118 Ma; (3) a late Cretaceous group (90–80 Ma), which includes Araxá; and (4) a late Paleocene group (~58 Ma).

By employing novel decay constants, Sonoki and Garda (1988) recalculated the ages of rocks in the Araxá Complex first estimated by Amaral et al. (1967). Two recalculated K/Ar ages of the phlogopitite in the Complex core were 97.6 ± 6.1 Ma and 89.4 ± 10.1 Ma; a K/Ar date for the phlogopite in the carbonatite was 77.4 ± 1.0 Ma.

14
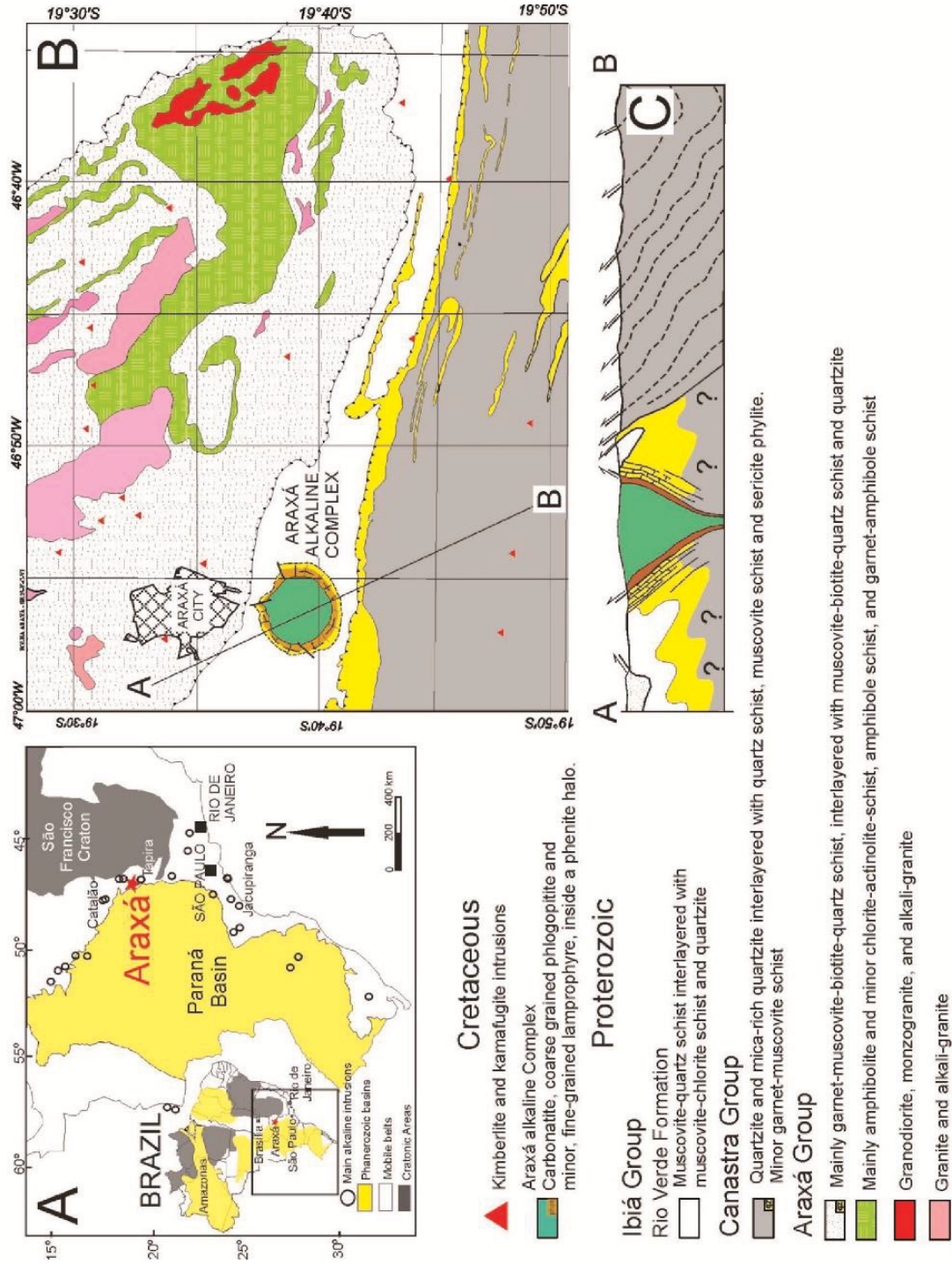
Fig. 2 – Tectonic and geological settings. (A) Indication of the main alkaline Complexes located in the southern part of Brazil. (B) Simplified geological map of the Araxá region (Modified from Seer et al., 2015). (C) Simplified regional geological section encompassing the Araxá alkali-carbonatitic Complex (modified from Seer et al., 2015).

Almeida (1983) geographically and tectonically classified the alkaline Complexes of southeastern Brazil, placing them into three groups. The largest of these three groups, which includes the Araxá Complex, contains alkaline intrusions near the edges of the Paraná sedimentary basin (Fig. 2A). These intrusions mainly lie on the eastern outer edge of the basin amid rocks of the Brasília folded belt between the São Francisco Craton and sedimentary basin. Almeida (1983) also grouped alkaline intrusions into alkaline provinces and related them to major lineaments, placing Araxá in the Alto Paranaíba arch, together with the Tapira, Catalão, Serra Negra and Salitre Complexes, among many others, as well as many kimberlitic and kamafugitic intrusions with smaller dimensions (Figs. 2A and 2B).

Grossi Sad and Torres (1971) made the first map of the Araxa alkaline complex, and Issa Filho et al. (1984) described the Araxá Complex, i.e., the former Barreiro Complex, and proposed a genetic model for its entire area, composed of alkaline rocks and carbonatites. Seer et al. (2015) published a geological map of the Araxá region at a scale of 1:100,000 (Folha Araxá, 2015), showing the Araxá Complex (Figs. 2B and 2C) hosted in poly deformed muscovite-quartz schist interlayered with muscovite-chlorite schist from the Rio Verde Formation within the Ibiá Group (Barbosa et al., 1970; Seer et al., 2000), Neoproterozoic age. The Araxá intrusion deformed and uplifted the quartzites and mica schists of the Ibiá and Canastra groups (Barbosa, 1970, Silva et al., 2012); therefore, the alkaline and carbonatite rocks currently occur inside a ring of phenitized quartzites and mica schists (Figs. 1 and 2A, B) (Grossi Sad and Torres, 1971, Seer et al., 2015).

Most surfaces inside the Complex are composed of laterally discontinuous lacustrine clayey sediments, whose thickness varies from 0 to 140 m. This type of sedimentation still occurs in lakes near Hotel Tauá (Fig. 1). These sediments and lateritic crusts obliterate all rocks and regolith (ores), which is why they are not shown in the maps and geological sections.

2.1.3 Analytical methods

The 20,162 samples from the CBMM database considered in the 2020 resource reassessment study were analyzed by SGS GEOSOL Laboratories. The samples obtained from the most recent drilling campaign were analyzed using the following methods: 20 oxides by XRF (%): Al_2O_3 and Fe_2O_3; MnO; P_2O_5 and SrO; U_3O_8 and BaO; K_2O and Na_2O; PbO, Ta_2O_5, V_2O_5, and CaO; La_2O_3 and Nb_2O_5; Pr_6O_{11}, and ThO_2; and CeO_2, MgO, Nd_2O_3, SiO_2, and TiO_2. LOI: Loss on ignition after calcination at 1,000 °C (%). Seventeen elements were analyzed by ICP-MS (ppm): Ce, Gd, Nd, Th, Yb, Dy, Ho, Pr, Tm, Er, La, Sm, U, Eu, Lu, Tb, and Y; the %S was analyzed by infrared spectroscopy.

Seventy-three new drill core samples were collected at the F–5IXK5, F–5XIJ3, and F–0XM9 drill holes and analyzed by ALS Labs (Australia) using the following methods: 13 oxides were analyzed by ICP–AES (%): SiO_2, Al_2O_3, Fe_2O_3, CaO, MgO, Na_2O, K_2O, Cr_2O_3, TiO_2, MnO, P_2O_5, SrO, and BaO. LOI: after calcination at 1,000 °C (%). Thirty-eight elements were analyzed by ICP–MS (ppm): Ba, Ce, Cr, Cs, Dy, Er, Eu, Ga, Gd, Hf, Ho, La, Lu, Nb, Nd, Pr, Rb, Sm, Sn, Sr, Ta, Tb, Th, Tm, U, V, W, Y, Yb, and Zr. The total %C and total %S were analyzed using infrared spectroscopy. Six elements were analyzed by ICP-MS (ppm): As, Bi, Hg, Sb, Se, Te, and Tl. Ten elements were assessed by ICP–AES (ppm): Ag, Cd, Co, Cu, Li, Mo, Ni, Pb, Sc, and

Zn. Niobium was reanalyzed by XRF; Ce, La, Nd, and Pr were reanalyzed by ICP-AES when an over limit occurred.

X-ray diffraction (XRD) analysis was performed using the powder method with a Bruker D8 Advance diffractometer operating with Cu-Kα radiation and a position-sensitive Lynxeye XE detector. The collection of diffractograms was performed in the range of 10° to 70°; at this range, a total reading of 3,080 steps was obtained, with a timestep of 0.4 s in increments of 0.02°. The crystalline phases were identified by comparing the diffractograms with the ICDD (International Centre for Diffraction Data) PDF database using the DiffracEva software. The reference intensity ratio (RIR) method was used to semi quantify the minerals based on the dimensioning of all diffraction data in relation to the diffraction of the standard reference materials. The samples were also analyzed by an SEM (scanning electron microscope), QUANTA 450 (FEI COMPANY™), coupled to an EDS (**Energy Dispersive Spectroscopy**) system (EDAX–AMETEK™). These analyses were used to validate and adjust the mineral semi-quantification resulting from the RIR. Appendix 2 shows the chemical compositions of these samples; Appendix 3 presents the minerals that compose them.

To determine the densities of the ores, the sand flask, hydrostatic balance, and template methods were used. A sand flask was used for the outcropping and friable materials. This method consists of digging an in situ hole with regular and well-defined walls. The material was then removed, weighed, and the flask filled with sand was weighed. The hole was then filled with sand, thus assigning a predefined density. The flask containing the remaining sand was weighed again; the volume of the hole was established. The density was calculated as the ratio between the mass and volume of the material in situ. The material collected in the excavation subsequently remained in a furnace for 6 h at 120 °C; it was then weighed again so that the moisture and dry base density could be defined.

2.1.4 Rock and mineralized body composition and location

The pits made by the mining companies operating in Araxa present a few outcrops of alkaline rocks and carbonatites. Some deep drill holes that surpassed the weathering front show that alkaline silicatic rocks predominate in the center of the Complex, mainly as phlogopitic breccia (Fig. 3A), magnetite-rich phlogopitite (Fig. 3B), and phlogopite-magnetite apatitites. These are all cut by carbonatite veins and venules (Fig. 3C). Surrounding the phlogopitic breccia and apatitite in the core is a carbonatite ring (Fig. 3D) with variable magnetite concentrations.

Resultados e discussão
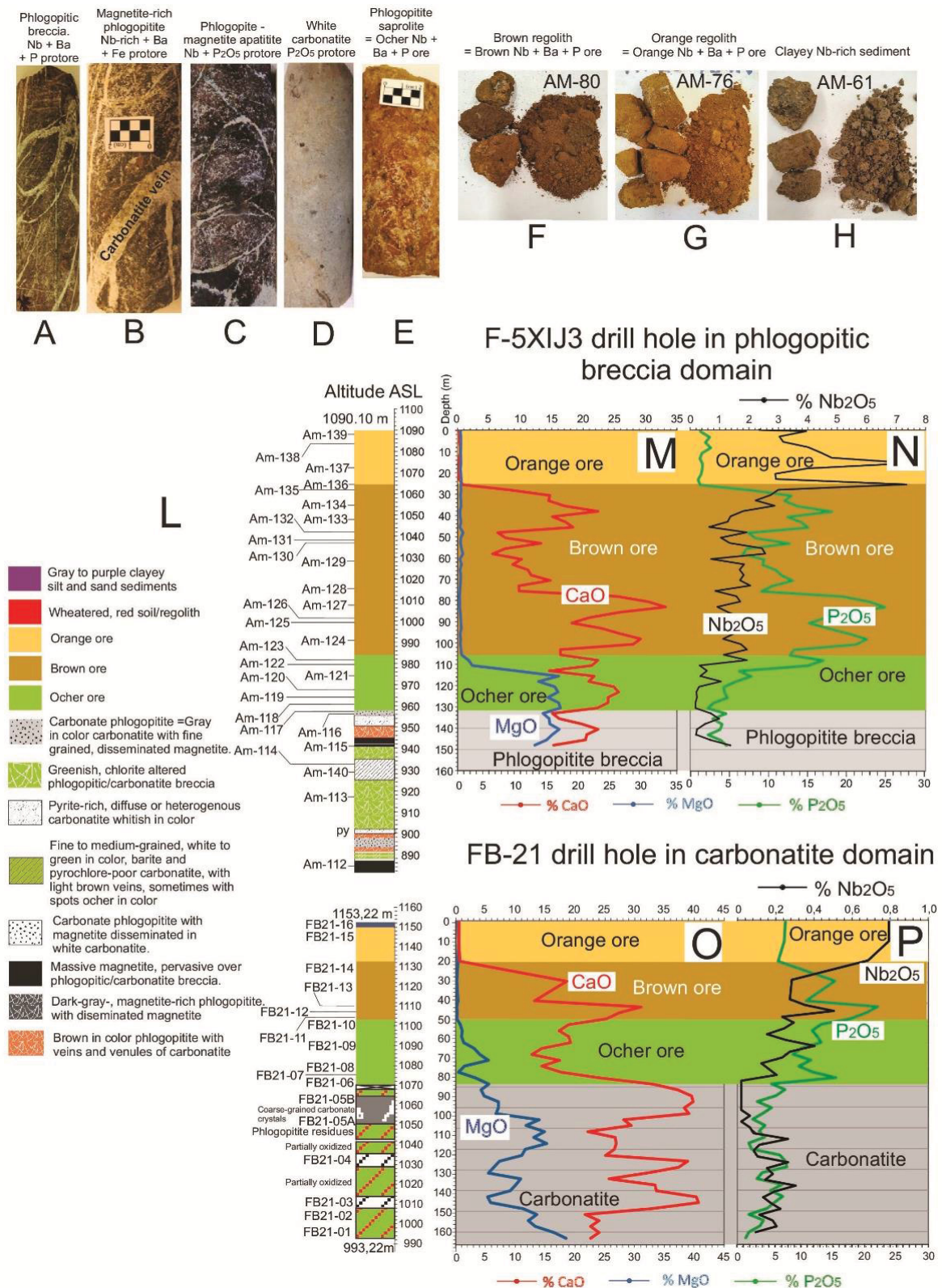
Fig. 3 – Characteristics of the ores and rocks in the Araxá Complex. (A to D) Complex main rocks. (E) Saprolytic ore. (F and G) Main regolithic ores. (H) Clayey sediments. (L) Description of the lithologies and ores from drill holes F-5XIJ3 (Complex core) and FB-21 (outer carbonatitic ring). Variation in the MgO and CaO (M) and Nb_2O_5 and P_2O_5 (N) in the core of the Complex. Variation in the MgO and CaO (O) and Nb_2O_5 and P_2O_5 (P) contents in the carbonatite outer ring.

Resultados e discussão

Contacts between the supergenic ores and rocks in the bedrock are often abrupt; the transition usually only occurs across a few centimeters but can expand to a few meters (Fig. 3L). The total thickness of the saprolithic and regolithic ores can exceed 200 m, with three types mainly distinguished by their CaO and MgO contents and predominant colors: (a) ocher saprolite (Fig. 3L, M, N, O, P, E) is sufficiently consistent to remain cylindrical in shape when sectioned by the drill crown. Its lower contact is with the rock while the upper contact is with the brown regolithic ore. (b) The brown regolith (Fig. 3L, M, N, O, P, F) is powdery and lies in an intermediate position above the ocher saprolite and below the orange regolith. (c) The orange regolithic ore (Fig. 3L, M, N, O, P, G) is also powdery and often covered by lateritic soil or clayey sediments (Fig. 3L, H), both presenting high SiO_2, Fe_2O_3, and Al_2O_3 contents; Nb_2O_5 may also occur. We note that both phlogopitites and carbonatites are subject to sudden changes in CaO and MgO (Fig. 3L, M, N, O, P). On the phlogopitic breccia, the ocher ore contains approximately 15% MgO and 20% CaO (Fig. 3M). The MgO content decreases to < 2% in the brown ore, whereas the CaO content varies from 15 to 30%. In the orange ore, the MgO content is similar to that of CaO, both decreasing from 20–25% to < 2% (Fig. 3M). The same variations occur when the saprolite ore substrate is carbonatite (Fig. 3O).

Fe_2O_3, BaO, CaO, and MgO compose most of the rock and ore masses; however, the magnitudes of the CaO and MgO contents in the supergenic ores indicate different levels of weathering and consequently different mineralogical compositions. These factors influence the pyrochlore mineral beneficiation processes, as well as the mining orientation. Therefore, the different types of ore were chemically defined by the contents of the following oxides: (a) orange ore, < 2.0% MgO and CaO (Figs. 3M, O and 4A), (b) brown ore < 2.0% MgO and > 2.0% CaO (Figs. 3M, O and 4B) and (c) ocher ore, > 2.0% MgO and CaO (Figs. 3M, O and 4C).
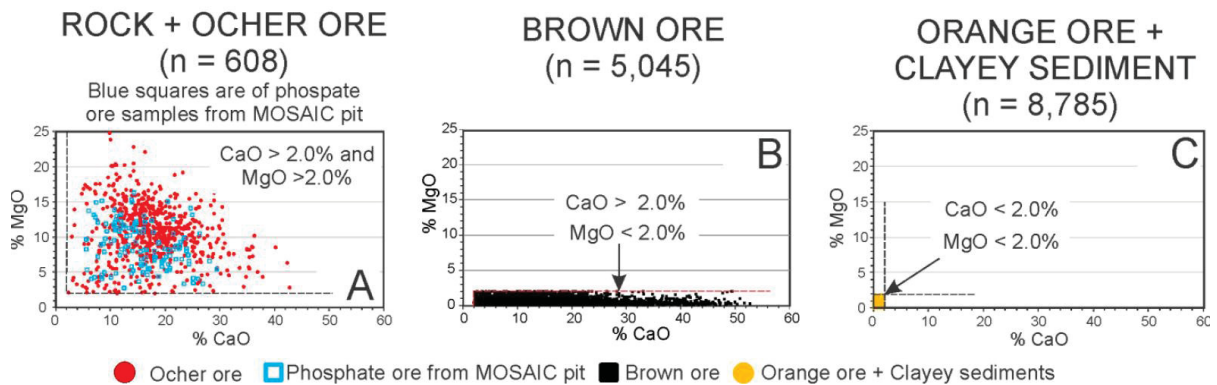
Fig. 4 – Chemical characterization of ocher saprolite (A), brown regolith (B) and orange regolith and clayey soil (C) ores based on CaO and MgO contents. Note that the points corresponding to the analysis of 8,785 samples of orange + clay ore are in the small domain of Fig. 4C, delimited by CaO and MgO contents lower than 2%. These diagrams and the following were plotted based on CBMM.

This definition of the ore types allows for a visualization of their distributions within the Complex using block models built for MgO (Fig. 5A–C) and CaO (Fig. 5D–F) substances. By still considering the chemical parameters that define the ores, the edges of the ocher, brown, and orange ore bodies were defined in SW–NE (Fig. 5G, H) and SW–NE (Fig. 5I, J) sections in the block models. Initially, the line separating the ocher ore bodies from those with brown ore was determined in sections 5G and 5I (red lines). This line separates the ores containing > 2.0% MgO (ocher ore) from those

Resultados e discussão

with < 2.0% (brown ore). Given that the orange ore has < 2.0% MgO and CaO, figures 5H, J presents a line separating the brown ore from the orange (yellow line). Therefore, the mineralized bodies with ocher ore between the rocky substrate and red line, brown ore between the red and yellow lines, and orange ore between the yellow line and the surface were delineated. We note that the yellow lines in figures 5H, J were moved to figures 5G, I.
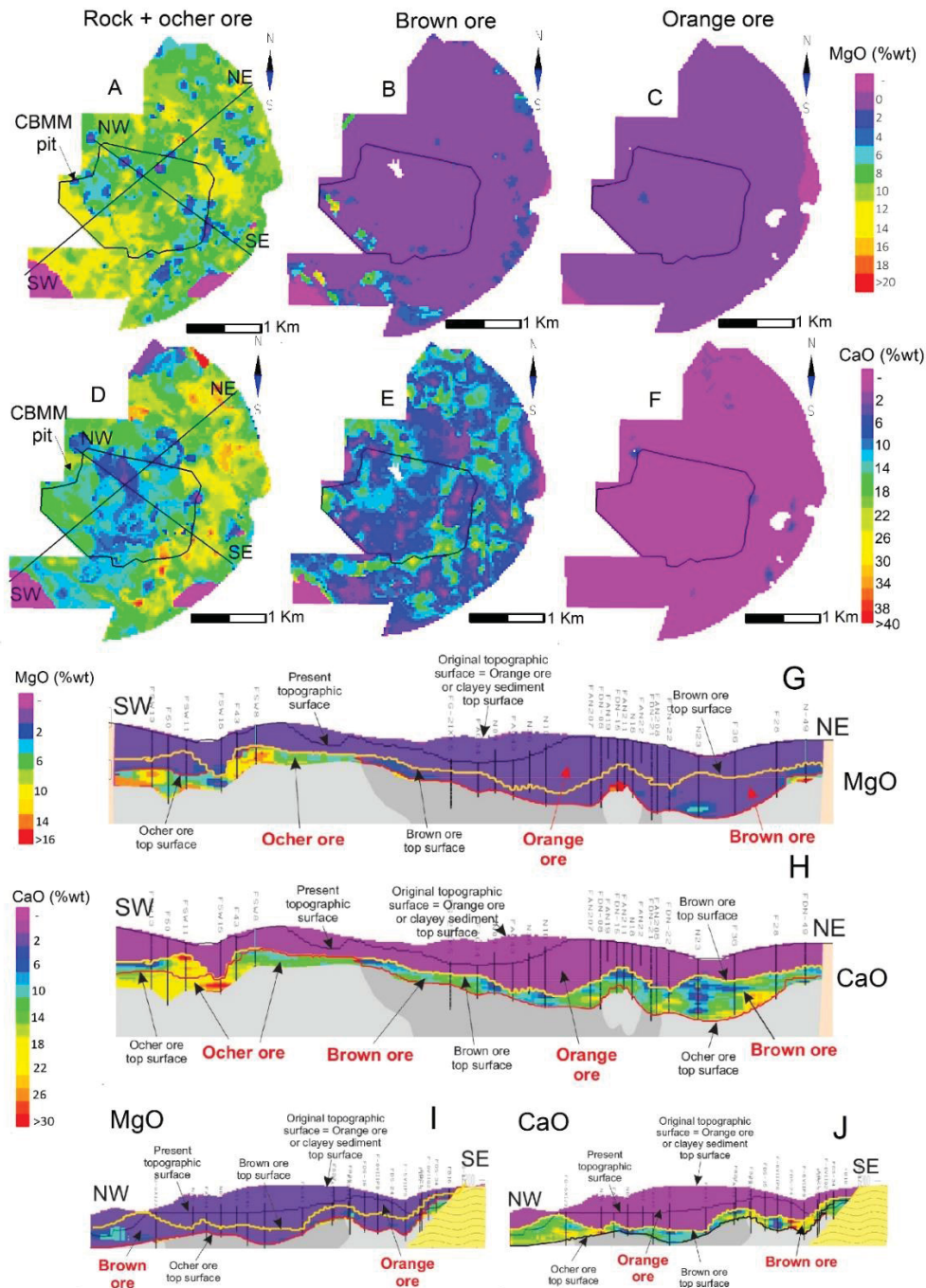
Fig. 5 - Geological delimitating of the mineralized bodies in the Araxá deposits based on the MgO and CaO contents of the ores, calculated on the block model used by the CBMM. (A–C) Map of the distribution of MgO contents. (D–F) Map of the distribution of CaO contents. Boundaries of the mineralized bodies defined in section: SW–NE (G–H), and NW–SE (I–J).

Figures 6A-1 to 6J-3 show the spatial distribution of blocks in a block model constructed for the ocher (6A-1 to 6J-1) and brown (6A-2 to 6J-2) ores, as well as the orange (6A-3 to 6J-3), calculated to obtain the distribution of ore substances. The distribution of Nb_2O_5 is shown in Fig. 6A-1 to A-3, Fe in 6B-1 to B-3, P in 6C-1 to C-3, BaO in 6D-1 to D-3, S in 6 E-1 to E-3, REOs in 6F-1 to F-3, TiO_2 in 6G-1 to G-3, SiO_2 in 6H-1 to H-3, K_2O in 6E-1 to I-3), and Al_2O_3 in 6J-1 to J-3. In these figures, the reference location is the CBMM mine pit (Fig. 1). Because of the simplified sampling carried out in the ITAFOS area (Fig. 1) and the lack of survey data for the drill hole samples collected in the Mosaic area (Fig. 1), the block model did not cover these two areas.

Resultados e discussão
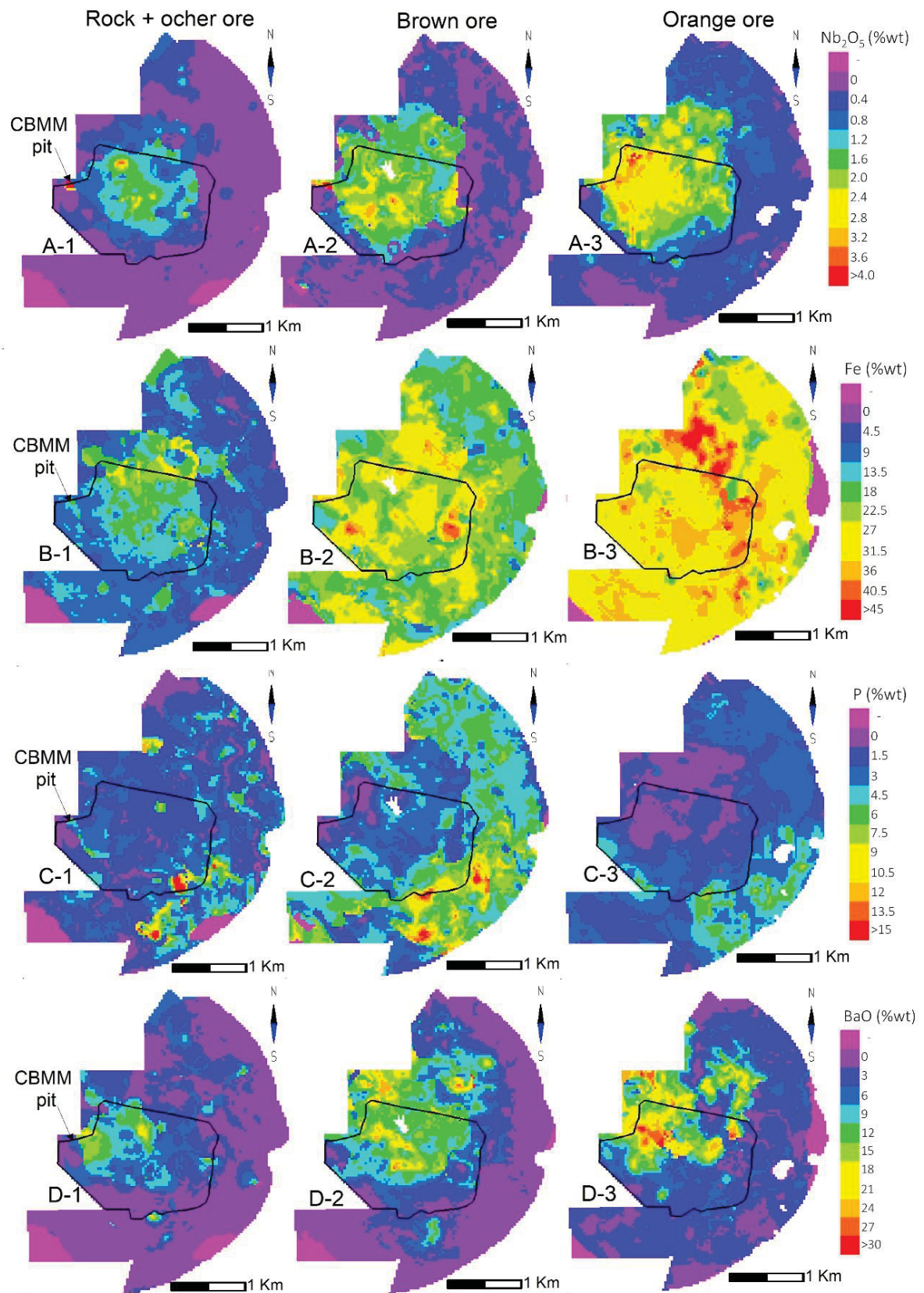
Resultados e discussão
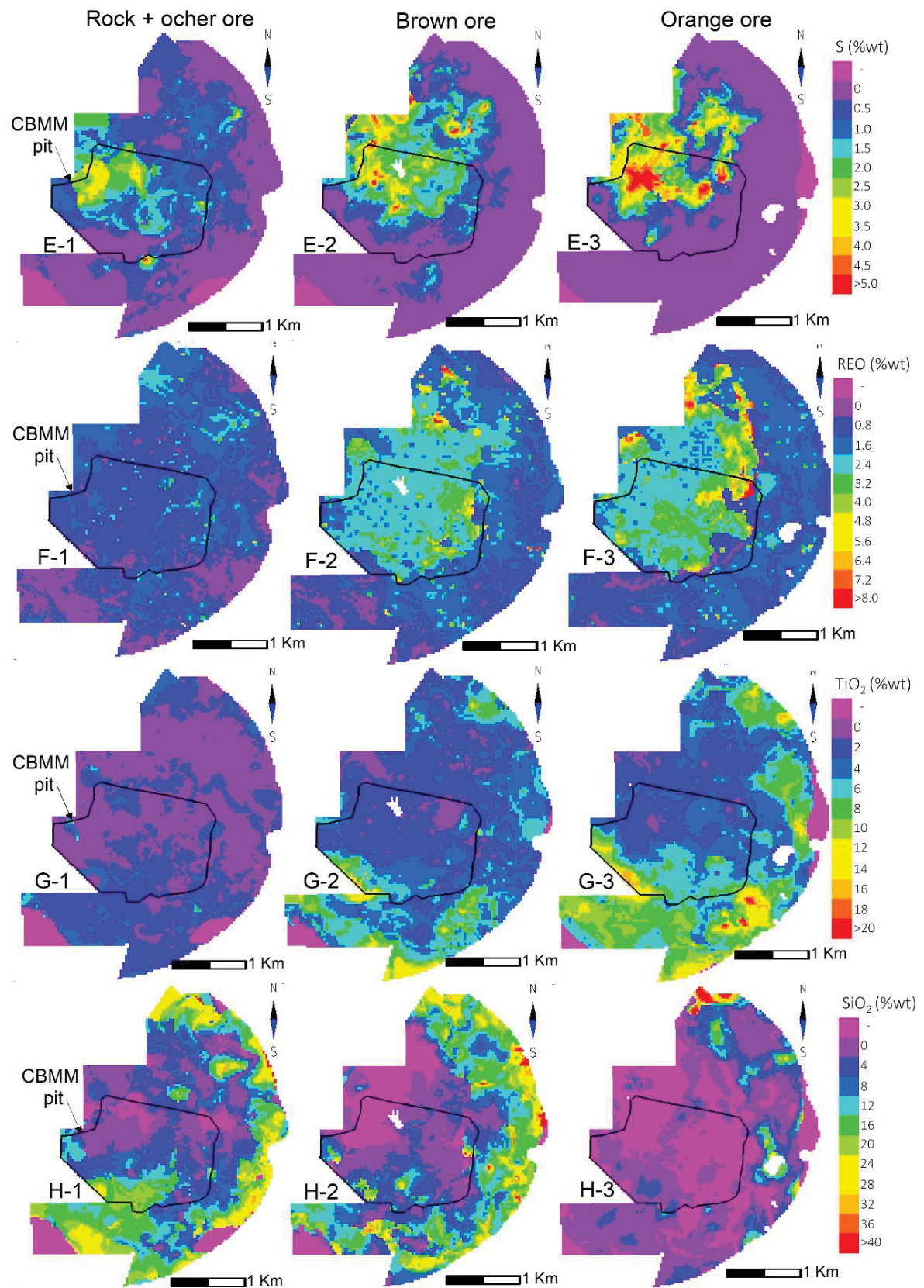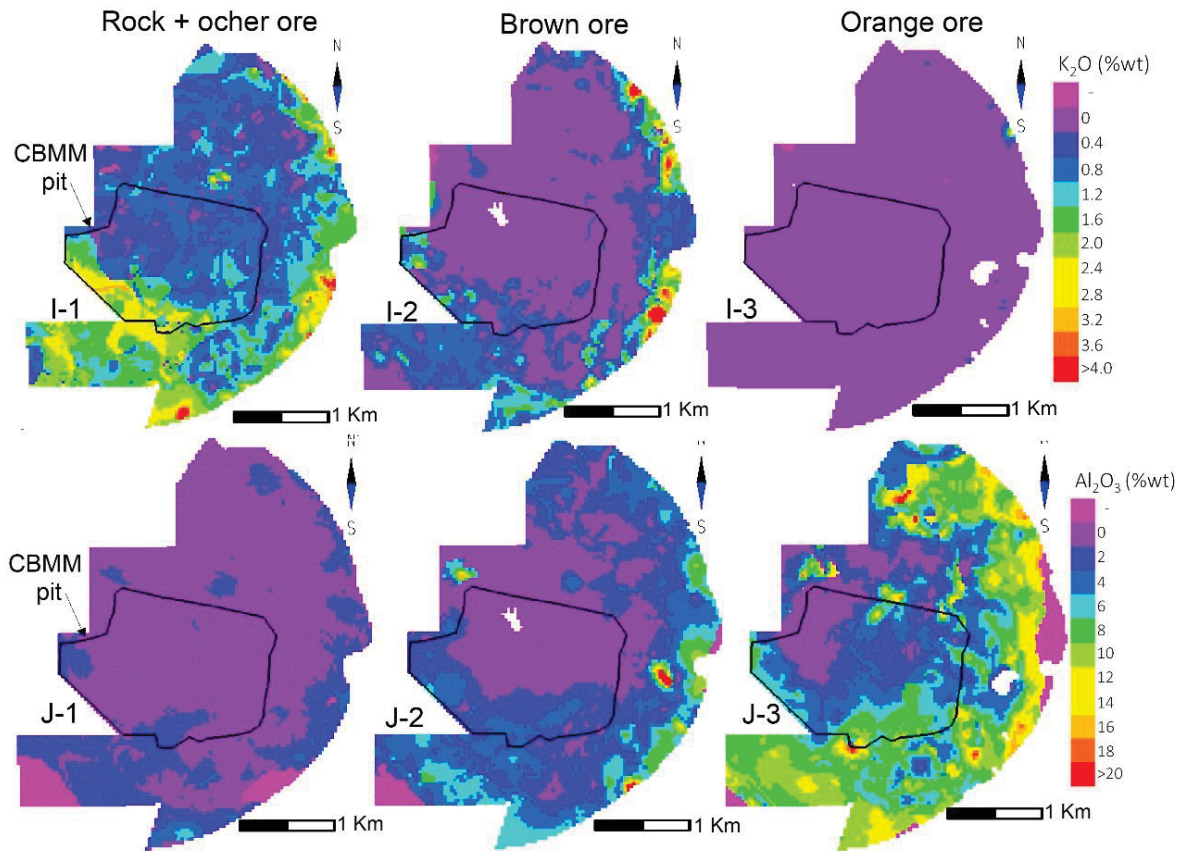
Fig. 6 - Distribution of the contents of the main substances that constitute the Araxá orebodies according to the block models of the deposits: Nb2O5 (A-1 to A-3), Fe (B-1 to B-3), P (C-1 to C-3), BaO (D-1 to D-3), S (E-1 to E-3), REO (F-1 to F-3), Ti (G-1 to G-3), SiO2 (H-1 to H-3), K2O (I-1 to I-3), and Al2O3 (J-1 to J-3).

The Nb_2O_5 contents (Fig. 6A-1 to A-3), present in various types of pyrochlore (Appendix 3), varied depending on the region of the Complex. In the central region of the phlogopitic breccia and magnetite apatitites domain, the Nb_2O_5 content increased from 0.4% in the ocher ore (Fig. 6A-1) to approximately 4.0% in the orange ore (Fig. 6A-3). In the ores occurring on the carbonatitic ring, the Nb_2O_5 content varied from 0.0 to 0.6%. The Fe content (Fig. 6B-1 to BD-3) in the ocher ore ranged from 18 to 27% (corresponding, respectively, to 26 to 39% Fe_2O_3) and was concentrated in the core; however, the concentrations and coverage area increased radially from the core to the edges of the Complex, from the brown regolith (26 to 65% Fe_2O_3) to the orange (32 to 65% Fe_2O_3) ore. Figures 6A-1 and 6B-1 show that the area occupied by the ocher ore was simultaneously enriched in Nb_2O_5 and Fe, whereas the contents of these substances were always low in the carbonatite ring. The orange regolith occupies the entire surface of the Complex, with Fe_2O_3 contents between 20 and 65%; the highest concentrations occur near the eastern and northern edges of the CBMM pit (Fig. 6B-3).

The P content (Fig. 6C-1 to 6C-3) of the ocher saprolites was low, varying from 0.0 to 3.0% (P_2O_5 from 0.0 to 7.0%) in almost the entire Complex. They were high only in the south-eastern part of the Complex, in the F4 pit region (Fig. 1), and in the ITAFOS deposit in the northern part, where the saprolites contain F-apatite (Appendix 3) and

the P content ranges from 4 to 15%. In the brown regoliths (Fig. 6C-2), the P_2O_5 contents were higher and the regoliths presented contents above 10.0%, occurring in most of the Complex; however, the region with the highest content was still that of the F4 pit (Figs. 1 and 6C-2). Owing to the presence of gorceixite (Appendix 3) in the orange regolith, the P_2O_5 content decreased to < 21.0% across the entire region, commonly below 7%, including the F4 pit region.

The distribution of BaO (Figs. 14B-1 to 14B-3) mimics that of Nb_2O_5. The BaO content is high in the core, ranging from 20.0% in the ocher saprolite to 33.0% in the orange regolith; however, it is often low in the saprolite and regolith occurring in the carbonatitic ring, where it does not exceed 6.0% (Fig. 6D-3). This was also the case for the S content (Fig. 6E-1 to 6E-3). The core saprolites had S contents of up to 3.5%, whereas in the orange regolith, the S content was < 0.5%. Similar to BaO, S experienced an increase in this area, with a high content in the core to the NE (compare Fig. 6D-2, D-3 to 6E-2, E-3). No S occurred in the carbonatite ring, except for the area to the NE of the Complex.

The saprolite in the core of the Complex did not contain significant REE contents (Fig. 6F-1). Mineralization occurred in the brown (Fig. 6F-2) and orange (Fig. 6F-3) regoliths, encompassing the central and northeastern areas of the Complex. The highest content, up to 8.0% REOs, occurred in the northeastern part of the nucleus and in the ITAFOS deposit. In the saprolites and regoliths on the carbonatitic ring, the REO content was low, varying from 0.0 to 1.6%, occasionally reaching 2.4%.

No ocher ore had TiO_2 (Fig. 6G-1). Here, TiO_2 contents between 6 and 10% occurred in the brown ore above the carbonatitic ring (Fig. 6G-2) and reached up to 20% in the orange ore (Fig. 6G-3). The distribution of the TiO_2 content did not coincide with that of Fe.

In the central and northern parts of the Complex, the ocher ores had low SiO_2 contents (0.0 to 12.0%), as depicted in Fig. 6H-1 to 6H-3. However, the brown regolith experienced a gradual increase in its SiO_2 content: up to 40% on the edge of the Complex, near the ring of phenitized quartzite and muscovite schist that surrounds the carbonatite ring. Generally, the SiO_2 contents decreased in the orange regolith, remaining high only on the NE edge of the Complex. The K_2O contents (Figs. 6 I-1 to 6 I-3) also only increased on the outer edge of the carbonatite ring, where they reached 4.0% in the saprolite. The K_2O content decreased in the brown regolith and disappeared in the orange (Fig. 6 I-3).

The ocher and brown ores were practically devoid of Al_2O_3 (Figs. 6J-1 and 6J-2), with contents lower than 4.0%. In the orange regolith located on the outer edge of the carbonatitic ring, the Al_2O_3 content was higher, ranging from 6.0 to 14.0% (Fig. 6J-3). In this type of regolith, Al_2O_3 occurred as Al-phosphates, gibbsite and kaolinite (Appendix 3). The behavior of the TiO_2 content (Fig. 6G-1 to 6G-3) was similar to that of Al_2O_3.

Resultados e discussão

2.1.5 Chemical and mineral characteristics of saprolitic and regolithic ores

General chemical and mineral characteristics of rocks and ores from Araxá Complex

Seventy-three samples were collected from the drill cores recovered from drill holes FG-5IXK5 (21 samples), F-5XIJ3 (23 samples), and F-0XM9 (29 samples) (Fig. 1). Table 3 presents a summary of the results of the analyses. They showed that Fe_2O_3 was the most common substance, with contents between 14.8 and 79.3%, followed by BaO, varying from 0.7 to 33.5%, and P_2O_5, ranging from 1.01 to 21.5%. The CaO contents varied from 0.05 to 26.4% while those of MgO ranged from 0.12 to 14.95%. The Nb_2O_5 contents, between 0.23 and 7.57%, were higher in the orange regolith. The P_2O_5 content was the highest in the brown regolith; the BaO and S contents were high, especially in the brown and orange regoliths. The contents of La_2O_3 (0.2 to 5.0%), Ce_2O_3 (0.2 to 8.0%), and Nd_2O_3 (0.07 to 2.00%) were high, mainly in the brown and orange regoliths.

Table 3 – Summary of new chemical analyses of ores from the core of the Araxá Complex.

Analyte XRF (wt%)	Ocher ore + rock (n = 4)				Brown ore (n = 20)				Orange ore (n = 43)			
	Mean	SD	Min	Max	Mean	SD	Min	Max	Mean	SD	Min	Max
Al_2O_3	0.9	0.6	0.23	1.48	0.9	1.0	0.09	3.93	0.6	0.4	0.1	1.84
BaO	9.6	3.6	5.3	14.1	13	8	3.26	32	15	8	1.65	33.5
C	1.0	1.0	0.23	2.32	0.20	0.10	0.08	0.45	0.07	0.03	0.03	0.15
CaO	13	5	6.3	18.5	14	6	1.96	26.4	0.2	0.3	0.05	1.74
Fe_2O_3	32	6	26.8	41.1	37	12	14.85	59.1	53	13	18.6	79.3
K_2O	0.49	0.18	0.32	0.73	0.05	0.04	0.01	0.19	0.02	0.01	0.01	0.05
LOI	9.3	2.1	6.54	11.5	5.2	1.5	3.02	7.97	6.6	1.6	2.95	10.5
MgO	5.6	3.4	2.5	10.4	0.5	0.4	0.15	1.6	0.34	0.14	0.12	0.74
MnO	0.57	0.13	0.42	0.71	0.9	0.5	0.26	2.11	1.3	0.5	0.5	2.7
Na_2O	0.17	0.08	0.09	0.27	0.09	0.05	0.01	0.2	0.02	0.02	0.01	0.08
Nb_2O_5	2.0	0.8	1.57	3.21	1.5	0.8	0.231	3.02	3.0	1.3	0.62	7.57
P_2O_5	9	5	4.85	15.35	12	5	2.54	21.5	2.7	1.4	1.01	7.74
S	1.9	0.9	0.76	2.91	2.7	1.8	0.29	6.65	2.8	1.8	0.14	6.8
SiO_2	8.6	4.2	6.15	14.85	4	3	0.59	11.6	4	4	0.64	17.3
SrO	1.02	0.32	0.56	1.26	1.1	0.4	0.57	2.23	0.27	0.15	0.05	0.66
TiO_2	2.3	0.5	1.81	2.89	3	3	0.36	12.65	3.2	1.3	0.58	7.82
Σ(total)	97.6	1.7	96.2	99.43	96	2	89.13	99.22	94	5	80.8	101.49

Resultados e discussão

Table 3 (cont.)

LA-ICPMS (ppm)	Ocher ore + rock (n = 4)				Brown ore (n = 20)				Orange ore (n = 43)			
	Mean	SD	Min	Max	Mean	SD	Min	Max	Mean	SD	Min	Max
Ag			<0.5	1.6			<0.5	4.4			<0.5	2.7
As	7.1	1.7	5.1	9.2	18	22	3.8	106.5	8	6	1.2	25.9
Bi	6	4	0.58	11.3	2.2	2.4	0.31	9.16	7	12	0.08	46
Cd			<0.5	2.0			<0.5	3.3			<0.5	1.0
Co	85	39	44	127	110	100	44	497	198	95	76	508
Cr	140	117	40	310	151	150	10	590	92	57	30	270
Cs	1.0	0.5	0.36	1.46	0.18	0.15	0.08	0.75	0.3	0.3	0.06	1.43
Cu	56	37	29	111	42	41	6.0	183	77	52	12	214
Ga	24	10	18.3	39.8	27	17	7.3	91.2	55	36	19.4	189.5
Ge			<5	6.0			<5	11			<5	22
Hf	29	18	16.30	53.7	20	13	7.0	60.4	31	18	7.6	103.5
Hg	0.010	0.004	0.01	0.01	0.02	0.01	0.01	0.05	0.02	0.02	0.007	0.087
In	0.32	0.17	0.17	0.56	0.5	0.3	0.14	1.17	1.0	1.3	0.141	6.21
Li	40	22	10	60			<10	30			<10	10
Mo	3.8	1.3	2.0	5.0	11	12	4.0	58	10	7	3	39
Ni	82	38	51	135	135	81	37	322	67	32	25	119
Pb	483	281	105	773	366	304	81	1,250	1,408	2,082	38	9,190
Rb	24	10	14.6	34.6	2.0	1.6	0.4	5.2	0.49	0.20	0.20	1.00
Re	0.005	0.004	0.002	0.01	0.005	0.001	0.002	0.008	0.006	0.002	0.003	0.01
Sb	1.0	0.3	0.70	1.36	2	3	0.41	12.35	1.0	0.7	0.31	3.48
Sc	18	8	6.0	25	34	20	9	84	32	14	11	64
Se			<0.2	0.30			<0.2	1.8			<0.2	0.5
Sn	35	9	27	48	40	25	12	121	56	21	13	105
Sr			4,350	>10,000			4,340	>10,000	2,412	1,167	829	5,730
Ta	42	43	5.2	102	42	67	1.1	305	52	54	2.6	283
Te	0.21	0.13	0.09	0.36	0.14	0.12	0.04	0.54	0.3	0.4	0.02	1.55
Th			752.00	>10,000			151	>10,000			288	>1,000
Tl	1.1	0.5	0.54	1.67	4	5	0.51	22.8	1.8	1.8	0.33	9.35
U	168	117	35.1	294	113	162	17.25	597	123	89	18.55	341
V	317	85	244	436	333	150	129	594	529	184	128	989
W	195	358	12	732	25	40	3	189	25	12	7.0	77
Y	140	40	94	189	174	59	69.4	297	255	142	93.7	845
Zn	458	200	289	747	789	345	398	1,700	947	573	310	2,600
Zr	1,308	964	584	2,690	840	644	282	3,110	1,304	913	261	5,110

Resultados e discussão

Table 3 (cont.)

LA-ICPMS (ppm)	Ocher ore + rock (n = 4)				Brown ore (n = 20)				Orange ore (n = 43)			
	Mean	SD	Min	Max	Mean	SD	Min	Max	Mean	SD	Min	Max
La	2,245	1,340	940	4,120	3,051	3,448	913	16,500	9,509	9,003	1,630	39,700
Ce	4,760	2,478	2,350	8,220	5,899	5,629	1,765	27,400	16,240	14,224	4,030	71,300
Pr	506	248	268	855	584	443	181	2,200	1,362	1,080	396	5,700
Nd	1,697	736	948	2,710	1,982	1,342	609	6,660	4,424	3,104	1,315	17,000
Sm	196	55	129.5	260	225	88	72.1	445	392	190	151	1,200
Eu	47	10	35.8	55.9	54	18	18.5	80.6	82	33	34.5	196.5
Gd	99.4	22.7	70.6	118.5	112	36	39.7	165.5	166	62	74.3	344
Tb	11.0	2.4	8.36	13.7	13	4	4.77	19.75	18	7	7.72	37.4
Dy	46	11	34	57.6	52	17	21	84.2	73	28	31.6	130.5
Ho	6.3	1.6	4.62	8.25	7.4	2.5	3.04	12.4	10	5	4.27	25.6
Er	12.5	3.2	8.81	16.5	15	5	6.09	25.7	21	10	8.14	54.5
Tm	1.2	0.3	0.87	1.66	1.6	0.5	0.7	2.63	2.1	1.1	0.84	6.04
Yb	6.0	1.6	4.32	8.11	7.8	2.7	4.17	12.8	10	6	3.66	31.2
Lu	0.8	0.2	0.6	1.13	1.1	0.4	0.55	1.92	1.4	0.8	0.51	4.66
Σ(REE)	9,635	4,884	4,803	16,433	12,004	10,928	3,703	53,518	32,311	27,509	7,943	135,679

Appendix 3 shows the mineral compositions of these 73 samples, as determined by SEM and XRD. In the three ore types, Nb occurred as crystallized hydroxycalciopyrochlore, as determined by SEM and XRD (Issa Filho et al., 2011). Hydrokenopyrochlore, identified by Miyawaki et al. (2021), occurred in the brown and orange ores (Appendix 3). Fluorcalciopyrochlore was detected only in one sample of the ocher (AM-61) and orange (AM-137) ores. Phosphorus preferentially exists in fluorapatite, which occurred in the ocher and brown ores (Appendix 3); however, it was detected in one orange ore sample (AM-67) near the contact with the brown ore. Gorceixite was detected in the orange and brown ores. Exceptionally, gorceixite, along with goyazite, rutile, kaolinite, gibbsite, hematite, and goethite, also occurred in the clayey soil and sediments that cover the orange ore.

In alkaline rocks, norsethite, detected in sample AM-61, was the main Ba mineral (Issa Filho et al., 2011). However, among the three ore types that formed in the center of the Complex, barite was the main Ba host. LREEs occurred alongside P in monazite. Monazite and goyazite generally occurred only in the orange ore and were detected in only one brown ore sample (AM-120). Monazite occurred in the brown and ocher (Appendix 3) ores only in drill hole F-0XM9 (Fig. 1). Iron occurred in all three ore types, crystallized as magnetite, hematite, and predominantly goethite. Ilmenite and anatase were rare, occurring in the orange ore and on top of the brown ore, but only in samples from drill-hole F-5XIJ3. Dolomite occurred in the ocher ore and rarely in the brown ore base. Quartz occurred in all of the ore types. Vermiculite was less common and occurred only in the ocher ore of the F-5XIJ3 hole.

Resultados e discussão

Additionally, the rocks, saprolite, and regoliths of the Complex remain locally bathed by S-rich water, which contains 420 mg/L SO_4^{2-}, 0.12 mg/L Ba^{2+} and 3,400 mg/L HCO_3^- (Raposo, 2011).

Main chemical characteristics of saprolitic and regolithic ores

Figure 7A shows that there is a direct correlation between the Nb_2O_5 and Fe_2O_3 contents of the three ore types. In the ocher ore, Nb_2O_5 generally varies between 0 and 3.0%, whereas Fe_2O_3 varied between 3 and 30% (Fig. 7A). In the brown ore, the Nb_2O_5 contents varied from 0 to 4.0% and Fe_2O_3 ranged from 3 to 40%. In the orange ore and clayey sediments, the Nb_2O_5 contents varied from 0 to 7.0% while Fe_2O_3 varied between 0 and 60%.
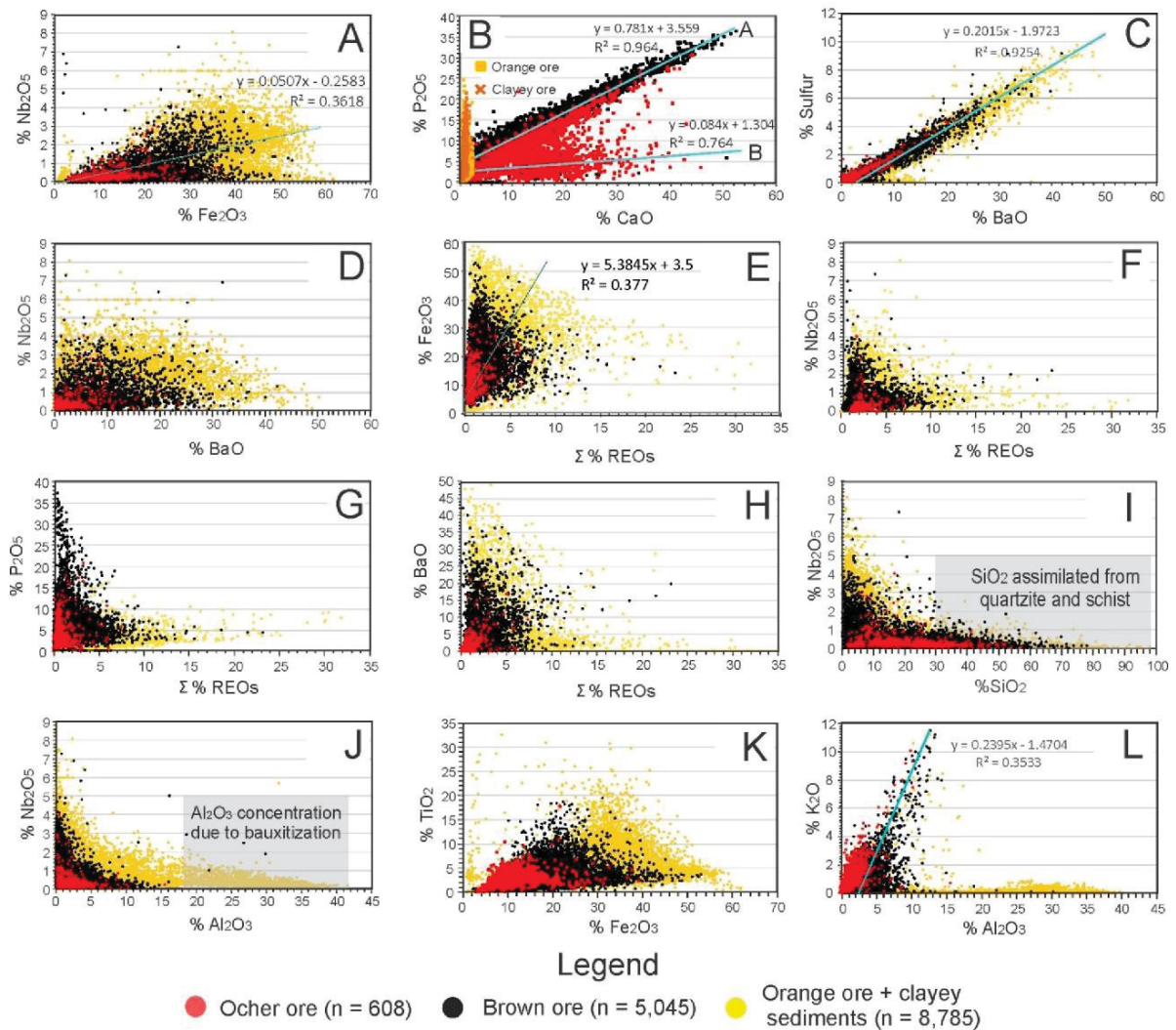
Fig. 7 - Main chemical characteristics of the ocher, brown, and orange ores from the Araxá orebodies: (A) Fe_2O_3 vs. Nb_2O_5, (B) CaO vs. P_2O_5, (C) BaO vs. S, (D) BaO vs. Nb_2O_5, (E) ΣREOs vs. Fe_2O_3, (F) ΣREOs vs. Nb_2O_5, (G) ΣREOs vs. P_2O_5, (H) ΣREOs vs. BaO, (I) SiO_2 vs. Nb_2O_5, (J) Al_2O_3 vs. Nb_2O_5, (K) Fe2O3 vs. TiO_2, and (L) Al_2O_3 vs. K_2O.

Figure 7B shows the correlation, with an R^2 of 0.96, between CaO and P_2O_5 in the ocher and brown ores, reflecting the stoichiometric proportions of this substance in apatite. This type of correlation did not exist in the orange ore and clayey sediments.

There is another mode that correlates (R^2 = 0.76) CaO with lower P_2O_5 contents. The highest P_2O_5 contents in the ocher ore were approximately 27% (Fig. 7B) while the P_2O_5 contents of this ore were confused with those of the brown ore when < 22%. The P_2O_5 contents of the brown ore were the highest, reaching 36%, and this type of ore was predominant, presenting the best quality. The P_2O_5 mineral in the brown and ocher ores was fluorapatite (Appendix 3). This mineral did not exist in the orange regolith owing to a lack of CaO. The P_2O_5 content in the orange ore, lateritic soil, and clayey sediments was between 0 and 24%; the same substance was present in the gorceixite, monazite, and goyazite (Appendix 3). Mineralized saprolites, with P_2O_5 contents < 5%, identified by line B in figure 7B, occurred adjacent to the rocky substrate and constitute the ocher saprolite. Ocher ore outcrops occur in the Mosaic pit and was described as micaceous weathered ore and saprolite in Graço (2015). In this pit most of the brown and orange regoliths have been mined. Outside the Mosaic pit, brown ore is observed in pit F4 (Fig. 1) and its vicinity. Outside of the Mosaic and F4 pits, as well as the ITAFOS deposits, carbonatite is not mineralized with P_2O_5. In these regions, weathered rock and saprolite dominate, with P_2O_5 contents of < 5%.

Reflecting the stoichiometric proportions of barite, Fig. 7C shows that the BaO content is linearly and directly proportional to the presence of S in the ocher, brown, and orange ores (R^2 = 0.92), formed at the Complex nucleus because barite is the main Ba ore mineral in the three ore types (Appendix 3). In the ocher ore, the BaO contents ranged from 0 to ~25% (fig. 7C) while those of S varied from 0 to 5%. In the brown ore, the BaO content varied from 0 to 35% and S from 0 to 8%. However, in the orange ore, BaO varied from 0 to 48% and S ranged from 0 to 10%. There was no correlation between the BaO and Nb_2O_5 content (Fig. 7D).

The REOs had poor correlations with Fe_2O_3 (Fig. 7E); the REOs and Fe_2O_3 concentrations increased from the ocher to the orange ore. The REO and Nb_2O_5 concentrations increased from the ocher to orange ore, where the REO content exceeded 15% and the Nb_2O_5 content reached 6.0% (Fig. 7F). Overall, the REO concentrations were inversely proportional to those of P_2O_5 (Fig. 7G) and BaO (Fig. 7H). Previous studies on the CBMM by the LCT–USP (Laboratory of Technological Characterization of the University of São Paulo) (LCT-USP, 2016) reported that REOs occur in monazite and rhabdophane in the brown and orange ores.

Figure 7I shows that regolith with Nb_2O_5 contain up to 90% SiO_2. It is noteworthy that the SiO_2 content increased from the ocher to orange ore; within the three types, there were samples with SiO_2 contents of more than 60%. Figure 7J shows that the orange ores could contain up to 42% Al_2O_3, but the contents in the brown and ocher ores were significantly lower, i.e., < 15%. The Fe_2O_3 and TiO_2 were weakly correlated in the three ore types (Fig. 7K); Al_2O_3 and K_2O were correlated in the ocher and brown ores, but not in the orange ores (Fig. 7L).

2.1.6 Discussion

Maps and sections of mineralized bodies

Variations in mineralized body compositions: Figures 6A-1 to A-3, compared with figures 6B-1 to B-3, 6D-1 to D-3, and 6E-1 to E-3 show that in the core of the Complex, in the ocher ore over phlogopitic breccia domain, Nb_2O_5, Fe, BaO, and S occupy coincident positions. As the intensity of weathering increases, rock-bearing Nb, BaO,

and S are partially weathered, but remain in or near the core while Fe_2O_3 is also partially destroyed and Fe is mobilized. The brown (Fig. 6B-2) and orange (Fig. 6B-3) ores gradually occupy larger areas constituting lateritic crusts. In the phlogopitic breccia, Fe occurs in magnetite and ilmenite, whereas in the brown and orange ores, adjacent to the core, Fe is also present in hematite, and goethite. Barite is the main Ba + S mineral, followed by gorceixite in significantly smaller amounts. Hydroxycalciopyrochlore and hydrokenopyrochlore represent the main mineral phase, accounting for the largest amount of Nb extractable from all ore types. The concentrations of pyrochlore and barite decrease with increased distance to the core and exist in low amounts on the carbonatite ring.

At the center of the Complex, the ocher ore contained no P (Fig. 6C-1), which was locally concentrated around the core. The highest concentrations were in the Mosaic area, in the F4 pit, and in the ITAFOS deposit (Figs. 1 and 6C-1 to C-3): areas where the P content exceeded 13%. Crystallized as fluorapatite, P was concentrated in these regions in the ocher and brown ores. Phosphorus is disseminated in the brown ore, with contents between 4.5 and 7.5%, throughout the region surrounding the core (Fig. 6C-2), always in fluorapatite, and, to a significantly less extent, in gorceixite or monazite.

Figure 6F-1 shows that there is no REEs in the ocher ore anywhere in the Complex. Apparently, when the supergenic monazite ± rhabdophane crystallized and formed the brown and orange ores, the REE concentration increased and the LREO contents reached values between 4.0 and 8.0% (Figs. 6F-2 and 6FD-3). We note that after this process occurred during the formation of the brown ore, the REO contents increased with an elevated weathering intensity. The result was that the REO contents were slightly higher in the orange ore, however the perimeter of the area containing the high REOs contents in the orange ore (Fig. 6F-3) practically did not change when compared with the brown ore REE mineralization perimeter (Fig. 6F-2).

Titanium, crystallized as anatase and ilmenite (Appendix 3), was concentrated only on the carbonatite ring to the south and southeast of the Complex (Fig. 6G-1 to 6G-3), where the contents locally exceeded 12%. This distribution was not clear: perhaps it was due to specific intrusions of anatase and/or ilmenite carbonatite that did not interact with any of the existing drill holes.

The high SiO_2, K_2O, and Al_2O_3 contents near the Complex host rocks (Figs. 6H-1 to H-3, 6 I-1 to I-3, and 6J-2 to J-3) were likely a consequence of the assimilation of muscovite-quartz schists and muscovite-chlorite schists from the Rio Verde Formation (Fig. 2B). Currently, SiO_2 and K_2O, which are easily mobilized by meteoric water, are concentrated differently in ores: SiO_2 occurs in all three ore types and occupies a wide band around the core of the Complex, whereas K_2O, which is more mobile than SiO_2, leaves the weathering system when weathering reaches its maximum value and forms orange ore (Fig. 6 I-3). Furthermore, Al_2O_3 is practically immobile, which is why it is concentrated, reaching contents greater than 14% (Fig. 6J-3) only in the orange ore on the edge of the Complex, likely not far from the original location of assimilation.

Maps of ore body top surfaces: The compilation of the information contained in the maps on the distribution of substances according to the block model of the deposits (Figs. 6A-1 to J-3) allowed for the construction of maps of the top surfaces of the ore bodies (Figs. 8A–C). Most of the brown and orange ore in the Mosaic area had already been mined when Grasso (2015) was published. In the maps, the clayey sediment and

soil cover that lie on the orange orebody (Fig. 11A) were not positioned. In the nucleus, the ocher ore (Fig. 8A) contained Nb_2O_5 + P_2O_5 + $BaSO_4$ + Fe_3O_4, with Nb_2O_5 contents between 1.2 and 4.0%. Around the ocher, encompassing part of the core and extending over the carbonatites, is the ocher ore with P_2O_5 contents between 3.0 and 15.0% and average Nb_2O_5 of 1.0% (closest to the core) and 0.3% (over the carbonatites). In the Mosaic and F4 pits and their vicinity, also in small bodies mineralized in a random distribution over the carbonatites, the P_2O_5 contents in the ocher ore were higher, i.e., between 5.0 and 28.0%. The ITAFOS deposit contains ocher ore with P_2O_5 contents between 0.0 and 28.0% (Mean = 11.0%), REOs between 0.0 and 10.0% (Mean = 2.6%), and Nb_2O_5 contents between 1.2 and 4.0% (Mean = 1.98%). These contents would be a consequence of the occurrence of phlogopitic breccia in the local rocky substrate that were likely not assimilated by the carbonatites that surround the core.

Resultados e discussão

Fig. 8 - Top surface maps of: (A) ocher, (B) brown, and (C) orange orebodies. In the eastern area of the Complex where the Mosaic pit is located, brown and orange ores occur; the extent of the areas covered by these mineralized bodies is not known.
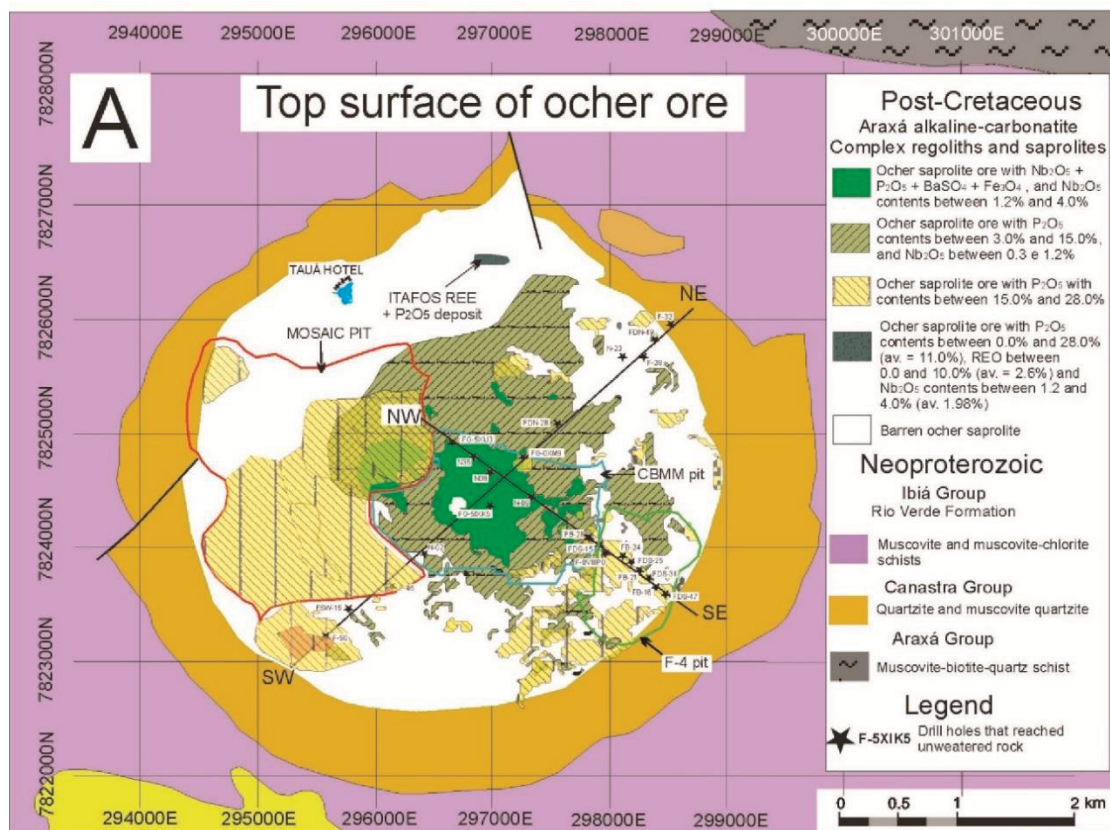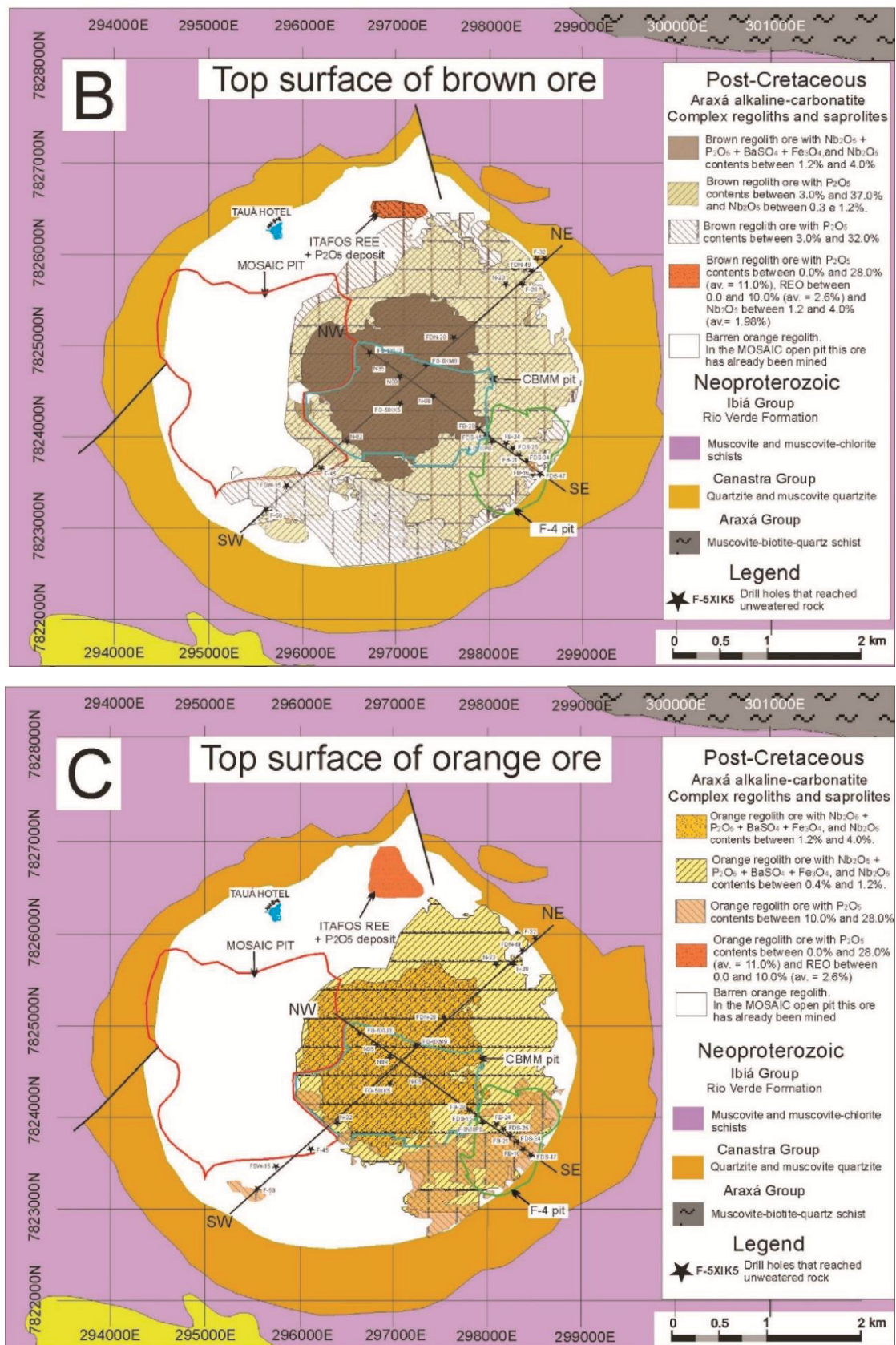
In the core, the orebodies with brown ore (Fig. 8B) contained Nb_2O_5 + P_2O_5 + $BaSO_4$ + Fe_3O_4, with Nb_2O_5 contents between 1.2 and 4.0% (Mean = 1.7%). On the carbonatites, involving the core and close to its adjacent areas, brown ore had a P_2O_5 content of 3.0 to 37.0%. P_2O_5 occurs, with predominate contents under 10%. In this ore body, the P_2O_5 content of the brown ore varied from 3.0 to 32.0%, mainly under 5.0%. In the ITAFOS deposit, brown regolith ore occurred, characterized by P_2O_5, REOs, and Nb_2O_5 mineralization (Clay and Ackroyd, 2012).

The orange ore located within the nucleus was found to comprise of Nb_2O_5, P_2O_5, $BaSO_4$, and Fe_3O_4, with the presence of Nb_2O_5 ranging between 1.2% and 4.0%, a similarity to the brown ore (Fig. 8C). An adjacent body of orange ore was also identified, exhibiting similar mineral composition, however, with reduced Nb_2O_5 content, ranging between 0.4% and 1.2%. The P_2O_5 content of the orange regolith was observed to be less abundant, with values ranging between 0.5% and 28.0%, in comparison to the brown regolith. It should be noted that the absence of identified minerals containing P_2O_5 in this region is likely due to the fact that they may exist in an amorphous form, rendering them undetectable through X-ray diffraction (XRD) analysis. Gorceixite, though present in small quantities, could not be considered as the source of the P_2O_5 content between 10% and 28%, (Fig. 8C), which was analyzed in this ore.

Areas occupied by the mineralized bodies containing Nb_2O_5 + P_2O_5 + $BaSO_4$ + Fe_3O_4 increased from the ocher to orange ores (Figs. 8A–C). Thus, the halo of the orange ore, enriched in Nb_2O_5 + P_2O_5 + $BaSO_4$ + Fe_3O_4, surrounding the core (Fig. 8C) did not reflect the carbonatitic composition of the rocky substrate. This halo formed via lateral and radial dispersion of the orange ore in the Complex nucleus with weathering intensification. This halo contained the same elements as the core; the only difference was the low ore mineral content. This is similar to the outermost rim of the brown ore, which had a lower P_2O_5 content than the inner rim (Fig. 8B). The lower P_2O_5 contents in the orange ore were a consequence of apatite destruction owing to weathering (leaching of CaO) and caused the crystallization of gorceixite and REE-phosphates.

Geological sections: Figures 9A–E show the SW–NE sections while figures 9F–J shows the NW–SE, whose traces are on the maps in figures 1 and 8. These sections were constructed on maps derived from the block models (Figs. 6A-1 to J-3); figures. 5G – J shows the boundaries of the mineralized bodies.

Resultados e discussão
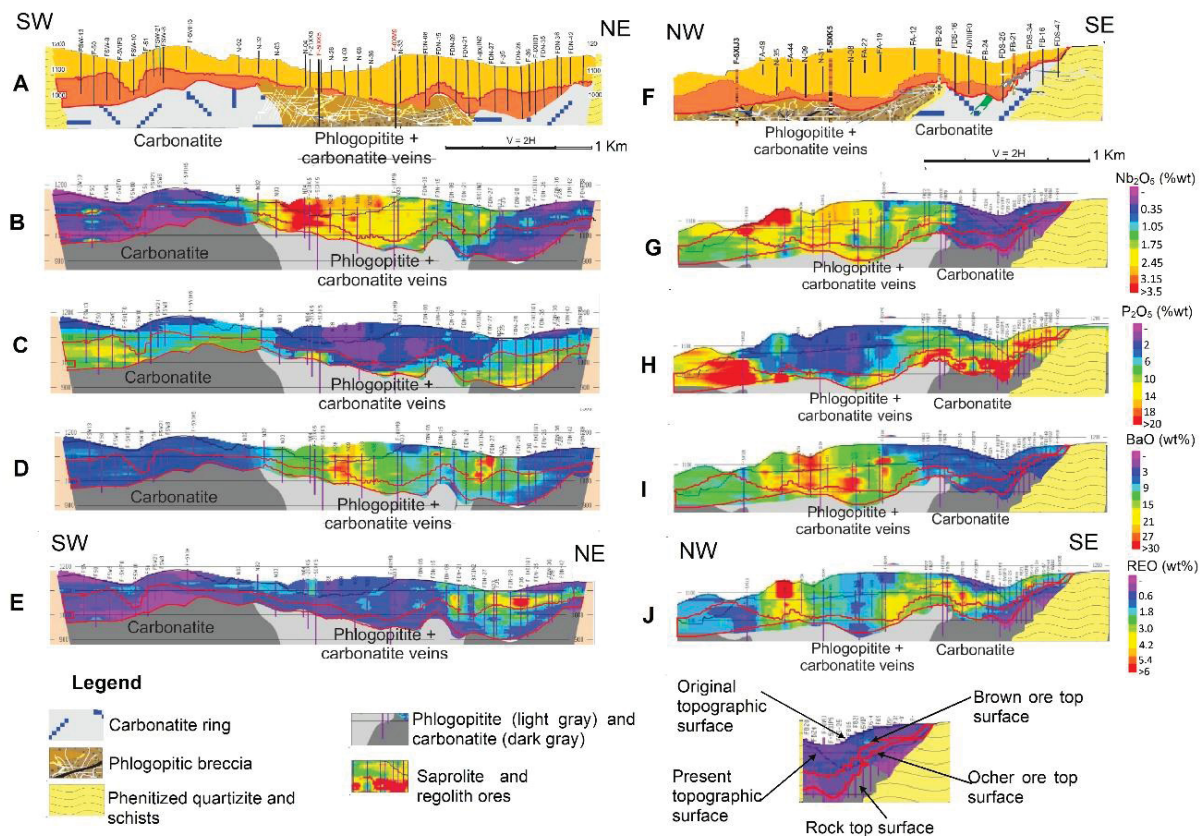
Fig. 9 - Cross-sectional representations of the boundaries of the mineralized bodies on the bedrock are presented in Figs. 9A and 9F, respectively depicting the SW-NE and NW-SE sections. The chemical analysis of the ores is performed along the cross-sectional lines designated on the maps in Figs 8A-C, and the results are displayed in Figs Fig. 9B-E and 9G-J. The distributions of Nb_2O_5, P_2O_5, BaO, and REOs are depicted in the ocher, brown, and orange ores along the SW-NE axis and similarly along the NW-SE axis.

Figure 9A (SW–NE section) and F (NW–SE section) are sections that show the bedrock of the ocher, brown, and orange ore bodies. The other figures show the distribution of the main substances that constitute the ore bodies.

Sections 9B + 9G and 9D + 9I show that Nb_2O_5 and BaO occur over the phlogopitic breccia, although the edges mineralized with Nb_2O_5 and BaO in the orange ore advanced over the carbonatites (NE in Figs. 8B + 8C and 9B + 9D). Ores with P_2O_5 contents > 3% occurred on phlogopitic breccia (Figs. 8A–C) and carbonatites (Figs. 8C - H), but regolith with P_2O_5 contents greater than 15% can occur only on carbonatites (Figs. 8B-C and 9C + 9H). High REO contents occurred in the ocher, brown, and orange ores formed on carbonatites and in the ITAFOS deposit (Figs. 8A–C and 9E +9J), as well as on the phlogopitic breccia (Fig. 9J). Notice that the highest Nb_2O_5 and BaO contents were in the orange ore (Figs. 9B + 9G and 9D + 9I, respectively); the highest P_2O_5 contents were observed in the brown ore (Fig. 9C, H).

In the geological sections (Fig. 9), pyrochlore was more concentrated in the phlogopitic breccia, simultaneously forming brown and orange ores with Nb_2O_5 contents above 3.0% (Fig. 9B), or only in the orange ore (Fig. 9G). Simultaneous concentrations likely occurred when the rocky substrate (phlogopitic breccia and magnetite apatitite) was rich in Nb. Niobium concentrations above 3% only occurred in the orange ore, which could be a consequence of the residual concentration, i.e.,

progressing from the top (surface) of the orange ore to the rocky substrate. This is why the pyrochlore concentration is higher near the surface. The process of lateral and radial dispersion, which occurs simultaneously with weathering, can explain the sections with ores containing Nb_2O_5 (Figs. 9B, G) and BaO (Figs. 9D, I) formed in the core also occur in the orange ore found on carbonatites (NE of Figs. 9B and 9D). This Nb mineralization above the carbonatite ring were likely displaced from the nucleus region.

Furthermore, P_2O_5 was concentrated in the brown ore on phlogopitic breccia and carbonatites (Fig. 9C), where the P_2O_5 content varied between 0.0 and 42.0% (Mean = 17.5%), or simultaneously in the brown and orange ores (Fig. 9H), with P_2O_5 contents above 18%. Phosphate was selectively concentrated in the Mosaic (Fig. 8A) (Grasso, 2015) and F4 pits (Figs. 6C-1 to C-3 and 9C) and in the ITAFOS deposit (Fig. 8A to 8C). With the exception of the ITAFOS area, the best explanation for this selective distribution is that the outer carbonatite ring is composed of distinct carbonatite intrusions, with or without apatite, which led to the formation of mineralized sites, presenting a gradient of grades and non-mineralized sites.

Barium contents greater than 27%, occurred in the brown and orange ores formed on the Complex core (Figs. 6D-1 to D-3 and 9D, I). Figure 9D shows a strong concentration of barite in the orange ore in the transition between substrates (phlogopitic breccia and carbonatites), in which the contents were also higher than 27% BaO. The barite, despite being an authigenic mineral, must be the product of the residual concentration that occurred from top to bottom, similar to the Nb concentration (Fig. 9G). In this case, as the barite was residually concentrated, the orange ore spread laterally and radially, carrying the barite, which would have originally been above the core zone, to the outer zones. In the orange ore, REOs had higher contents, i.e., above 5.0% (Figs. 9E, J); however, below these locations, the brown ore always presented REOs at lower concentrations, i.e., between 2.0 and 4.0%. The REO concentrations occur indistinctly in ores on carbonatite (Fig. 9E and ITAFOS deposits), phlogopitic breccia (Fig. 9J), and in the transition from phlogopitic breccia to carbonatite zones (Fig. 9J). This behavior suggests that the original REO concentrations did not depend on the original or unaltered underlying rocks. This could be a consequence of a late, possibly hydrothermal, process, which indistinctly covered the core and carbonatite zones.

Characteristics of saprolites and regoliths containing Nb, P, Ba, REE, and Fe + Ti

The Fe_2O_3 and Nb_2O_5 contents were positively correlated (Fig. 7A), which suggests that, in the substrate rock of the Complex core (Figs. 6A-1 and B-1), pyrochlore and magnetite crystallized simultaneously as a result of the same mineralization process. There was no proportionality between the Nb_2O_5 and BaO contents (Fig. 7D); therefore, pyrochlore and barite are minerals of different paragenesis. We note that barite and pyrochlore exist mainly in the core of the Complex. As the barite paragenesis differs from that of pyrochlore, the rock it generates differs from that from which pyrochlore was derived. Therefore, in the core domain, the Nb_2O_5 and BaO contents increased from ocher to orange ore as weathering intensity increased.

Sulfur and BaO had a good correlation, reflecting the stoichiometric proportions of Ba and S in barite (Fig. 7C). The existence of a single population indicated that barite

is the only mineral containing Ba and S in the ores. Unlike apatite (Fig. 7B), figure 7C shows that the correlation between Ba and S in the nucleus of the Complex also exists in the orange ore, implying that barite was not destroyed when weathering reached its highest intensity. The BaO and Nb_2O_5 contents (Fig. 7D) gradually increased from the ocher to the orange ore. This increase, having no proportionality, was only due to an increase in the residual concentration of pyrochlore and barite, following an increase in the weathering intensity of different rocks.

The simultaneous increase in the Nb_2O_5 + Fe_2O_3 + BaO contents with the REOs (Figs. 7E, F, H) suggests that the concentrations of pyrochlore, magnetite, barite, and minerals with REEs increased simultaneously. Pyrochlore and magnetite were likely residually concentrated while minerals with REEs, mainly monazite, crystallized during the weathering process. Crystallization of minerals with REEs may explain the inverse relationships between the REO concentrations and P_2O_5 (Fig. 7G), indicating that most of the REOs in the ores are not in pyrochlore, apatite, or gorceixite, but crystallized in monazite, rhabdophane, or florencite during brown and orange ore formation.

Contrary to that reported above, when examining the presence of REOs in weathered rocks and soils from the Araxá Complex, Mariano and Mariano Jr. (2012) observed that most REO resources occur in the weathering products of carbonatites and laterites, where REOs are products of carbonate and apatite destruction. According to that study, REOs may recrystallize as monazite, rhabdophane, gorceixite, goyazite, florencite, and churchite, inextricably associated with iron oxides, forming secondary REO concentrations with high contents, as observed in the orange ore. In their review on the presence of REE-rich monazite in carbonatite-related REE deposits, Chen et al. (2017) observed that most monazite related to carbonatites is a product of alteration or weathering, almost always occurring in association with apatite, as observed by Oliveira and Imbernon (1998) in Catalão, and by Santos et al. (2018) in Floresta Azul. Monazite partially or completely replaces apatite, generating a replacement halo, whose thickness and REO content depend only on the availability of REEs. In Araxá, the presence of monazite, and absence of apatite in the orange ore, presence of apatite, and absence of monazite in the brown and ocher ores (Appendix 3) suggest that monazite and rhabdophane crystallized owing to the destruction of apatite by weathering, thus inheriting the REEs within the apatite. The monazite observed in the orange ore from the Complex core occurs in microcrystalline aggregates and is easily recognized in the orange ore due to its greenish color (Figs. 11B, C). In some locations, such as in the F-0XM9 drill hole (Fig. 1 and Appendix 3), monazite occurs in the brown and ocher ores.

Toledo et al. (2004) showed the effects of weathering and recrystallization processes involving Catalão apatite, which generate secondary apatite, likely with low REE contents, together with monazite, rhabdophane, and florencite, with high and varied REO contents.

The tendency for a decrease in the Nb_2O_5 content, following an increase in the Al_2O_3 content (Fig. 7J), suggests that the soil formed via the weathering of the orange ore, destroying most of the pyrochlore and concentrated Al_2O_3. The weathering that formed the orange ore followed the destruction of part of the pyrochlore and Nb dispersion, which likely adsorbed on goethite. Locally, soil bauxitization occurs, where alumina and silica are concentrated, while magnetite is leached and/or transformed into goethite, which also adsorbs Nb. Figure 7J shows Al_2O_3 contents greater than 40%, figure 7I shows SiO_2 contents up to 80%, and figure 7L shows K_2O contents up

Resultados e discussão

to 14%. The regolithic ore with SiO₂ contents greater than 30%, formed on the phlogopitic breccia (10% when formed on carbonatites, as well as more than 5% on both bedrocks) must be a consequence of the assimilation of regional schists and quartzites that occurred when the alkaline rocks became lodged and formed the alkaline-carbonatitic Complex. Likewise, ores with Al₂O₃ contents higher than 18%, normal for phlogopitic breccia, must be a consequence of bauxitization and not of assimilation because the ocher and brown ores had Al₂O₃ contents lower than 18%.

Weathering evolution and weathering lines

Figures 10A, C, E, G, I show the evolution of the weathering (weathering lines) that generated ores on the phlogopitic breccia, whose original SiO₂ contents varied between 10 and 40% (Appendix 1, Fig. 7I). Figure 10B, D, F, H, J shows the evolution of carbonatite weathering, with SiO₂ contents of less than 10% (Fig. 7I) and CaO + MgO greater than 30%.

Resultados e discussão

Ores from phlogopitic breccia domain

Ores from carbonatite ring domain
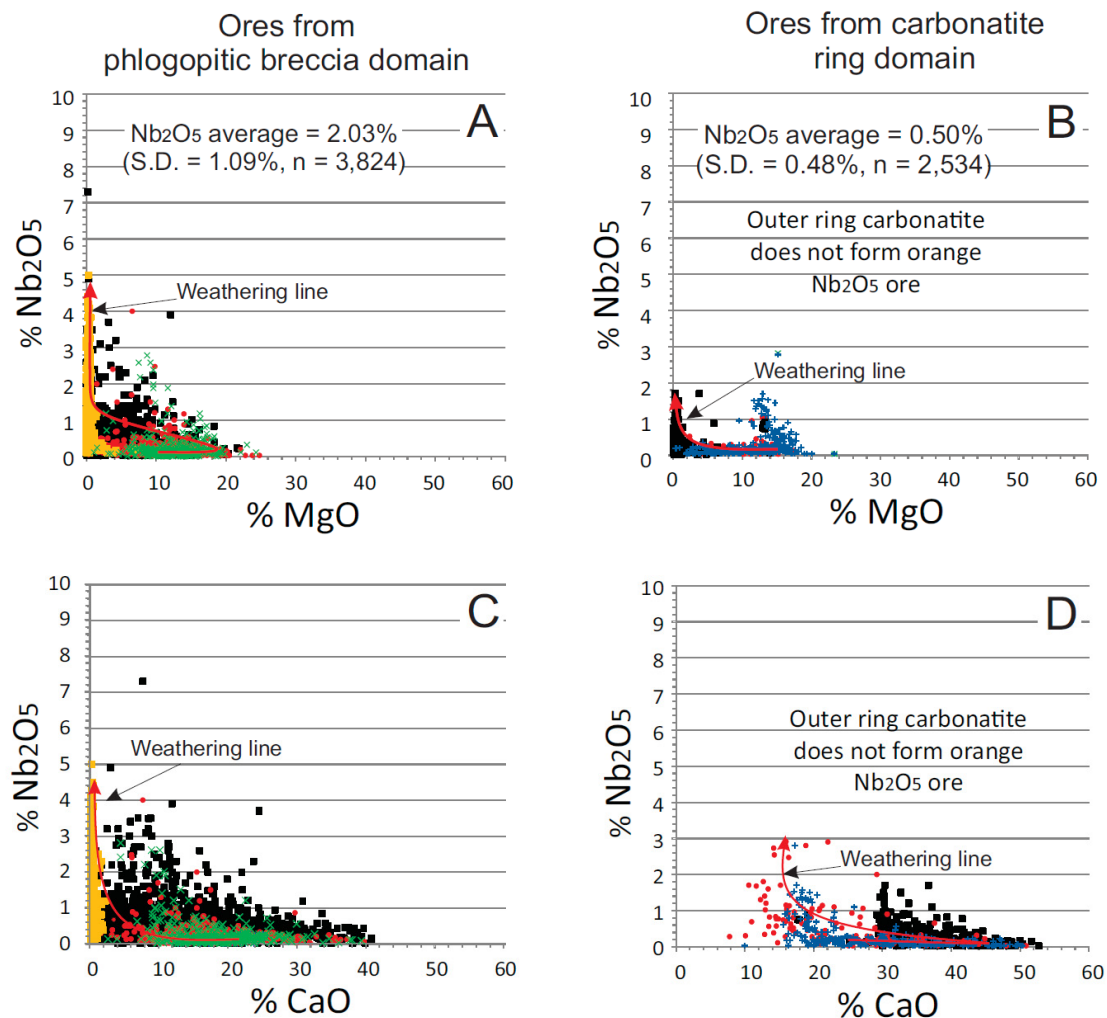
Resultados e discussão
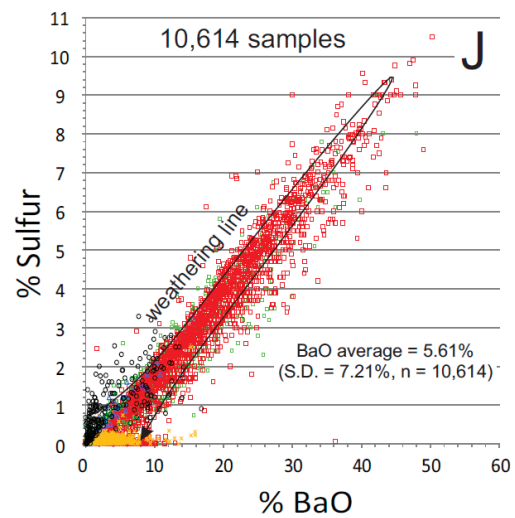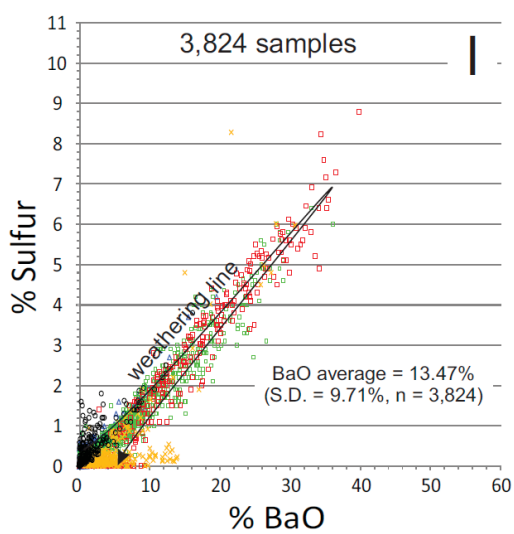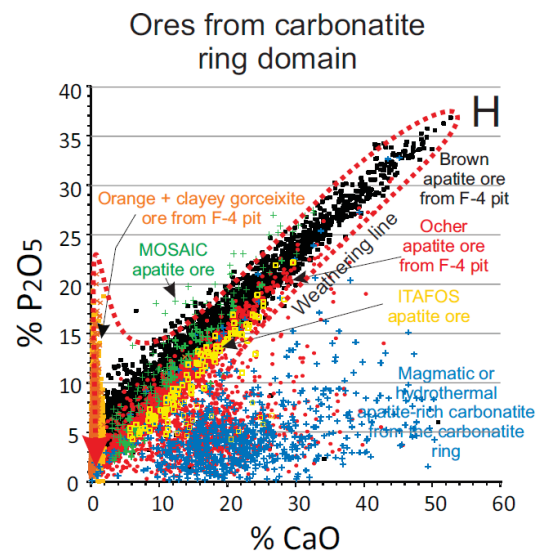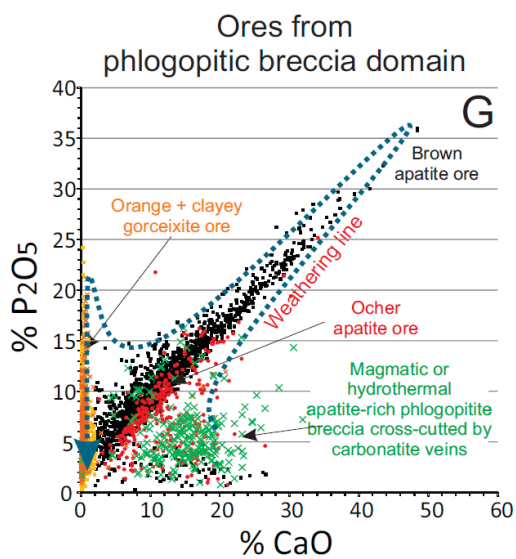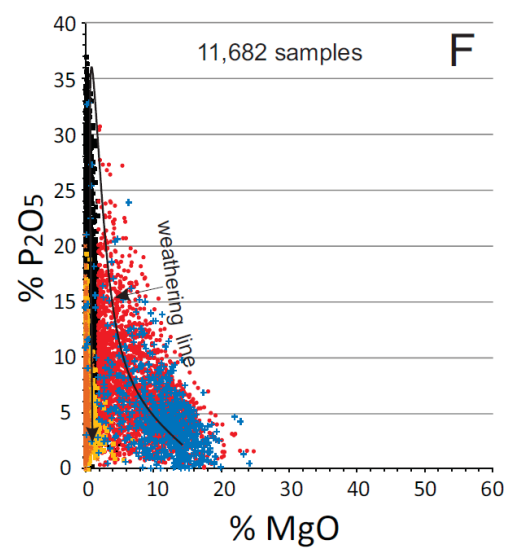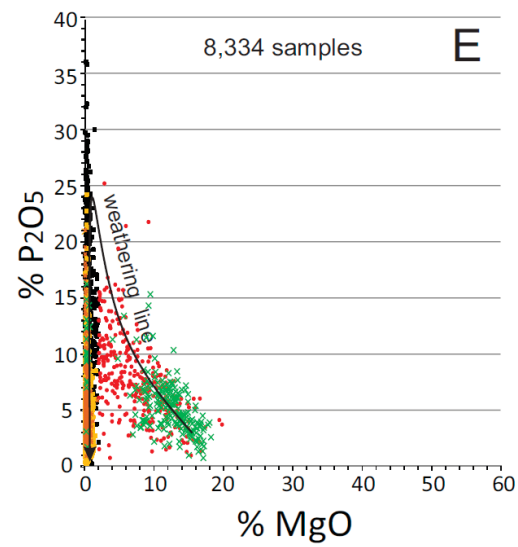
Legend

■ Nb₂O₅ and P₂O₅ brown ore

● Nb₂O₅ and P₂O₅ ocher ore

■ Nb₂O₅ and P₂O₅ orange ore

✳ Clayey soil

＋ Brown P₂O₅ ore and regolith from MOSAIC pit

▫ Brown P₂O₅ ore and regolith from ITAFOS deposit

✕ Phlogopitite breccia cross-cuted by carbonatite veins

＋ Carbonatite from the external ring

○ Norsethite [BaMg(CO₃)₂] mineralized rock

△ BaSO₄ ocher ore and saprolite

▫ BaSO₄ brown ore and regolith

▫ BaSO₄ orange ore and regolith

✕ BaSO₄ clayey ore and soil

Fig. 10 - Lines of evolution of weathering and the genesis of the Araxá ores. On the left side: evolution of weathering for the ores formed in the core of the Complex, where phlogopitic breccia and magnetite apatitites containing SiO_2 between 10 and 40%. (A) CaO vs. Nb_2O_5, (B) CaO vs. Nb_2O_5, (E) MgO vs. P_2O_5, (G) CaO vs. P_2O_5, and (I) BaO vs. S. On the right side: evolution of weathering of ores formed on carbonatites, characterized by SiO_2 contents lower than 10% and CaO + MgO contents greater than 30%. (B) MgO vs. Nb_2O_5, (D) CaO vs. Nb_2O_5, (F) MgO vs. P_2O_5, (H) CaO vs. P_2O_5 and (J) BaO vs. S.

As shown in figures 3M–P, rock oxidation can form an ocher ore. Brown ore forms when MgO is removed from the ocher ore; orange ore forms when CaO is removed from the brown ore. The concentrations of pyrochlore and magnetite (not shown in the figures) on the phlogopitic breccia are simply caused by the removal of MgO followed by CaO (red arrows in Figs. 10A, C), which increases the Nb_2O_5 concentration from less than 1.0% in the rock to up to 5% (Mean = 2.03% Nb_2O_5, n = 3,842 and SD = 1.09) in the orange ore. The formation of orange ore causes an even greater pyrochlore concentration, which is only destroyed in the last stage of weathering; part of the Nb migrates to goethite, such that there is a decrease in the Nb content of the orange ore. In locations where phosphate is mined from weathered carbonatites, Nb_2O_5 orange ore do not form; the Nb_2O_5 average content in this region was 0.50% (n = 2,540 and SD = 0.48%) (Figs. 10B, D).

Figures 10G–H show how weathering evolved to form P_2O_5 ores. Unlike the results for Nb_2O_5 (comparing the trajectories of the weathering lines in figures 10A to 10D with those in figures 10E–H), MgO was rapidly leached from both the phlogopitic breccia (Fig. 10E) and carbonatites (Fig. 10F), concentrating residual apatite and increasing the P_2O_5 content of approximately 5% in the rock (1.0–15%) to over 25% in the ocher ore and over 35% in the brown ore. The removal of CaO then destroyed the apatite in the brown ore, reducing the P_2O_5 content to less than 2.0% (between 0.0 and 24.0%) in the orange ore on both the phlogopitic breccia and carbonatites (Figs. 3N + 3P and 10F + 10H). A small part of the P_2O_5 in the orange ore was in gorceixite, but the minerals   that contained most of the P in the orange ore were likely the REE-phosphates. Apart from the presence of magnetite apatitites, associated with the phlogopitic breccia, P_2O_5 contents of up to 30% in the brown ore over the phlogopitic breccia and up to 22% in the orange ore indicate that the phlogopitic breccia is cut by carbonatite veins with P_2O_5, such as those that form the Mosaic and the F4 deposits.

The linear and direct correlation between BaO and S was maintained both for the ore formed in the core (Fig. 10I) and on the carbonatite in the outer ring (Fig. 10J); however, the general average content was higher in the core (BaO = 13.47%) than that in the outer ring (BaO = 5.61%). More barium in the rocky substrate of the core,

where there is less carbonatite than in the outer ring, can be explained by the presence of Ba carbonate in the core, forming norsethite carbonatite (Appendix 3; ocher ore from the F-5XIJ3 drill hole).

The process of weathering, which leads to the concentration of barite, starts with the release of barium (Ba) from norsethite in Ba-rich carbonatites (Figs. 10I, J). During this stage of weathering, the formation of ocher ore containing barite is negligible. In both the core of the Complex (Fig. 10I) and the carbonatitic ring (Fig. 10J), following the release of Ba from norsethite, Ba becomes attached to sulfur (S) and crystallizes into barite, which is residually concentrated in the brown and orange ores, yet is destroyed during soil formation (Figs. 10I, J). This is likely due to the outcropping location of the norsethite-bearing rocks during weathering, as barite was not found to be concentrated in the clay-rich sediments.

Crystallization of fluorapatite vs. gorceixite, monazite, and rhabdophane: To understand the apatite, gorceixite, monazite, and rhabdophane distributions in the ores, we calculated the number of moles of P and Ca that could crystallize as apatite, considering that each mole of apatite $[(Ca_5(PO_4)_3(Cl, F, OH)]$ contains 3 moles of P and 5 moles of Ca. The average Ca and P contents of the ocher, brown, and orange ores, as listed in Table 4, were used.

Table 4 - Crystallization of apatite and/or gorceixite, monazite, and rhabdophane based on the average Ca and P contents of the Araxá ores.

Ore type	#sample	Phosphorous (P)		Calcium (Ca)		Apatite molar ratio (*)	Mineral that may crystallize
		Mean (wt%)	#moles	Mean (wt%)	#moles	$\dfrac{\text{\#moles (Ca)/5}}{\text{\#moles (P)/3}}$	
Ocher ore	4	4.1	0.132	9.4	0.235	1.071	Apatite and Carbonate
Brown ore	20	5.2	0.169	9.7	0.241	0.855	Apatite, Al-phosphate and REE-phosphate
Orange ore	43	2.2	0.071	0.2	0.004	0.032	Al-phosphate and REE-phosphate

(*) Considering the general formula of apatite: $Ca_5(PO_4)_3(OH,F,Cl)$

The molar ratios of Ca/P presented in Table 4 suggest that, following apatite + carbonate crystallization and residual concentration in the ocher ore, exhaustion of Ca occurred, leading to the presence of P. In the brown ore, further crystallization of P is evident in the form of apatite + gorceixite + monazite (+ rhabdophane) + an undetermined Al-phosphate compound. Conversely, the orange ore displays substantial amounts of Al-phosphate + monazite, resulting in the absence of apatite and the presence of small quantities of gorceixite, monazite, and apatite in the brown ore. Mining data obtained from the orange ore consistently demonstrates a lack of significant gorceixite; it is believed that the majority of P is present either as a REE-phosphate or as an unclassified substance, potentially a non-crystalline Al-phosphate.

Resultados e discussão
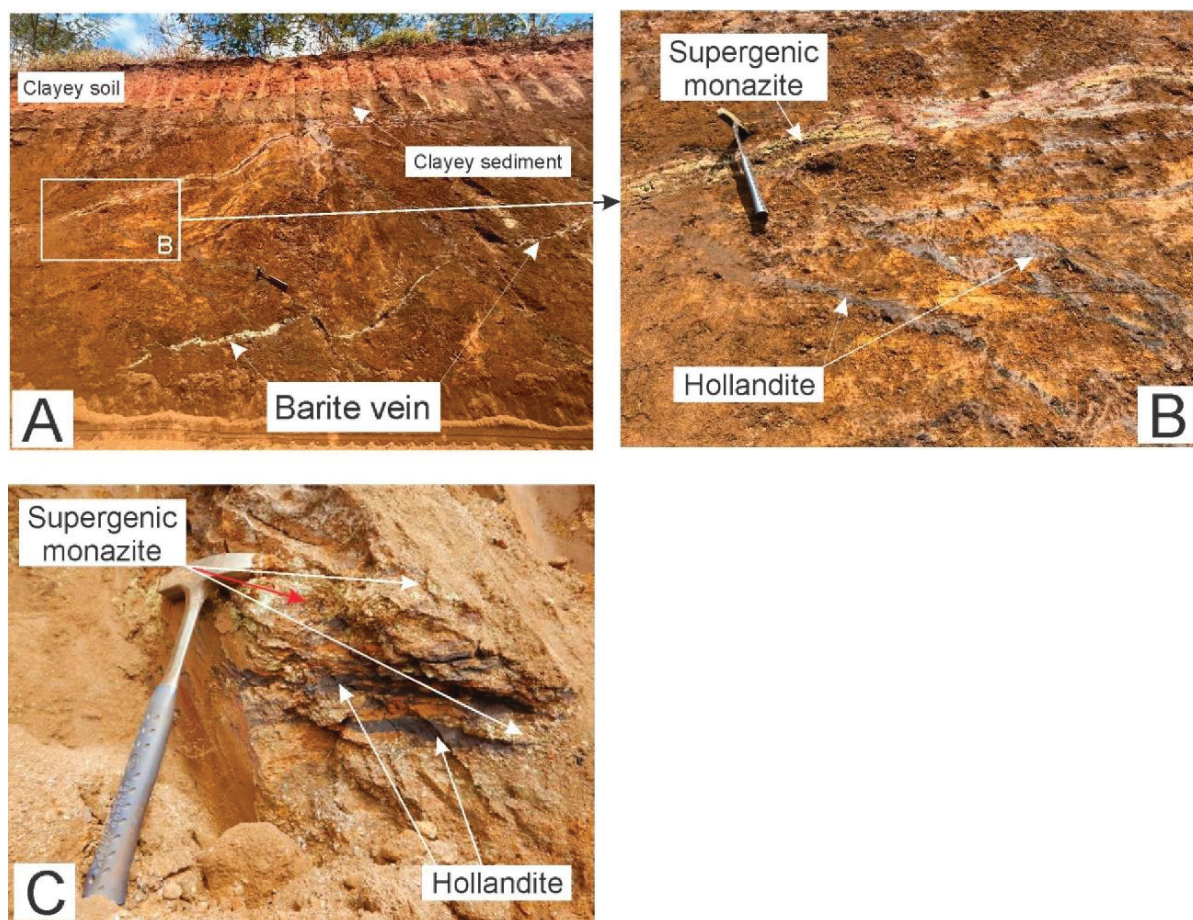
Fig. 11 - All images are of orange ore features observed in the interior of the CBMM open pit. (A) Massive barite veins covered by clayey sediments and soil. (B) Stratiform concentration of the supergenic monazite and hollandite veins. (C) Occurrence of supergenic monazite and hollandite.

Excess of Ba over S: In the Araxá Complex, excess Ba occurs in all of the ore types, where barite veins and venules (Fig. 11A) are common and barite vein fragments are present in the soil. To quantitatively estimate whether the Araxá ores bear non-crystallized Ba as barite, the CBMM database BaO and S analysis was performed (Table 1), which allowed for a comparison between the number of moles of Ba and S in the ores (Table 5). A Ba/S molar ratio greater than one indicates the presence of barite in all ore types, mainly in the orange ore, confirming Ba excess compared with S.

Table 5 - Excess of Ba over S and the crystallization of barite in the Araxá ores.

| Ore type | # sample | Barium (Ba) | | Sulfur (S) | | Barite molar ratio (*) |
		Mean (wt%)	# moles	Mean (wt%)	# moles	$\dfrac{\#moles\ (Ba)}{\#moles\ (S)}$
Ocher ore	4	8.6	0.063	1.9	0.059	1.057
Brown ore	20	11.6	0.085	2.7	0.084	1.007
Orange ore	43	13.4	0.098	2.8	0.087	1.120

(*) Considering the general formula of barite: $BaSO_4$

The excess Ba in the weathered ores may crystalize as gorceixite, hydrokenopyrochlore, or hollandite (Fig. 11B, C), but the concentrations of these minerals observed during the mining and beneficiation process do not explain the excess Ba and amount of barite present in the ores or on the surface of the Complex. This excess Ba in the ore likely resides in aqueous solutions, which disseminates elemental Ba in all the ores, quite often reacting to form aqueous sulfur-rich solutions (Raposo, 2011). These solutions precipitate barite and form massive barite veins in the brown and orange ores (Fig. 11A). Sulfur solutions exist at present outcrops near the Tauá Hotel (Fig. 1), which are thought to permeate the regoliths and have existed since the formation of the Complex.

General model of the mineralization process

Figure 12 presents a general schematic model showing the relative dispositions of the three types of ore (ocher, brown, and orange) in relation to the rocks from which they derived, the likely meteoric water (which weathered these rocks) flow lines, and of the S gases and solutions that must have percolated through the rocks since the beginning of magmatism that yielded the Complex. The mineralized bodies are stratiform and horizontal, as shown in figures 5G–J and 9. These geometries suggest that meteoric water permeated through the rocks while removing and mobilizing substances in a lateral, radial, and horizontal flow pattern, as indicated by the arrows, which also indicate radial growth of the various mineralized bodies as weathering progressed (Figs. 8A–C). Notice that the thickness of the orange orebody is large whereas that of the ocher body is narrower. Furthermore, S solutions have percolated through the rocks and ores.

Resultados e discussão
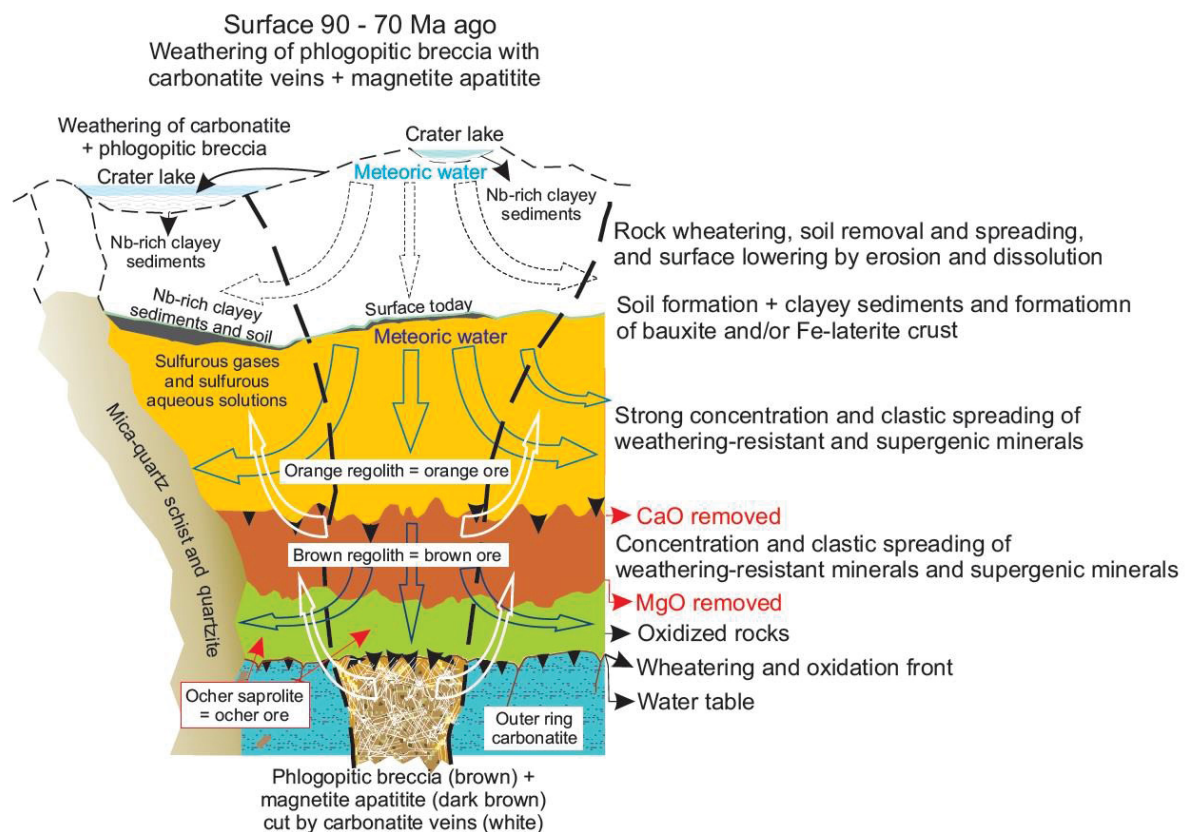
Fig. 12 - General schematic genetic model showing the position of the Araxa orebodies and how weathering evolved through a horizontal and radial flow regime of meteoric water (blue arrows) and S solutions (white arrows). The presence of clayey sediments partially covering the orange ore suggests the past existence of one or more crater lakes at the bottom of which these sediments originally settled.

We note the presence of a layer of Nb_2O_5-bearing clayey sediments discordantly settled on the orange regolith. This layer, with thicknesses between 0 and 40 m, on the regolith was derived from the phlogopitic breccia; thicknesses from 0 to 150 m on the regolith were derived from the carbonatites. During some periods after the emplacement of igneous rocks, crater lakes formed where these sediments settled. The presence of Nb in these sediments indicates that their source areas contained this element, i.e., they must have originated from outcropping parts of the phlogopitic breccia and magnetite apatitites or their weathering products, perhaps the saprolites corresponding to the ocher ore.

Volume variations and chemical gains/losses during ore formation: Volume variations were estimated according to the Gresens equations (1967) modified by Grant (1986); Table 6 presents the results, section "Phlogopitic breccia zone" and "Carbonatite ring zone." The average specific weights of the rocks and ores used in the calculations were as follows: unoxidized rock = 2.71 t/m^3; ocher ore = 2.43t/m^3; brown ore = 2.13 t/m^3; orange ore = 2.01 t/m^3; and siliceous bauxite = 1.64 t/m^3.

Table 6 - Volume changes in the weathering of phlogopitic breccia and carbonatites.

	Carbonatite rig zone					Phlogopitic breccias zone		
Drill-hole	Rock to ocher ore	Ocher ore to Brown ore	Brown ore to Orange ore	Orange ore to Clayey soil	Drill-hole	Rock to ocher ore	Ocher ore to Brown ore	Brown ore to Orange ore
FDS-25	-7	-48	-23	8	F-5XIJ3	-20	-64	-35
FDS-16	-17	-54	-14	24	F-5IXK5	-11	-51	17
FDN-47	-17	-47	-15	7	F-0XM9	-8	-10	-33
FDN-25	-10	-63	-13	134	F-3VIIK7	-27	-49	-30
FDN-24	-14	-48	-20	49	F-0XN0	-36	-50	-11
Mean	**-13**	**-52**	**-17**	**44**	F-0IXM0	-24	-58	-35
SD (n = 5)	4	7	4	53	**Mean**	**-21**	**-47**	**-21**
					SD (n = 6)	10	19	21

Figure 13 shows examples of isocons plotted based on the average contents of the F-5XIJ3 drill hole core samples (Fig. 1) according to the technique proposed by Grant (1986) to estimate the volume variations when the ocher, brown, and orange ores formed. Adjustments to the isocon lines were performed based on the contents of TiO_2, Fe_2O_3, Nb_2O_5, and Al_2O_3, which are considered immobile or almost immobile during weathering. The same procedure was applied to all of the other drill holes.

A

$$\frac{Ma}{Mo} = 0.8938 \quad \text{Mass decrease of 11\%}$$

Va/Vo = Ma/Mo.(ga/go) = 0.8938.(2.43/2.71) = 0.8015

Volume decrease of 19.9%

B

$$\frac{Ma}{Mo} = 0.4139 \quad \text{Mass decrease of 58.6\%}$$

Va/Vo = Ma/Mo.(ga/go) = 0.4139.(2.13/2.43) = 0.3628

Volume decrease of 63.7%

C

$$\frac{Ma}{Mo} = 0.6894 \quad \text{Mass decrease of 31.1\%}$$

Va/Vo = Ma/Mo.(ga/go) = 0.6894.(2.01/2.13) = 0.6506

Volume decrease of 34.9%
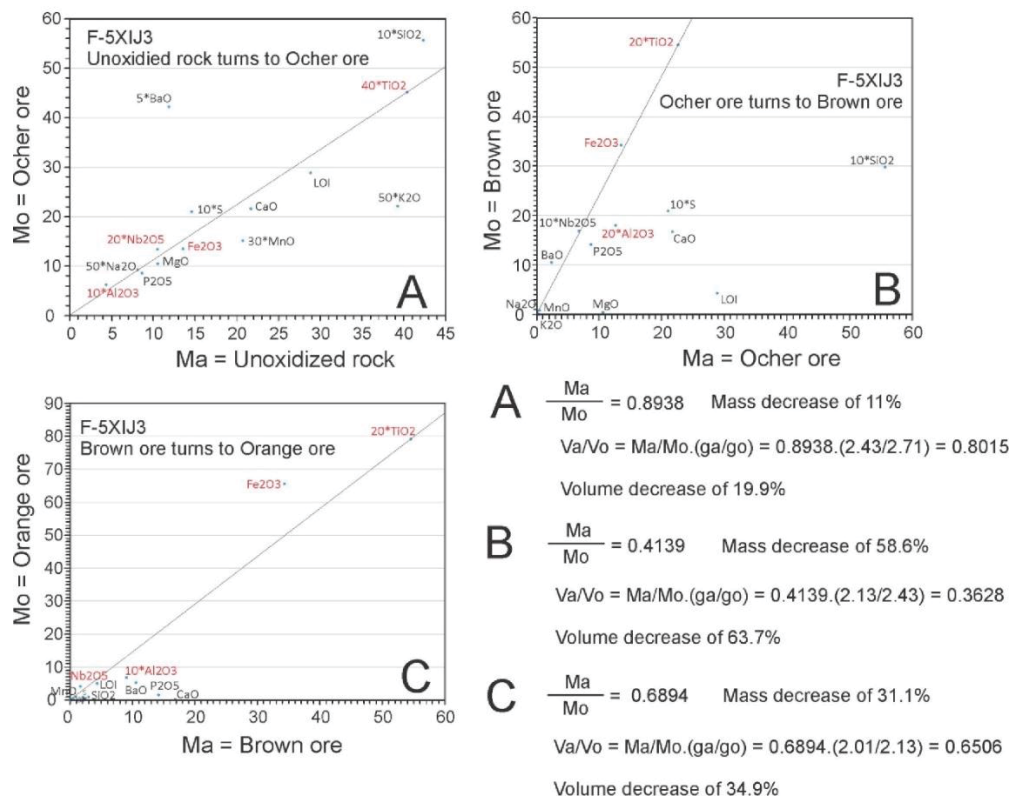
Fig. 13 - Examples of isocons plotted based on the average contents of the drilling samples from the F-5XIJ3 drill hole. The straight lines were fitted considering the TiO_2, Fe_2O_3, Nb_2O_5, and Al_2O_3 contents.

Due to the heterogeneity of the rocky substrate, weathering developed in a highly varied manner, achieving very different results in places only a few tens of

meters distant from another. Estimates of the volume variations and the chemical losses and gains were obtained with the average compositions of the six drill hole core samples located in the core region and five other drill holes situated in the carbonatite domain of the outer ring (Table 6, Appendices 4, 5, 6 and 7). Thus, the average volume changes and compositions of the rocks and ores observed in the drill hole core analysis were significantly different, which is reflected in the high values for the standard deviations of the volume variations listed in Table 6 and Appendices 6 and 7. Therefore, we considered the orders of magnitude of the "volume variation" and "chemical losses and gains" variables that occurred during weathering.

To estimate the volume variations, drill holes 5XIJ3, F-5IXK5, F-3VIIK7, F-0XN0, F-0XM9, and F-0IXXN0 were selected because they are located in the core of the Complex (Figs. 1, 8, and 9) and have surpassed the weathering front. The contents of the samples collected in each of these drill holes allowed for the calculation of the average composition of unweathered rocks and of each type of ore at each location (Fig. 1 and Appendix 4). The volume changes (Table 6) were determined for each drill hole location when mineralized rock (first protore) was transformed into saprolitic ocher ore, when the ocher ore (second protore) was transformed into a regolithic brown ore, and the brown ore (third protore) was transformed into orange regolith ore. Finally, the average values of the volume changes in these six drill-holes (Table 6, "average" line) were used to estimate how weathering evolved to form ores with Nb, P, Ba, REEs, and Ti-Fe in the nucleus of the Complex. Based on these results, figures 14A–H was constructed simulate the evolution of weathering in this region.
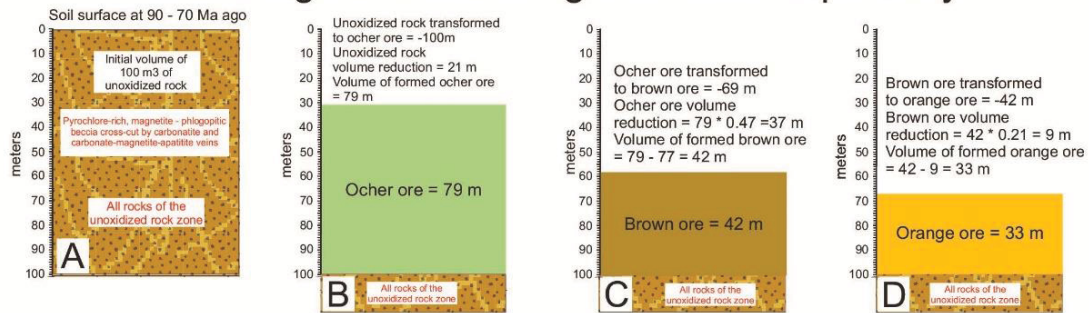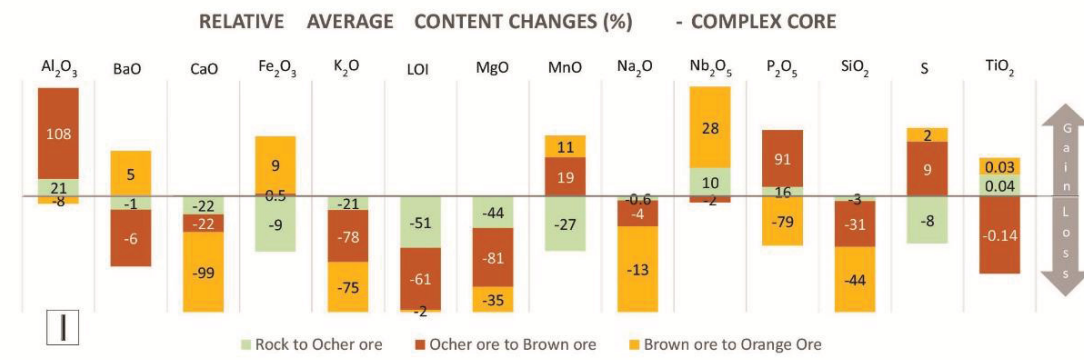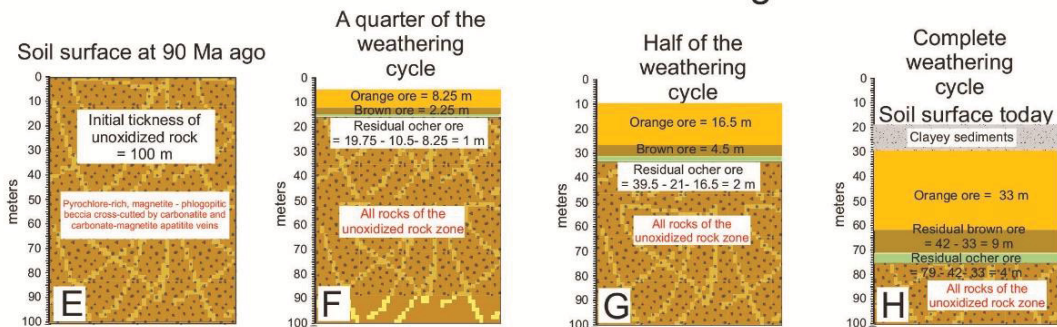
Fig. 14 - (A to H) Results of the weathering simulation of a 100-m-thick rock column in the core of the Complex. See text for explanation. (I) Relative losses and gains due to weathering based on the average compositions of the cores from drill holes F-5IXK5, F-5XIJ3, F-0XM9, F-3VIIK7, F-0XN0, and F-0IXM0, made in the core region.

To plot these figures, the volumes of the ores generated from a 100-m-thick rock column were considered as a "weathering stage" (Fig. 14A). Calculated separately, the thicknesses of the ocher (Fig. 14B), brown (Fig. 14C) and orange (Fig. 14D) ores formed from 100 m of rock were 79, 42, and 33 m, respectively, which may correspond to a complete "weathering stage." When the rock began to weather, the three ores formed simultaneously. Thus, weathering began to form the ocher ore. Immediately afterwards, brown ore formation began, consuming the ocher and forming the orange ore, which consumed the brown. The ore column formed at the end of "one stage" of weathering would be that shown in figure 14H, totaling 33 m of orange ore, 9 m of brown ore, and 4 m of ocher ore. Half a "stage" forms a column, as in figure 14G, and a quarter of a "stage" forms a column, as in figure 14F. Notice that the orange ore was the last to form and nothing can consume it, except erosion and/or surface leaching;

its thickness will increase over time. Furthermore, the ocher ore was consumed during the formation of the brown and orange ores, which became reasonably thick at the end of a "stage" of weathering, which was observed in the drill cores (Figs. 3M, N). The clayey sediment (Fig. 14H) settled in crater lakes (Fig. 12A). When the topography was reversed due to erosion and the lakes ceased to exist, these sediments settled on the surface of the orange ore and continued deformation as the weathering column thickened to form all of the ores.

Appendix 4 lists the average contents of the rocks and ores from drill holes 5XIJ3, F-5IXK5, F-3VIIK7, F-0XN0, F-0XM9, and F-0IXXN0. Figure 14I and Appendix 6 show the average chemical losses and gains in relative values that occurred during the formation of each type of ore in the Complex core according to the six drillholes. In the core of the Complex, the formation of the ocher ore involved a relative gain of approximately 10% Nb_2O_5, 16% P_2O_5, and 21% Al_2O_3 and losses of 44% MgO, 22% CaO, 21% K_2O, 1% BaO, 8% S, and 51% LOI; these values characterize the beginning of ore formation. During the formation of the brown ore from the ocher ore, relative gains on the order of 91% P_2O_5, 9% S, and 108% Al_2O_3 occurred and 2% Nb_2O_5, 6% BaO, 81% MgO, 22% CaO, 9% Fe_2O_3, 51% LOI, and 78% K_2O were leached. The formation of orange ore involved an increase in the relative Nb_2O_5 concentration of 28%, 5% BaO, 2% S, 9% Fe_2O_3, and 11% MnO and a loss of 79% P_2O_5, 99% CaO, 44% MgO, 75% K_2O, 13% Na_2O, and 44% SiO_2, which indicates laterization with lateritic ores rich in Nb and Ba.

Volume variations and chemical gains/losses during outer ring carbonatite ore formation: The variation in volume occurring during carbonatite weathering was estimated in the same manner as the phlogopitic breccia variations, whose the results are listed in Table 6, section "outer ring carbonatite zone." To estimate the volume variations, drill holes FDS-25, FDS-16, NDF-47, NDF-25, and NDF-24 were selected because they are in the outer carbonatite ring (Figs. 1, 8, and 9) and also because they surpass the weathering front in the rock. The contents of the core samples collected in each of these drill holes allowed for the calculation of the average composition of the unweathered rocks and each type of ore in each drill hole location (Appendix 5 and Figs. 1, 8, and 9). The same procedure was applied to the ores deriving from the phlogopitic breccia and we estimated the manner in which weathering evolved, i.e., ore formation with P_2O_5 on the outer ring carbonatites (Figs. 8 and 9). Figures 15A–I were constructed based on these results to simulate the weathering evolution. The same procedure used to plot figure 14 was applied to construct figure 15. Calculated separately, the thicknesses of the ocher (Fig. 15B), brown (Fig. 15C), and orange ore (Fig. 15D) formed from a 100-m-thick rock column were 87, 42, and 35 m, respectively, which would correspond to a complete "weathering stage." Half of the cycle formed a column, as shown in figure 15H, and a quarter of a cycle formed a column, as shown in figure 15G. Similar to the core domain, ocher ore was consumed during the formation of the brown and orange ores. At the end of the "weathering stage," the orange ore formed a mineralized body slightly thicker than that of the brown ore (Figs. 3O, P). Siliceous bauxite (Fig. 15E) settled on the orange regolith and likely formed later in some places where the carbonatites assimilated kaolinite from the host rocks. Gibbsite was concentrated when carbonatites and silica from kaolinite were leached.
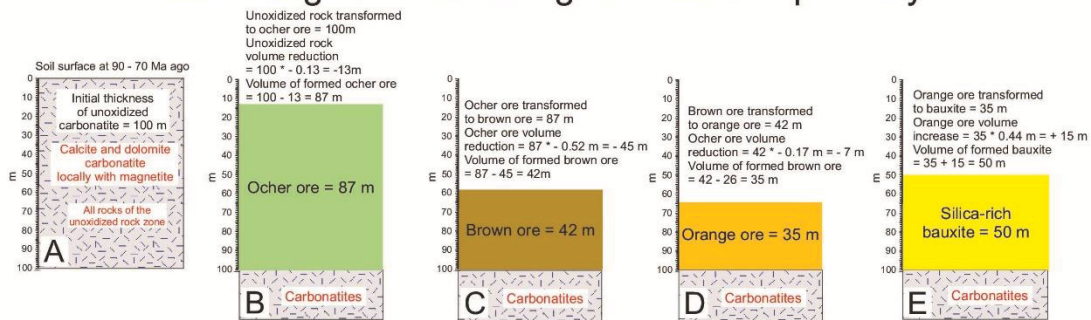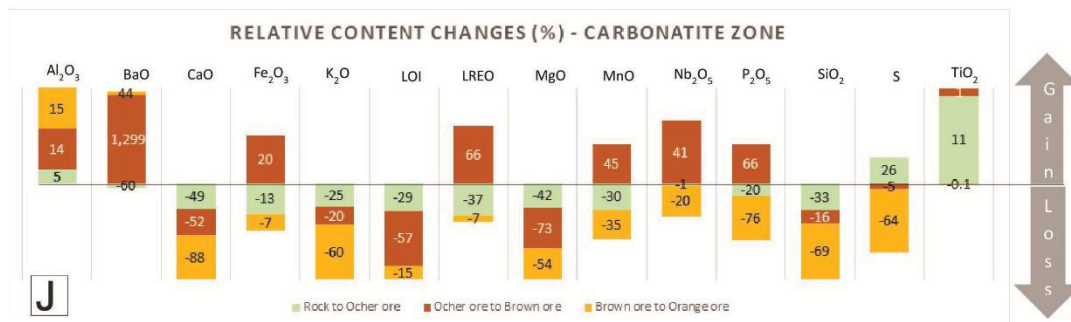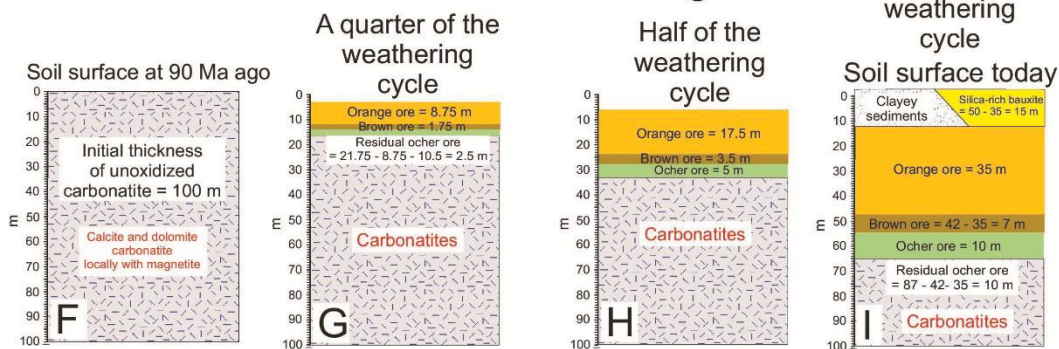
Fig. 15 - (A to I) Results of the weathering simulation of a 100-m-thick rock column in the core of the Complex. See text for explanation. (I) Relative losses and gains due to weathering based on the average compositions of cores from drill holes FDS-25, FDS-16, FDN-47, FDN-24, and FDN-25, made in the carbonatite region.

Figure 15J and Appendix 7 show the chemical losses and gains that occurred during the formation of each type of ore in relative values, considering samples from the five drill holes. In the carbonatitic ring, the formation of the ocher ore involved relative gains of 10% TiO_2, 26% S, and 5% Al_2O_3. There were losses of 20% Nb_2O_5, 20% P_2O_5, 60% BaO, 37% REO, 49% CaO, 42% MgO, 29% LOI, 33% SiO_2, and 25% K_2O. To form the brown ore, there was a gain of 41% Nb_2O_5, 66% P_2O_5, 1,299% BaO, 66% REO, 20% Fe_2O_3, 14% Al_2O_3, and 45% MnO. Furthermore, 73% MgO, 52% CaO, 5% S, 20% K_2O, 16% SiO_2, and 57% LOI were leached. The orange regolith formation contained 44% BaO, 15% Al_2O_3, and 20% Nb_2O_5; 76% P_2O_5, 64% S, 7% REO, 88% CaO, 54% MgO, 35% MnO, 7% Fe_2O_3, 69% SiO_2, and 15% LOI were leached. Along with the high relative gains of BaO, there were relative S losses of 33, 16, and 69% when the ocher, brown, and orange ores formed, respectively. Thus, the almost non-existence of barite in the ores formed on carbonatites was due to S leaching during

weathering, although BaO was heavily enriched in brown (1,299%) and orange (44%) ores owing to norsethite dissolution. The phosphorous concentration (76% P_2O_5) likely originated during the destruction of apatite and the crystallization of gorceixite when orange ore formed (Table 7B).

The formation of siliceous bauxite involved significant gains of 313% SiO_2, 598% Al_2O_3, 515% K_2O, and 53% BaO. These increases in the concentrations of mobile substances, such as SiO_2, K_2O, and BaO, suggest that the siliceous bauxite was sedimentary, likely forming during the existence of the crater lake that also created clayey sediments. Therefore, siliceous bauxites may not be products of the orange ore weathering.

2.1.7 Conclusions

The Araxá alkaline-carbonatitic Complex is composed of phlogopitic breccia and magnetite apatitites located in the core of the Complex and surrounded by a halo of carbonatites. During carbonatite emplacement, assimilation of the schists and quartzites that host the Complex occurred such that some rocks at the external edge of the carbonatite ring had more than 40% SiO_2, 14% Al_2O_3, and 4.0% K_2O.

In the Araxá Complex, the ores are saprolites and regoliths formed by the weathering of phlogopitic breccia and magnetite apatitites existing in the Complex core, as well as via the weathering of the outer ring carbonatites. Based on the sharp variation in MgO and CaO concentrations, three types of ore can be defined as ocher, brown, and orange ores.

The core of the Complex contains Nb, P, Ba, Ti, and Fe polymetallic ores, which locally contain REEs. On the outer ring carbonatites, saprolites, and regoliths containing P, low Ba contents, and occasional REEs were generated. The main Nb ore minerals were hydroxycalciopyrochlore and hydrokenopyrochlore. In the orange ore, part of the pyrochlore was destroyed and Nb was adsorbed on goethite. The concentrations of Nb and Fe had a proportional and direct correlation, which suggests that pyrochlore and magnetite belong to the same paragenesis in the igneous rocks. The remaining Nb ore resources in the Araxá Complex have been estimated at 896 Mt in the brown and orange ores, with an average content of 1.49% Nb_2O_5.

Apatite occurs in ocher ore as fluorapatite. In the orange ore, apatite was destroyed by weathering where P became bound to Ba and Al, resulting in the crystallization of gorceixite or as REE-phosphates. The highest concentrations of apatite occurred in the ores that formed on the outer ring carbonatites. The remaining phosphate resource in the weathered ores amounts to 770 Mt and has an estimated average content of 10.4% P_2O_5.

In the center of the Complex, barite occurs in the three ore types and is the main Ba ore mineral, to a significantly lesser extent, Ba-bearing minerals such as gorceixite, hydrokenopyrochlore, and hollandite. Although similar to pyrochlore and magnetite, barite also occurs in the core of the Complex; there is no correlation between the BaO contents and those of Nb_2O_5 and Fe_2O_3, indicating that barite does not belong to the original paragenesis with pyrochlore and magnetite. The weathering system resulted in a lower S concentration than that of Ba. The ores have an excess of Ba that likely resides in the aqueous solutions, which disseminates elemental Ba in all ores and quite often reacts with aqueous sulfur-rich solutions that form barite veins. Barium cations

were generated via the release of Ba from norsethite-bearing carbonatites; the binding of Ba to the S released by pyrite weathering (possibly also with S from sulfur-rich solutions) crystallized barite. The ores formed on the Complex core had between 20 and 33% BaO; those on the carbonatite outer ring had less than 6% BaO. Currently, Araxá contains 768 Mt of barite in the weathered ores with an average content of 20.1% $BaSO_4$.

The weathering evolution represented by weathering lines showed that the concentrations of pyrochlore and magnetite in the phlogopitic breccia were simply caused by the removal of MgO from dolomite and norsethite followed by CaO from apatite, which, at the end of weathering, increased the concentration of Nb_2O_5 from less than 1.0% in the rock to up to 5% in the orange ore. MgO was rapidly leached from both the phlogopitic breccia and carbonatite, concentrating residual apatite and increasing the P_2O_5 content by approximately 5% in the rock to over 25% in the ocher ore and over 35% in the brown ore. Unlike Nb_2O_5, at the end of weathering, the removal of CaO destroyed the apatite in the brown ore, reducing the P_2O_5 content to less than 2% in the orange ore that formed on both the phlogopitic breccia and carbonatites. The barite concentration increased with the release of Ba from the norsethite carbonatite, which bound to S and crystallized barite; this was residually concentrated in the brown and orange ores but was destroyed with soil formation.

As the weathering evolved, the REEs were concentrated in supergenic monazite and rhabdophane. These minerals appeared in the core of the Complex and in the carbonatite ring region, but the highest REO contents were in the core of the Complex. Although monazite is at least partially a primary mineral, there was evidence of autigenic and supergenic monazite/rhabdophane crystallization and REEs emerging from apatite destruction. The estimated remaining resources in the weathered ores are 352 Mt, with 5.6% REOs.

Maps of the top surfaces of the ocher, brown, and orange ores showed that the orebodies are stratiform and roughly horizontal. Saprolites and regoliths presenting this geometry indicate that the meteoric water flow lines that generated them migrated from the surface downward and inflected horizontally. This weathering process leached mobile substances, primarily K_2O, CaO, MgO, and SiO_2, and removed them from the weathering system laterally, horizontally, and radially. Thus, the concentrations of the minerals and ore depended equally on their concentrations in the weathered rocks and on accumulation caused by residual enrichment that occurred from the surface downward. From top to bottom, as the minerals concentrated, the ore minerals in the core of the Complex were displaced laterally as a result of the weathering of the phlogopitic breccia and magnetite apatites, thus concentrating in regions where the substrate was carbonatite and vice versa.

The weathering of rocks generates saprolites and regoliths, with volumes smaller than those of the original rocks. If a 100-m-thick column of phlogopitic breccia and magnetite is weathered, the ore column formed at the end of weathering will have 33 m of orange ore, 9 m of brown ore, and 4 m of ocher ore. If 100 m of carbonatites are weathered, the ore column will have 35 m of orange ore, 7 m of brown ore, and 10 m of ocher ore. Clay silt and clays in crater lakes constitute layers with thicknesses between 0 and 140 m, covering the orange regolith, locally buried laterite, and weathered volcanic tuffs. At present, these sediments are on orange ore and adapt to the changes that occur in the surface topography as the thickness of the ore body increases heterogeneous way.

Resultados e discussão

The residual enrichment of pyrochlore in the orange (28% relative Nb_2O_5 or 0.25% absolute) and ocher (10% of Nb_2O) ores and apatite in the brown (91% relative P_2O_5 or 4.14% absolute) and ocher (16% relative P_2O_5 or 0.91% absolute) ores are the most important characteristics imposed by the weathering of the phlogopitic breccia and magnetite apatitites in the core of the Complex, in addition to the loss of MgO and CaO during the formation of the three ore types. Similar to the core, there is also a residual concentration of pyrochlore (41% Nb_2O_5) and apatite (66% P_2O_5) in the carbonatites, but this concentration corresponds to only 0.08% by weight of Nb_2O_5 (= absolute content), whereas the relative P_2O_5 concentration corresponds to an absolute increase in content equal to 1.38%. The formation of siliceous bauxite involved very high gains of mobile substances, such as SiO_2, K_2O, and BaO, which suggests that the element was formed via sedimentation and not by weathering of the orange ore.

Resultados e discussão

References

Amaral, C., Bushee, J., Cordani, U.C., Kawashita, K., Reynolds, J.H., 1967, Potassiun-argon ages of alkaline rocks from Southern Brazil: Geochimica et Cosmochimica Acta, v.31, p. 117-142.

Barbosa, O., Braun, O.P.G., Dyer R.C., Cunha, C.A.B.R., 1970, Geologia da região do Triângulo Mineiro. Rio de Janeiro: Boletim 136 do DNPM/DFPM, 140p.

Chen, W., Honghui, H., Bai, T., Jiang, S., 2017, Geochemistry of Monazite within Carbonatite related REE Deposits: MDPI Resources, v.6, (51); doi:10.3390/resources6040051.

Clay, A.N., Ackroyd, B., 2012, A preliminary economic assessment in the form of an independent technical report on MBAC FERTILIZER CORPORATION (MBAC) Araxá Project located in Minas Gerais State, Brazil, as amended, prepared by VENMYN RAND (PTY) LIMITED (VENMYN), Internet, 112p.

Folha Araxá, 2015, Mapa Geológico da Folha Araxá - SE.23-Y-C-VI Escala 1:100.000, CODEMIG (Companhia para o Desenvolvimento de Minas Gerais).

Gomes, C.B. and Comin-Chiaramonti, P., 2017, Magmatismo Alcalino Continental da Região Meridional da Plataforma Brasileira: Editora EDUSP, 595p.

Grant, J.A., 1986. The Isocon Diagram - A Simple Solution to Gresens' Equation for Metasomatic Alteration: Economic Geology, v. 81, p. 1976-1982.

Grasso, C.B., 2015, Geologia e geometalurgia dos minérios de fosfato na base do manto de intemperismo da mina do Barreiro, Araxá: Doctor Thesis n° 126, Universidade de Brasília, Instituto de Geociências, 261p. (unpublished).

Gresen, R.L., 1967, Composition-volume relationships of metasomatism: Chemical Geology, v. 2, p. 47-55.

Grossi-Sad, J.H., Torres, N., 1971, Geologia e recursos minerais do Distrito do Barreiro, Araxá, Minas Gerais: Relatório DNPM/GEOSOL, Unpublished, 35p.

Issa Filho, A., Lima, P.R.A.S., Souza, O.M., 1984, Aspectos da geologia do Complexo caronatítico do Barreiro, Araxá, MinasGerais, Brasil. *In*: *Complexos carbonatíticos do Brasil – Geologia*. Brasilia, CBMM

Issa Filho, A., Riffel, B.F., Sousa, C.A.F., 2011, Some aspects of the mineralogy of CBMM niobium deposit and mining and pyrochlore ore processing – Araxá, MG – Brazil. In: International Symposium on Niobium. Proceedings. Orlando. Patherson, 15p.

LCT–USP, 2016, Caracterização em produtos de processamento de minérios de Terras Raras – Concentrados rougher e cleaner (*Characterization in rare earth ore processing products – rougher and cleaner concentrates*): Internal, unpublished report of the LCT - USP, 35p.

Mariano, A.N., Mariano Jr., A., 2012, Overview of REE Deposits and Mines in the World and in Brazil: Lecture with unpublished text, 67 slides.

Resultados e discussão

Miyawaki, R., Momma, K., Matsubara, S., Sano, T., Shigeoka, M., HoriuchI, H., 2021, Hydroxykenopyrochlore, $(A,Ce,Ba)_2(Nb,Ti)_2O_6(OH,F)$, A new member of the pyrochlore group from Araxá, Minas Gerais, Brazil: The Canadian Mineralogist, v.59, p.589-601 DOI: 10.3749/canmin.2000094

Oliveira, S.M.B, Imbernon, R.A.L., 1998, Weathering alteration and related REE concentration in the Catalão Carbonatite Complex, central Brazil: Journal of South American Earth Sciences, v. 11 (4), p. 379-388.

Raposo, D. B., 2011, Caracterização do aquífero associado ao Complexo Alcalino Carbonatítico do Barreiro, oeste de Minas Gerais. In portuguese: *Characterization of the aquifer associated with the Barreiro Alkaline Carbonatitic Complex, West of Minas Gerais*: Master Thesis. Universidade de Campinas. 126 p.

Santos, J. J.A., Conceição, H., Leandro, M.V.S., Rosa, M.L.S., 2018, Formation of monazite-(Ce, La) by fluid-apatite interaction: The Floresta Azul Alkaline Complex, Bahia, Brazil: Brazilian Journal of Geology, v. 48(4), p.721-733.

Seer, H.J., Dardenne, M.A., Pimentel, M.M., Fonseca, M.A., Moraes, L.C., 2000, O grupo Ibiá na sinforma de Araxá: um terreno tectono-estratigráfico ligado à evolução de arcos magmáticos: Revista Brasileira de Geociências, v.30(4), p.737-744.

Seer, H.J., Moraes, L.C., Silva, C.H., 2015, Mapa Geológico da Folha Araxá - SE.23-Y-C-VI Escala 1:100.000, CODEMIG

Silva, C.H., Simões, L.S.A., Damázio, W.L., Ferreira, S.N., Luvizotto, G.L., 2012, O Grupo Canastra em sua área-tipo, região de Tapira, sudoeste do estado de Minas Gerais: Revista do Instituto de Geociências – USP, Série Científica., v. 12(2), p. 8-98.

Sonoki, I.K., Garda, G.M., 1988, Idades K / Ar de rochas alcalinas do Brasil Meridional e Paraguai Oriental – Compilação e adaptação às novas constantes de decaimento: Boletim IG – USP, Série Científica, v.19, p.63-85.

Toledo, M.C.M., Lenharo, S.R.L., Ferrari, V.C., Fontan, F., De Perceval, P., Leroy, G., 2004, The compositional evolution of apatite in the weathering profile of the Catalão I alkaline-carbonatitic Complex, Goias, Brazil: The Canadian Mineralogist, *v*. 42, p. 1139-1158.

Ulbrich, H.H.G.J. and Gomes, C. B. 1981, Alkaline rocks from continental Brazil: Earth-Science Reviews, v. 17 p.135-154.

APPENDIX 1 – Chemical summary of CBMM database

Click here to access/download
Electronic Appendix (Excel etc.)
APPENDIX 1 - Chemical summary of CBMM
database.pdf

APPENDIX 2 – Chemical analysis – Drill hole samples

Click here to access/download
Electronic Appendix (Excel etc.)
APPENDIX 2 - Chemical analysis - Drill hole
samples.pdf

APPENDIX 3 – XRD Drill hole sample analysis

Click here to access/download
Electronic Appendix (Excel etc.)
APPENDIX 3 - XRD Drill hole sample analysis.pdf

APPENDIX 4 – Chemical content changes (phlogopitites)

Click here to access/download
Electronic Appendix (Excel etc.)
APPENDIX 4 - Content changes - phlogopitite.pdf

APPENDIX 5 – Content changes (carbonatites)

Click here to access/download
Electronic Appendix (Excel etc.)
APPENDIX 5 - Content changes - carbonatite.pdf

Resultados e discussão

APPENDIX 6 – Chemical contents (carbonatites)

Click here to access/download
Electronic Appendix (Excel etc.)
APPENDIX 6 - Chemical contents - carbonatite.pdf

Resultados e discussão
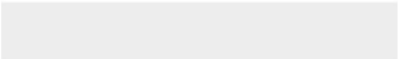
APPENDIX 7 – Chemical contents (phlogopitites)

Click here to access/download
Electronic Appendix (Excel etc.)
APPENDIX 7 - Chemical contents - phlogopitite.pdf

2.2 **Artigo 2** - Transition halos of Nb mineralization and the effects of their chemical and mineralogical characteristics on niobium recovery through flotation - Araxá Alkaline Carbonatite Complex, Minas Gerais, Brazil[1]

José Marques Braga Jr.[a*], João Carlos Biondi[b], Francisco Gregianin Testa[a]

[a] Companhia Brasileira de Metalurgia e Mineração (CBMM), Araxá, Minas Gerais, Brazil

[b] Universidade Federal do Paraná (UFPR), Departamento de Geologia, Curitiba, Paraná, Brazil

* Corresponding author

Tel.: +55 34998163581; e-mail Address: jose.marques@cbmm.com

---

[1] Abbreviations: CBMM, Companhia Brasileira de Metalurgia e Mineração; COMIPA, Companhia Mineradora do Pirocloro de Araxá; MR, metallurgical recovery; XRD, X-ray diffraction; ICDD, International Centre for Diffraction Data; RIR, reference intensity ratio; REE, rare earth elements; LREO, light rare earth oxides; REO, rare Earth oxides.

Abstract

Approximately 80% of the niobium sold worldwide is extracted from the Araxá alkaline–carbonatite complex in Minas Gerais, Brazil. In this complex, the Nb resources are in supergenic ores classified based on the variation of MgO and CaO as ocher, brown, and orange ores. Owing to the different behaviors observed during geometallurgical tests, it was determined that there are saprolites and regoliths mineralized in niobium whose metallurgical recoveries are inferior to those of the core ores mined from the seventies to the present day. These new types of ores form a transition halo surrounding the primary Nb-mineralized body. The formation of halo S primary ore is interpreted to occur via the simultaneous assimilation of phlogopitites from the core complex and mica-schists from the Ibia group by carbonatites housed around the phlogopitic core. The formation of halo N ores is interpreted to occur via the weathering of U-enriched carbonatite, which likely assimilates the phlogopitic breccia located in the north of the deposit, with possible subordinate hydrothermalism. The metallurgical recoveries of halo N and S ores are typically less than 0.65 NDD. This study explores three primary reasons to justify these low metallurgical recoveries: the presence of contaminating minerals, different niobium-bearing minerals, and morphological and textural aspects of pyrochlore. The halo S ocher and brown ores have low metallurgical recoveries due to the dolomite and vermiculite and halo S orange ore due to the clay minerals. In the halo N ocher ore dolomite causes low metallurgical recoveries, whereas in the halo N brown and orange ores suggest low metallurgical recoveries because of some other Nb-bearing mineral, such as uranopyrochlore, as indicated by the strong correlation between U_3O_8 and Nb_2O_5.

2.2.1 Introduction

Companhia Brasileira de Metalurgia e Mineração (CBMM) is the world's largest producer of niobium, having produced around 94 kT of FeNb equivalent in 2018. The Nb resources manufactured by CBMM are extracted exclusively by Companhia Mineradora do Pirocloro de Araxá (COMIPA) from the Araxá mine (former Barreiro mine, Fig. 1A), located in the state of Minas Gerais, Brazil. Given the current scenario of increased production of FeNb, properly characterizing the different types of ore that make up the company's mineral resources is necessary, especially for those with low metallurgical recovery than the present mineral beneficiation process. This need is justified by the difficulty in producing pyrochlore concentrates from ores with chemical and mineralogical characteristics different from the ore currently exploited, thus contributing to the company's productive growth plans.
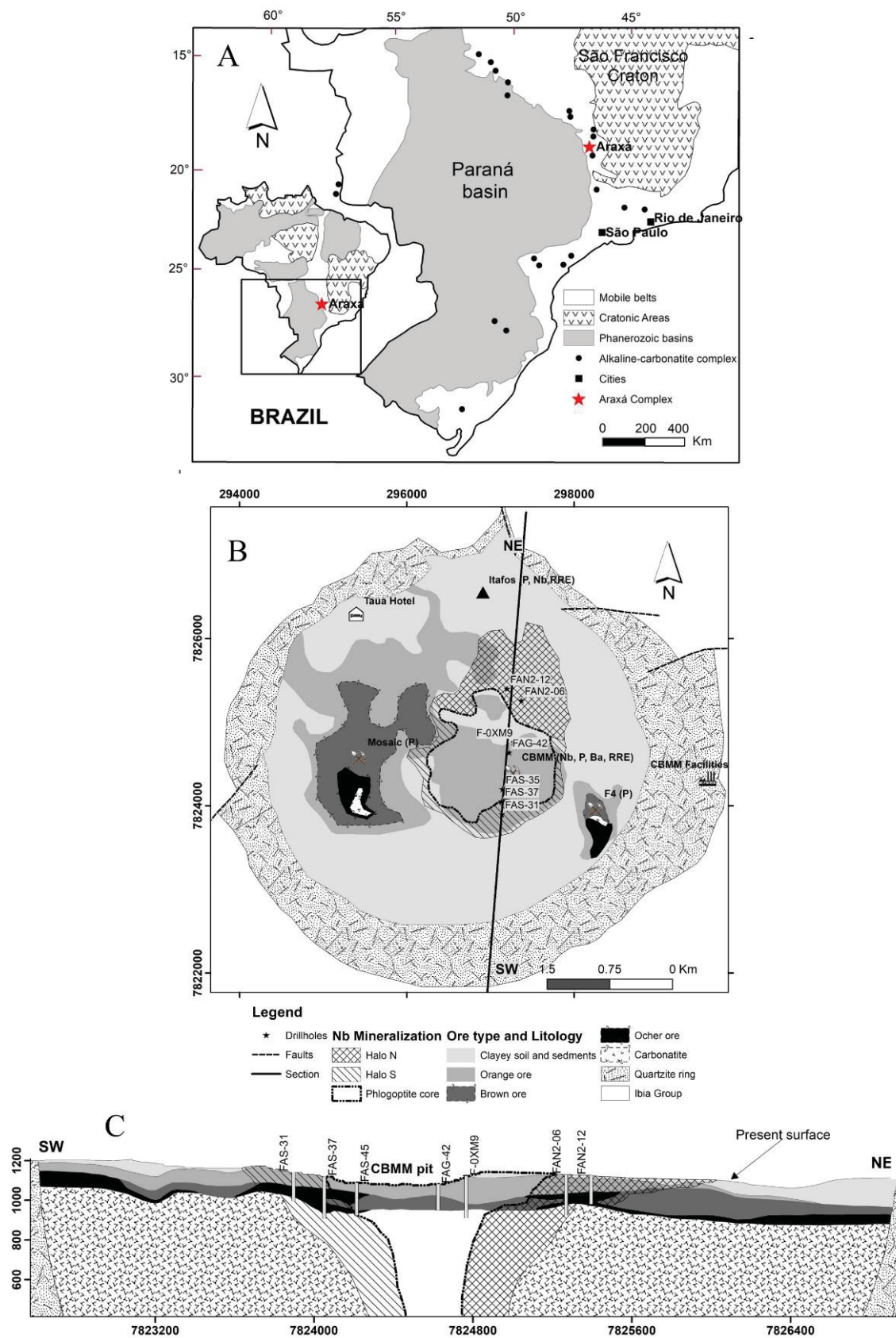
Fig.(A2) 1 - Geotectonic and geological settings. (A) Indication of the Araxá Complex and other alkaline Complexes in Brazil. (B) Simplified soil map of the Araxá Complex. (C) Simplified soil section encompassing the Araxá Complex.

Resultados e discussão

According to Braga and Biondi (2022), the niobium resources are in saprolites and regoliths, formed by the weathering of magnetite phlogopitites and apatite-magnetites existing in the core of the Complex, and the phosphate ores are in saprolites and regoliths formed by the weathering of carbonatites that form a ring surrounding the core of the Complex. Based on the sudden variation of MgO and CaO concentrations, Braga and Biondi (2022) defined three types of ores: ocher ore, a saprolite with MgO and CaO contents greater than 2.0%, brown regolith with MgO content less than 2.0% and CaO content greater than 2.0%, and the orange regolith, with MgO and CaO contents less than 2.0%.

Recently, due to the different behavior during the geometallurgical tests with drilling samples of the Nb ores of the Complex, it was observed that there are saprolites and regoliths mineralized in niobium whose properties are intermediate between those of the ores classified by Braga and Biondi (2022). This new type of ore forms a transition halo surrounding the main ore body located in the center of the Complex (Fig. 1B and C). Like the ores formed on the phlogopitites of the core or on the carbonatites surrounding the core, the transition halo also contains ocher, brown, and orange ores; however, its chemical compositions and the properties of its minerals are different from those of the core ores mined since the seventies. This mineralized body will henceforth be referred to as a "transition halo" or simply "halo." Knowing the characteristics of the transition halo ores, in addition to being economically relevant, complements and improves the understanding of the formation processes of the intemperic or secondary ores of Araxá, expanding this knowledge beyond what was published by Braga and Biondi (2022).

The variable "metallurgical recovery" (RM) denotes the proportion of industrially utilized niobium extracted from the ore via the employed mineral processing technique. It is quantified as the weight percentage ratio of niobium recovered in the concentrate to the niobium content in the ore subjected to the flotation process, ranging from 0% to 100%. This study normalized the RM data using the maximum and minimum methods to ensure information confidentiality. The normalization employed the formula $x_{nor} = (x_1 - x_{min}) / (x_{max} - x_{min})$, where x_1 represents the bench test value for sample 1, and x_{min} and x_{max} signify the minimum and maximum values of the entire result distribution, respectively. Consequently, the RM data exhibited a dimensionless distribution (NDD) from 0 to 1, with 0 corresponding to the lowest RM value in the actual distribution and 1 to the highest value. An identical procedure was applied to the U_3O_8 and U variables for the same reason.

The main stages of the beneficiation and treatment process of the Araxá niobium ore mix consist of primary and secondary crushing, magnetic separation, classification, conditioning, flotation, thickening, and filtration. In 2018, CBMM started with a new process to recover niobium from the ultrafine fraction to recover more metal and generate less waste. The product of the concentration plant is a niobium concentrate with about 55% Nb_2O_5, and the global average MR of the plant is approximately 64%. This concentrate is used exclusively by CBMM as an input in the subsequent stages of production: desulfurization, dephosphorization, metallurgy, chemistry to obtain oxides, and an electron beam furnace to obtain metallic niobium. The main products are standard iron-niobium, niobium oxides, metallic niobium, and niobium-zirconium, in addition to special alloys iron-niobium and nickel-niobium. Barite and magnetite are by-products of the niobium production process (da Silva Lima et al., 2022).

The main objectives of this study are (a) to know the chemical and mineralogical characteristics of the new ores recognized in the N and S transition halos and (b) to present the results of the pyrochlore flotation concentration tests of the regolithic and saprolitic ores of these transition halos. For this, the chemical, mineral, and flotation compositions typical of these new types of Nb ore are defined, and these characteristics are compared with those of the ores currently processed by CBMM. Additionally, a criterion is proposed to classify the Nb ores of transition halos.

2.2.2 Geotectonic, geochronological, and geological settings

Geotectonic and geochronological settings

In Brazil, hundreds of alkaline rock occurrences are known, which manifest as dykes, apophyses, necks, and differentiated intrusions that, except for kimberlitic and lamproitic bodies, have kilometric dimensions (Biondi, 2015). The map in Fig. 1A highlights the main Complexes formed by alkaline rocks in Brazil. The Alto Paranaíba Igneous Province, which encompasses the Araxá alkaline–carbonatite Complex (Almeida, 1983), is located on the northeast edge of the Paraná Basin (Fig. 1A), in a NW–SE alignment, coinciding with the Alto Paranaíba Arc, developed over the southern sector of the Brasília Folding Belt. The Brasília Belt outcrops on the western edge of the São Francisco Craton and extends for more than 1000 km in a north–south direction, covering the states of Minas Gerais, Goiás, Tocantins, and the Federal District (Almeida, 1967).

Gibson et al. (1995) discussed the age of magmatism in the Alto Paranaíba Province using new and old K/Ar, Ar/Ar, and U/Pb datings. They concluded that the alkaline magmatism of this province started less than 100 Ma ago. Radiometric ages in alkaline rocks of the Araxá Complex were determined for the first time by Ulbrich and Gomes (1981) and recalculated with new constants by Sonoki and Garda (1988). New dates were performed by Gomes et al. (1990), and all indicated ages between 98–77 Ma. Since then, the rocks of the Araxá Complex have been heavily weathered, forming a thick layer of soil up to 200 m thick, which constitute the Araxá ores (Braga and Biondi, 2022).

The intrusions of the rocks that make up the Complex deformed and raised the quartzites and mica-schists of the Ibia and Canastra groups, causing, currently, the alkaline and carbonatitic rocks to occur within a ring of phenitized quartzites and mica-schists (Grossi Sad and Torres, 1971) (Fig. 1B).

Local geology

The orange ore, which contains Nb, Ba, REE, and Fe, outcrops at the CBMM mine pit (Fig. 1B). The brown and ocher ores with P and potentially REE only outcrop within mine pits (Fig. 1B). The Nb, P, and REE deposit at ITAFOS in the north has not been explored. The surface of the Complex is mainly covered by lacustrine clayey sediments with a maximum thickness of 40 m in the central region (Fig. 1C and 2). Lateritic duricrusts and volcanic tuffs are present in some areas. Weathering causes the thickening of ores and the dispersal of ocher, brown, and orange ores, forming secondary halos of Nb mineralization (Braga & Biondi, 2022).

Resultados e discussão

Fig. 2 presents a schematic profile showing the ocher, brown, and orange ores formed by the weathering of phlogopites, carbonatites, and magnetite-apatitites and their variations in Nb_2O_5, P_2O_5, BaO, Fe_2O_3, CaO, MgO, Al_2O_3, SiO_2, K_2O, and LREO contents in the center of the Araxá Complex and the transition zones. The thicknesses of the ore bodies are up to 154 m in orange ore, 146 m in brown ore, and 89 m in ocher ore (Fig. 2). According to Braga and Biondi (2022), the substances Nb_2O_5, Fe_2O_3, BaO, Al_2O_3, S, TiO_2, and REO are residually concentrated from the rock to the orange ore, as can also be seen from the chemical profiles of these substances in Fig. 2. P_2O_5 residually concentrates from the rock to the brown ore and is partially leached during the formation of the orange ore (Fig. 2). MgO and K_2O are completely leached in the transition from ocher to brown ore, whereas CaO is fully leached in the transition from brown to orange ore (Fig. 2). SiO_2 is gradually removed from the rock to orange ore.
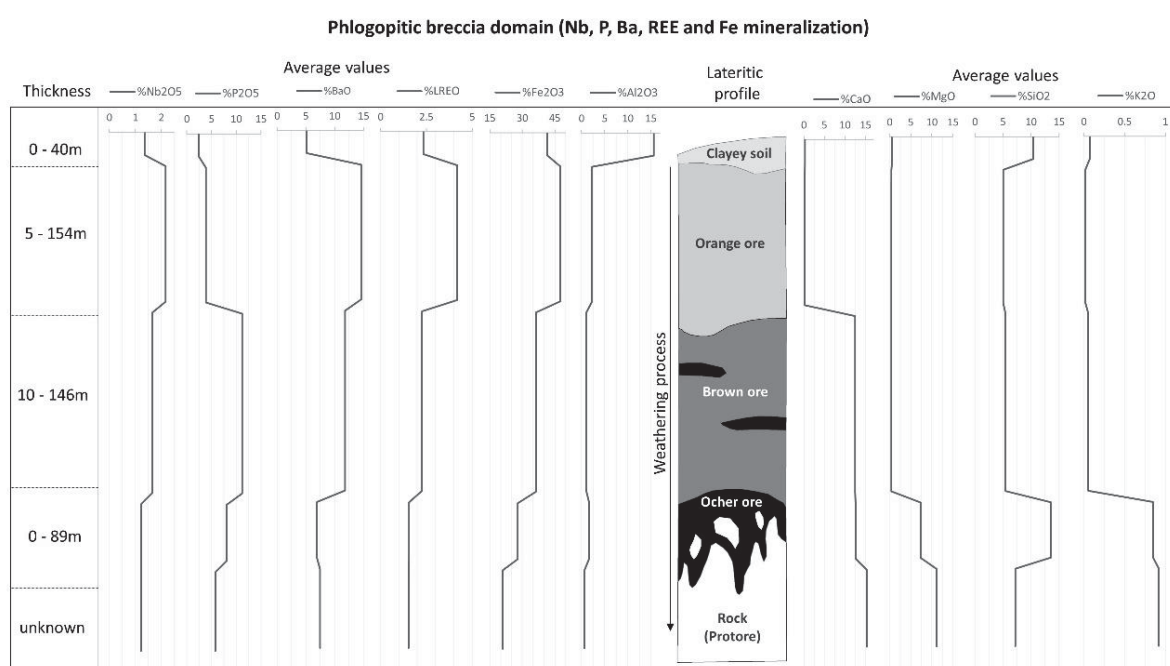
Fig.(A2) 2 - Lateritic and chemical profiles of the ores from the phlogopitic breccia domain.

The mineralized bodies that constitute the N and S transition halos (Fig. 1B) form two regions around the core of the main Nb mineralization. The sequence of supergenic ores observed in the core (ore, brown, and orange) also occurs in the N and S halo regions (Fig. 1C).

Analytical methods

Two-hundred-and-forty-six samples were selected from holes FAN2-06 (40), FAS-37 (41), FAS-31 (25), FAN2-12 (27), FAG-42 (24), FAS-35 (37), F- 0XM9 (29), and F-5XIJ3 (23) for chemical characterization (Fig. 1B and C). These samples were submitted to XRF analysis (%) for quantification of Al_2O_3, Fe_2O_3, MnO, P_2O_5, SrO, BaO, K_2O, Na_2O, PbO, Ta_2O_5, V_2O_5, CaO, La_2O_3, Nb_2O_5, Pr_6O_{11}, CeO_2, MgO, Nd_2O_3, SiO_2, and TiO_2. Loss on ignition was determined by calcination at 1000 °C (% LOI). The contents of Ce, Gd, Nd, Th, Yb, Dy, Ho, Pr, Tm, Er, La, Sm, U, Eu, Lu, Tb, and Y were determined by LA-ICP-MS. Total S was determined by non-dispersive infrared

cells of the sample submitted to combustion. All these analyzes were performed at SGS Geosol laboratories LDTA (Brazil).

The MR data used in this study were obtained from 194 samples from boreholes FAN2-06, FAS-37, FAS-31, FAN2-12, FAG-42, and FAS-35 (Fig. 1B and C), each sample corresponding to 5 m in length of the drill cores. All samples were submitted to laboratory process tests representing the industrial operation of preparation and concentration of niobium. These samples were physically homogenized, comminuted, and quartered. Two aliquots were used per sample for the test: one of 400 g for granulometric and chemical analyses of the initial sample and another of 3000 g for the mineral concentration tests. These tests were performed at CBMM's Ore Treatment Laboratory, simulating the industrial process of concentrating pyrochlore at Araxá. The 3000 g aliquots were initially wet sieved on a 42 µm mesh. The retained fraction, called coarse fraction, was ground in a ball mill and subsequently subjected to low-field magnetic separation, generating two products: a magnetic and a non-magnetic product. The mass and grinding time were adjusted such that the product has a D80 lower than 75 µm. The non-magnetic milled product was then incorporated into the passing fraction, called the fine fraction. An aliquot of 1000 g was submitted to the pyrochlore flotation test, which starts by mixing the ore with water in a stirred vat at a concentration of 40% solids, in which the surfactant reagents, pH modulators, and collectors were added and kept conditioning for 4 min. After this time, the air was injected into this vat and the air bubbles carried the pyrochlore particles to the surface, forming a mineralized foam; this foam was removed with the aid of shovels by the operator and corresponded to the concentrate. After obtaining the concentrate from the first flotation stage (rougher), two cleaner flotation stages were performed until the final concentrate was obtained. The products obtained in the flotation tests were flocculated, dewatered by decanting, and oven dried. After drying, the material was weighed and then quartered. Aliquots of the concentrate, magnetic tailings, and other tailings were analyzed by X-ray fluorescence in the CBMM chemical laboratory to determine the contents of Nb_2O_5, P_2O_5, CaO, Fe_2O_3, MgO, SiO_2, Al_2O_3, and $BaSO_4$.

The X-ray diffraction (XRD) analysis of these 177 samples from the drilling F-0XM9, F-5XIJ3, FAN2-06, FAS-37, FAS-31, and FAN2-12 (Fig. 1B and C) was performed using the powder method with a Bruker D8 Advance diffractometer operating with Cu-Kα radiation and a position-sensitive Lynxeye XE detector. The crystalline phases were identified by comparing the diffractograms with the International Centre for Diffraction Data (ICDD) PDF database with the aid of the Diffrac Eva software. The reference intensity ratio (RIR) method was used to semiquantify the minerals based on the dimensioning of all diffraction data in relation to the diffraction of the standard reference materials. Table 1 lists the summary of the chemical compositions of these samples, and Table 2 presents the minerals composing them.

Table(A2) 1 - Chemical summary of the Nb ores from the core and halos

XRF (wt%)	Ocher ore						Brown ore						Orange ore					
	halo N n = 14		core n = 5		halo S n = 31		halo N n = 19		core n = 20		halo S n = 10		halo N n = 31		core n = 45		halo S n = 25	
	Mean	SD	Mean	SD	Mean	SD	Mean	SD	Mean	SD	Mean	SD	Mean	SD	Mean	SD	Mean	SD
Al_2O_3	0.71	0.70	1.0	0.5	2.0	0.5	0.33	0.46	0.86	0.97	2.4	0.5	0.93	0.82	0.71	0.80	3.4	0.8
BaO	4.8	3.1	7.8	4.0	3.6	2.4	9.1	4.7	13	8	5.9	1.9	8.8	5.9	14	8	4.0	1.0
CaO	12	4	13	4	10	3	13	8	14	7	8.4	2.5	0.11	0.04	0.21	0.27	0.33	0.27
Fe_2O_3	36	6	29	7	28	5	46	15	37	12	39	3	67	8	54	13	56	3
LOI	11	5	12	6	7.6	2.4	4.5	1.1	5.2	1.5	7.6	0.7	5.2	1.5	6.7	1.6	8.0	1.3
MgO	8.1	3.7	7.5	5.1	7.6	3.4	0.49	0.36	0.49	0.36	0.65	0.56	0.57	0.23	0.36	0.15	0.40	0.08
MnO	0.73	0.12	0.54	0.13	0.76	0.19	0.77	0.15	0.94	0.50	1.2	0.3	1.3	0.3	1.2	0.5	1.6	0.4
Nb_2O_5	0.95	0.28	1.8	0.8	1.6	0.6	1.6	0.6	1.5	0.8	2.6	0.8	2.3	0.7	3.0	1.3	2.3	0.7
P_2O_5	6.3	3.1	8.3	4.6	8.6	2.8	12	5	12	5	11	2	2.1	0.7	2.7	1.4	6.1	1.2
PbO	0.027	0.020	0.055	0.028	0.042	0.037	0.039	0.013	0.042	0.035	0.072	0.037	0.044	0.017	0.161	0.235	0.082	0.044
SiO_2	11	6	9.8	4.4	18	3	3.4	2.0	3.8	3.3	11	4	2.6	1.0	4.4	3.7	7.3	3.3
SrO	0.38	0.36	0.96	0.30	1.1	0.2	0.54	0.34	1.1	0.4	0.94	0.23	0.04	0.06	0.27	0.15	0.52	0.10
Ta_2O_5	0.004	0.016	0.006	0.005	0.000	0.000	0.027	0.030	0.005	0.008	0.000	0.000	0.031	0.029	0.01	0.01	0.000	0.000
TiO_2	2.3	0.7	2.3	0.5	3.8	0.7	2.5	0.9	3.2	3.1	4.8	0.7	3.9	1.0	3.2	1.3	6.4	0.7

Resultados e discussão

Table 1 (cont.) - Chemical summary of the Nb ores from the core and halos

| LA-ICPMS (ppm) | Ocher ore | | | | | | Brown ore | | | | | | Orange ore | | | | | |
| | halo N n = 14 | | core n = 5 | | halo S n = 31 | | halo N n = 19 | | core n = 20 | | halo S n = 10 | | halo N n = 31 | | core n = 45 | | halo S n = 25 | |
	Mean	SD	Mean	SD	Mean	SD	Mean	SD	Mean	SD	Mean	SD	Mean	SD	Mean	SD	Mean	SD
La	1,984	598	1977	1,306	3,976	2,045	4,121	2,050	3,051	3,448	5,370	2,506	2,875	1,217	9,340	8,835	6,516	3,028
Ce	4,235	1,093	4,200	2,485	7,599	3,237	6,916	2,597	5,899	5,629	10,470	3,535	6,721	1,823	15,983	13,953	13,337	3,840
Pr	448	119	446	253	703	364	650.8	180	584	442.5	1,103	338	730.4	182	1,340	1,060	1,330	340
Nd	1518	394	1497	778	2319	977	2,135	603	1,982	1,342	3,136	797	2,656	702	4,351	3,053	3,787	804
Sm	178	41	174	68	304	180	247	52	224.7	88.2	370	72	334	74	386	189	456	140
Eu	41	9	42	14	70	45	58	14	53.72	17.57	80	19	79	16	80	33	106	34
Gd	80	15	88	32	154	95	120	33	112.41	35.86	179	47	157	31	162	63	236	80
Tb	8	2	10	3	15	8	12	4	12.577	4.059	18	5	16	3	17	7	24	8
Dy	32	10	41	15	51	26	50	19	52.48	16.92	70	25	63	16	71	29	91	32
Ho	4	1	6	2	6	3	7	3	7.385	2.47	9	4	8	2	10	5	13	5
Er	8	3	11	4	13	5	14	6	14.91	5.24	19	8	17	5	20	10	30	11
Tm	1	0	1	0	1	1	1	1	1.559	0.549	2	1	2	1	2	1	4	1
Yb	4	1	5	2	9	4	7	3	7.83	2.713	14	5	9	3	10	6	22	8
Lu	1	0	1	0	1	1	1	0	1.11	0.3995	2	1	1	0	1	1	3	1
Σ REE	8,540		8,500		15,221		14,340		12,005		20,842		13,667		31,774		25,955	
Th	554	108	749	193	910	563	881	199	626.4	247.2	1,377	424	1330	574	745	248	1108	298
Y	93	31	124	49	147	68	151	59	173.6	59	216	91	181	52	247	144	362	141
U (NDD)	0.350	0.201	0.215	0.160	0.016	0.011	0.572	0.220	0.154	0.244	0.055	0.034	0.624	0.197	0.170	0.131	0.053	0.025

Resultados e discussão

Table(A2) 2 - Average mineralogical compositions of ores from the core, halo N, and halo S regions.

Mineral (Mean)	XRD(%)	ocher ore			brown ore			orange ore		
		halo N	core	halo S	halo N	core	halo S	halo N	core	halo S
		n = 14	n = 4	n = 31	n = 19	n = 16	n = 10	n = 30	n = 28	n = 25
Hydrokenopyrochlore		<0.5	<0.5	<0.5	2	1	2	4	4	4
Hydroxycalciopyrochlore		1	2	2	1	2	2	n.d.	n.d.	n.d.
Fluorapatite		16	20	14	26	24	13	n.d.	n.d.	n.d.
Gorceixite/goyazite		1	n.d.	n.d.	1	3	13	4	2	16
Monazite		n.d.	<0.5	n.d.	1	<0.5	1	3	7	5
Barite		6	8	3	10	16	3	10	10	n.d.
Magnetite		3	5	1	7	3	4	7	3	n.d.
Hematite		4	5	6	10	9	12	18	10	9
Goethite		5	13	13	19	22	26	32	40	41
Ilmenite		3	2	1	3	3	2	3	3	2
Anatase/rutile		1	1	3	1	2	4	2	2	5
Dolomite		33	14	6	n.d.	n.d.	n.d.	n.d.	n.d.	n.d.
Norsethite		n.d.	2	n.d.	n.d.	n.d.	n.d.	n.d.	n.d.	n.d.
Quartz		5	9	14	4	3	9	3	5	7
Kaolinite		1	n.d.	n.d.	n.d.	n.d.	n.d.	n.d.	n.d.	n.d.
Gibbsite		<0.5	<0.5	n.d.	n.d.	n.d.	n.d.	n.d.	n.d.	n.d.
Vermiculite/Hydrobiotite		5	13	22	1	n.d.	n.d.	n.d.	n.d.	n.d.
Dickite		n.d.	n.d.	1	n.d.	n.d.	n.d.	n.d.	n.d.	n.d.
Illite		n.d.	n.d.	2	n.d.	n.d.	n.d.	n.d.	n.d.	n.d.

CBMM performed mineralogical studies at the mineral characterization laboratory of the University of São Paulo in 2016, in which an internal report was generated for CBMM with the identification of several mineral phases containing niobium (LCT-USP, 2016). Quantitative mineralogy was performed by the Mineral Liberation Analyzer (MLA-FEI) system coupled to a scanning electron microscope by energy dispersion. This study was performed only with samples of the orange ore from the core; none was from the halo regions. Three types of pyrochlore were identified: Ba-pyrochlore (69–75% of Nb_2O_5), Ca-Ba-pyrochlore (71–76% of Nb_2O_5), and a mineral composed of Nb+Ba+P+Th+REE+(OH) (45–62% of Nb_2O_5), interpreted as a product of Ba-pyrochlore weathering. In addition to pyrochlore, anatase, with up to 2.5% Nb_2O_5, goethite, with up to 7.5% Nb_2O_5, Nb+Fe(Ti+Si) oxide, with up to 64.3% Nb_2O_5, and Fe+Nb+Ti+Mn(+Al) oxide, with up to 37% Nb_2O_5 were also identified.

The LCT-USP (2019) characterized samples of the orange ore from the core using MLA-FEI with an emphasis on determining the mineralogical associations of pyrochlore. In the granulometric range in which pyrochlore is floated in Araxá, the release of pyrochlore in the characterized samples ranged from 65–86%, with pyrochlore primarily associated with goethite and gorceixite.

The data MR, U and U_3O_8 were subjected to normalization utilizing the minimum and maximum method. This methodology was employed for the purpose of maintaining confidentiality. Within the context of this article, these variables " are represented as non-dimensional data (NDD).

2.2.3 Geochemical, mineralogical, and pyrochlore flotation characteristics of ores from the core and the transition halos

Chemical characteristics of ores from the core and halos

To know the variation of the chemical contents of the halo N and S ores in relation to the ores of the core, the chemical analyzes of the 194 drill-core samples of the F-0XM9, F-5XIJ3, FAN2-06, FAS-37, FAS-31, and FAN2-12 drill-holes were considered (Fig. 1B and C). The same samples were analyzed with XRD for mineral identification. The region where Nb mineralization occurs was defined from the Nb_2O_5 contents of all drill-core samples present in the CBMM database. The outer perimeter of the transition halo was established based on a 0.5% Nb_2O_5 cut-off content, which corresponds to the Nb_2O_5 background of the carbonatite ring surrounding the core of the Complex. The average Nb_2O_5 contents of the ocher, brown, and orange ore in the main ore body, called "core," are respectively 1.8, 1.5, and 3.0%, while the average Nb_2O_5 contents in the halo N region were respectively 0.95, 1.6, and 2.3% and in the halo S region were 1.6, 2.6, and 2.3%.

The variations in the contents of Ce vs P_2O_5 (Fig. 3A-1–A-3), U vs PbO (Fig. 3B-1–B-3), Al_2O_3 vs SiO_2 (Fig. 3C-1–C-3), SrO vs TiO_2 (Fig. 3D-1–D-3), and CaO vs P_2O_5 (Fig. 3E-1–E-3) show how the chemistry of ocher, brown, and orange ores vary in the core, halo N, and halo S domains.

Resultados e discussão
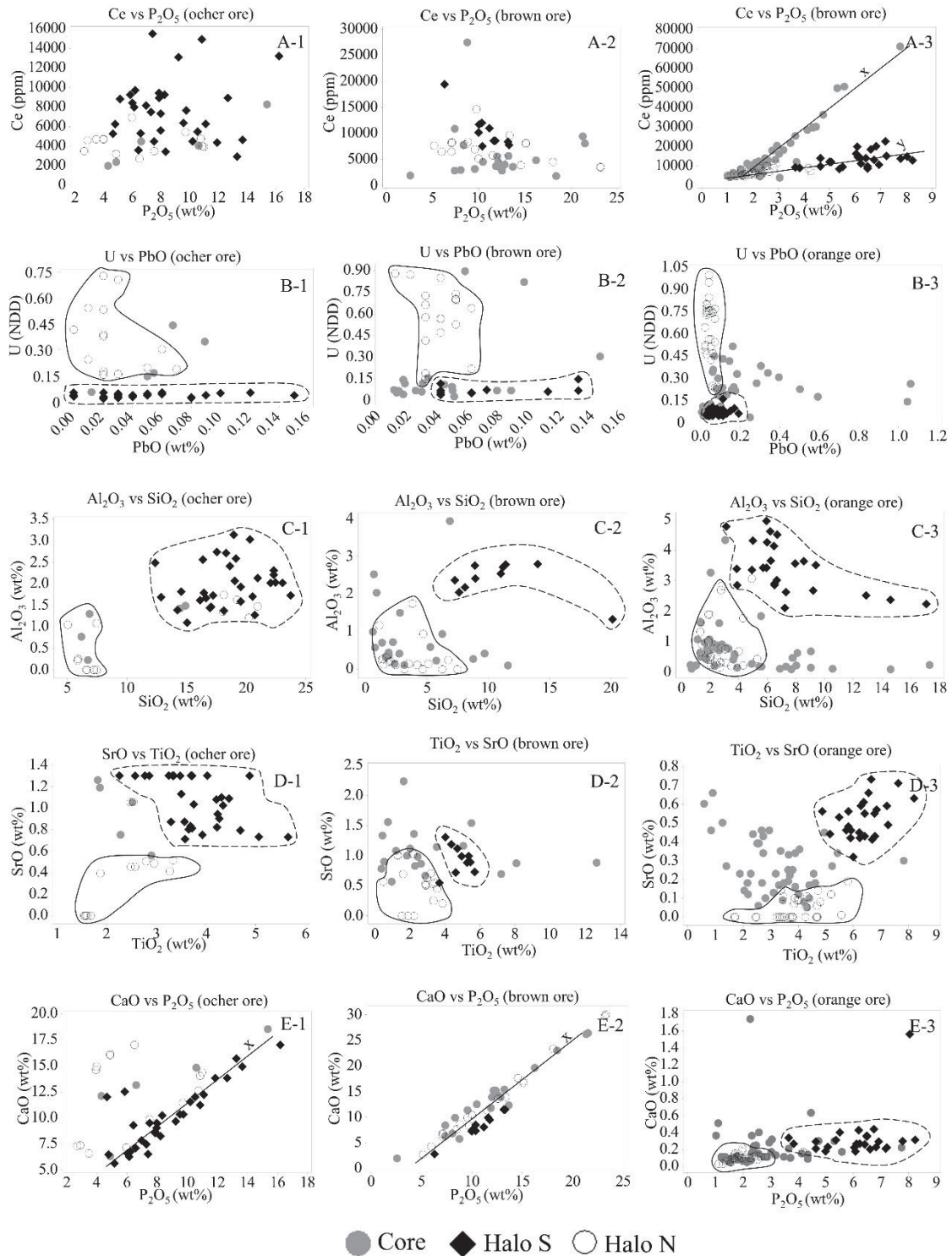
Fig.(A2) 3 - Scatter plot of oxides and elements in the three types of ore (ocher, brown, and orange). Ce vs P_2O_5 (A-1 to A-3), U vs PbO (B-1 to B-3), Al_2O_3 vs SiO_2 (C-1 to C-3), SrO vs TiO_2 (D-1 to D-3), CaO vs P_2O_5 (E-1 to E-3).

The variation of Ce vs P_2O_5 contents in the ocher and brown ores for the halo N, halo S, and core regions are equivalent (Fig. 3A-1 and A-2); however, with the

formation of the orange ore, we observed two correlation trends between these variables, one indicated by the "x" line and the other by the "y" line. Core samples follow the x-line trend, while halo N and halo S samples follow the y-line trend.

The U and PbO contents separate the three types of supergenic ores in the halo S region from that of the halo N region. (Fig. 3B-1–B-3). Halo S ores have lower U content than those observed in halo N for the three ore types (ocher, brown, and orange). The PbO concentrations in the ocher and brown ores of the halo S tend to be higher than those of the halo N. In the orange ore, the PbO contents of the halo N and the halo S are similar.

The SiO_2 and Al_2O_3 contents also separate the supergenic ores of the halo S and halo N (Fig. 3C-1–C-3). In this diagram, the SiO_2 and Al_2O_3 contents of the ocher, brown, and orange ores of the halo S are higher than those of the halo N, whereas the core ores present intermediate values to the ores of these two regions. In halo N ocher ore, the SiO_2 contents are less than 8%, and the Al_2O_3 contents are less than 1.2%, whereas, in the halo S, the Al_2O_3 contents are greater than 1.0%, and the SiO_2 contents are greater than 12% (Fig. 3A-1). In halo N brown ore, SiO_2 contents are less than 8%, and Al_2O_3 contents are less than 2%, whereas, in halo S, Al_2O_3 contents are greater than 2%, and SiO_2 contents are greater than 7% (Fig. 3B-1). In halo S orange ore, SiO_2 contents range from 4 to 18% and Al_2O_3 contents are greater than 2.0%, unlike in halo N orange ore, where SiO_2 contents are less than 6% and Al_2O_3 contents are less than 3% (Fig. 3C-3).

In the TiO_2 vs SrO diagram, SrO contents tend to be higher in the three types of ore in the halo S domain when compared to the ore from halo N and core domain (Fig. 3D-1–C-3). TiO_2 concentrations are also higher in halo S ores, particularly in orange ore, where TiO_2 contents reach 8%, against 4% for halo N (Appendix 1).

The CaO and P_2O_5 contents of the ocher and brown ores from the three regions (halo N, halo S, and the core) show similar behavior (Fig. 3E-1 and E-2). In the orange ore, this ratio between CaO and P_2O_5 individualizes the halo S and halo N ores (Fig. 3E-3). The halo S orange ore has higher P contents, reaching 8.5%, whereas the P contents of the halo N orange ore do not exceed 3%.

Mineral characteristics of ores from the core and the transition halos

Table 2 shows the average mineral compositions of the ores from the core, halo N, and halo S regions. The pyrochlore contents are similar for the three types of ore in each of these regions. In the orange ore, the amount of hydrokenopyrochlore for the ores of the three regions varies on an average from 3% to 4%, and hydroxycalciopyrochlore was not detected. Hydroxycalciopyrochlore appears in the brown ore of the three regions in average concentrations ranging from 0.8% to 1.8%; however, hydrokenopyrochlore is still the predominant Nb mineral in this ore, with average content ranging from 1.0% to 2.5% (Fig. 4A). In the ocher ore, hydroxycalciopyrochlore is the predominant Nb mineral, with content ranging from 1.0% to 2.0%, whereas the hydrokenopyrochlore in the halo S and core ranges from 0% to 1%, and it was not detected in the N halo (Fig. 4A).

Resultados e discussão
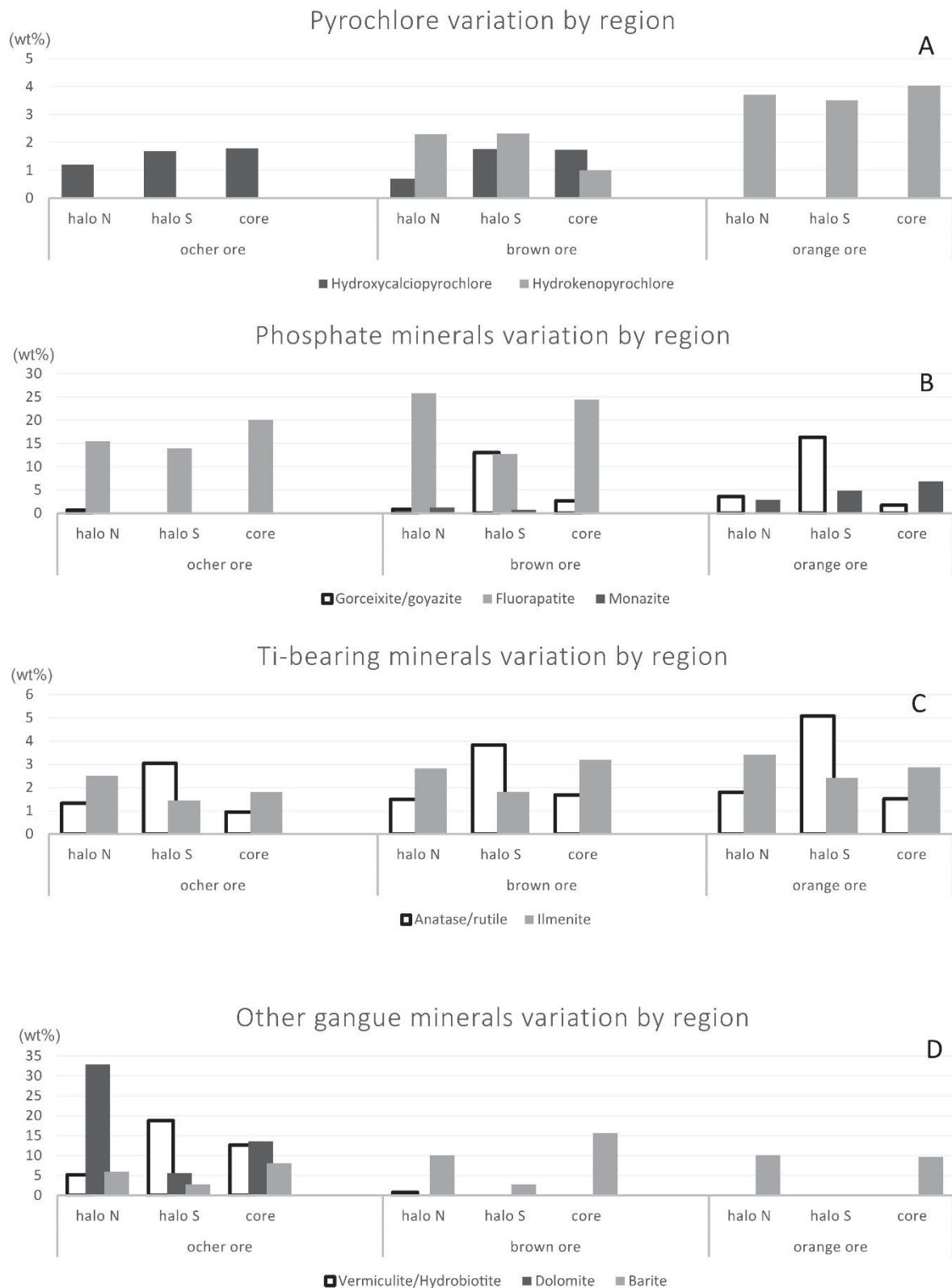
Fig.(A2) 4 - Bar graphs with the main minerals determined and quantified by XRD. (A) Pyrochlore variation by ore type and region. (B) Phosphate minerals variation by ore type and

Resultados e discussão

region. (C) Ti minerals variation by ore type and region. (D) Vermiculite/hydrobiotite, dolomite, and barite variation by ore type and region.

Fluorapatite is the predominant phosphate mineral in ocher and brown ores in the three regions (halo N, halo S, and the core). The contents of gorceixite and monazite gradually increased from ocher to orange ore. Fluorapatite was not detected in the orange ore of the three regions. The concentrations of gorceixite were higher in the orange ore of halo S, averaging 16%. In halo N, this value dropped to 4%. In the core, it was 2%. Monazite concentrations were higher in the core orange ore, with an average of 7% (Fig. 4B).

The halo S region had the highest anatase/rutile contents in the three types of ore, with an average content of 3%, 4%, and 5%, in ocher, brown, and orange ores, respectively (Fig. 4C). In the core, halo N, and halo S regions, the average ilmenite contents were similar, ranging from 1% to 3% in the three types of ore (Fig. 4C).

In the ocher ore, the highest concentrations of dolomite were in the halo N, with an average content of 33%. In halo S, the mean concentration of dolomite was 6% (Fig. 4D). Vermiculite was more concentrated in the halo S ocher ore, with an average concentration close to 22%, whereas in halo N, the average concentration was 5%. In the ocher ore, the barite contents of the core region and halo N were similar, ranging on an average from 6% to 8%. In halo S, this average concentration was 3%. Barite concentrations increased in the brown ore, exceeding by 10% the average concentration in halo N ore, 16% in the core, and 3% in halo S. Barite was not detected in the halo S orange ore, whereas there was barite, on an average of 10%, in the core and halo N orange ore (Fig. 4D).

The mineral dickite was found in samples of ocher ore from the FAS-31 drill-hole in the halo S region, in concentrations ranging from 0 to 11%. The illite mineral was found in the halo S ocher ore, specifically in samples from the FAS-37 drill-hole, in concentrations of up to 36% (Appendix 1).

MR of the ores from the core and transition halos

Samples of ocher, brown, and orange ores from the three regions (core, halo N, and halo S) were submitted to mineral processing tests, as described in the Analytical Methods. The best MR (NDD) results were for the brown and orange ores from the core region, with average values of 0.84 and 0.87, respectively (Table 3). In the ocher ore, only one sample from the core region had a value of 0.13, whereas the other tests with samples of this ore, regardless of the region, did not produce pyrochlore concentrate (Fig. 5). The halo N brown and orange ores showed the worst performance during the flotation test, with an average MR of 0.22 NDD. Normalized metallurgical

recoveries of halo S ores are intermediate between halo N and the core, with average values of 0.44 in brown ore and 0.66 in orange ore (Table 3).
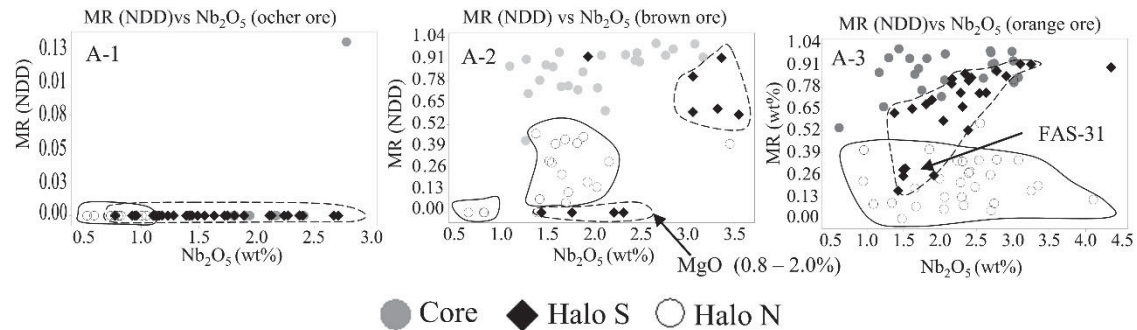
Fig.(A2) 5 - Scatter plot of the Nb_2O_5 vs MR. (A-1) In the ocher ore. (A-2) In the brown ore. (A-3) In the orange ore.

Table (A2) 3 - Summary of the metallurgical recovery results

Region	Variable	ocher ore (n = 54)				brown ore (n = 53)				orange ore (n = 82)			
		Mean	SD	Min	Max	Mean	SD	Min	Max	Mean	SD	Min	Max
halo N	MR (NDD)	0.00	0.00	0.00	0.00	0.22	0.17	0.00	0.46	0.23	0.17	0.00	0.82
	Nb_2O_5 (wt%)	0.9	0.3	0.5	1.4	1.6	0.6	0.7	3.5	2.3	0.7	0.9	4.1
core	MR (NDD)	0.02	0.05	0.00	0.13	0.84	0.14	0.14	1.00	0.84	0.14	0.14	1.00
	Nb_2O_5 (wt%)	2.1	0.4	1.6	2.8	2	0.6	1.1	3.2	2.3	0.7	1.4	4.4
halo S	MR (NDD)	0.00	0.00	0.00	0.00	0.44	0.40	0.00	0.92	0.66	0.23	0.17	0.91
	Nb_2O_5 (wt%)	1.6	0.6	0.8	2.7	2.6	0.8	1.4	3.5	2.1	0.7	0.6	3.1

2.2.4 Discussion

South halo ores formation

The main characteristics that differentiate the halo S ocher ore from the ocher ore of other regions are the high concentrations of vermiculite and anatase/rutile (Fig. 4C and 4D), the lower concentration of CaO, the significantly high concentrations of SiO_2 and Al_2O_3 (Table 1), and the presence of dickite and illite (Table 2). Vermiculite indicates that the rock that gave rise to the ocher ore in this region probably contained high concentrations of phlogopite and/or tetraferriphlogopite, as observed by Azzone and Ruberti (2010) in the Catalão I alkaline–carbonatitic ultramafic Complex. According to these authors, vermiculite and hydrobiotite would be products of the weathering of phlogopite and tetraferriphlogopite. In rocks, these phyllosilicates may belong to different paragenesis, including phlogopite/tetraferriphlogopite formed by metasomatic processes in rocks containing pyroxene and/or olivine, as already observed by Issa Filho et al. (2001). Muscovite normally weathers directly to illite; therefore, the vermiculite/hydrobiotite observed in the halo S ocher ore could not be the result of the weathering of a rock formed by the assimilation of the mica-schists of the Ibia Group by the carbonatite. However, the high levels of Al_2O_3 and SiO_2 in the halo S ores (Fig.

3) and the presence of dickite and illite in the samples from the FAS-31 and FAS-37 drill-holes suggest possible assimilation of the mica-schists from the Ibia group by the carbonatites surrounding the phlogopitites of the Complex's core. For the simultaneous assimilation of the mica-schists and the phlogopitic breccia by the carbonatite to have occurred, the phlogopitic nucleus would have to be lodged first in the Complex, unlike what Issa Filho et al. (2001) and Traversa et al. (2001) claimed.

The halo S protore was likely a rock formed by the assimilation during carbonatitic magmatism, of phlogopitites and mica-schists, which generated a high concentration of vermiculite, anatase, SiO_2, and Al_2O_3 and the occurrence of dickite and illite. Vermiculite would have been better preserved in the ocher ore of this region due to a differential weathering, which could be related to this simultaneous rock assimilation as in the region of the core of the Complex, the thickness of the ocher ore is negligible, whereas, in the halo S region, it can reach 80 m (Fig. 1C).

Unlike vermiculite, which is more easily weathered, anatase is relatively stable, causing it to be residually concentrated during weathering. Their maximum concentrations are observed in the halo S orange ore (Fig. 4C). These titanium minerals indicate that the rock that gave rise to the halo S ores also contained high concentrations of these minerals, reinforcing the idea that this halo is a product of the assimilation, mainly of phlogopitites. Alternatively, according to the proposal by Ribeiro et al. (2014), the supergenic Ti deposits of Salitre, Serra Negra, and Tapira would have originated from the differentiation of alkaline and carbonatitic magmas, with the formation of bebedouritic rocks rich in perovskite. Different from what occurs in those Complexes, the higher concentration of anatase in the halo S ores could be associated with carbonatitic magmatism as in mica-schists, the concentrations of these minerals are small, and those of the core ores, generated from phlogopitites, are smaller than those of halo S.

North halo ores formation

The halo N ocher ore had the highest concentration of dolomite, with an average content of 33% (Table 2). The concentrations of the main minerals detected in the halo N are similar to those of the core ores (Fig. 4). In contrast, chemical signatures reveal ores with distinct characteristics. The high concentrations of U (Fig. 3B-1, B-2, and B-3) in the halo N ocher, brown, and orange ores have the most evident differences. Furthermore, the halo N ores are also characterized by low concentrations of Al_2O_3, SiO_2, SrO, and TiO_2, when compared to the contents of these elements in the halo S and core ores (Fig. 4).

In halo N, U contents are positively correlated with Nb_2O_5 in the three types of ores (Fig. 6). The best correlation ($R^2 = 0.63$) was observed in the orange ore, where the Nb_2O_5 and U contents are higher. The positive correlation of these elements indicates that pyrochlore could be associated with some U-bearing mineral or that U could be in the pyrochlore structure. According to Huang et al. (2022), in the polymetallic deposit of U-Nb, in the orogen north of Qinling (central China), uraniopyrochlore associated with uraninite occurs. These authors argue that the mineralization in U could be associated with the carbonatitic magmatism of this province and the high-temperature hydrothermal events enriching the carbonatite with more U. In addition, they believe that the perfect correlation between U and Nb of this deposit suggests that the higher U contents would be a consequence of the magmatic

origin, and some samples with a higher or lower Nb/U ratio locally represent the enrichment or impoverishment of the rock caused by the hydrothermal alteration. In the present work, only mineralized regoliths and saprolites were analyzed, and extracting information on the primary origin of U and Nb would not be simple. However, it is likely that the enrichment in U also occurred in two phases: one magmatic, due to the intrusion of carbonatite enriched in U and, eventually, in Nb, which would have assimilated the phlogopitic rock rich in Nb, and another hydrothermal. The hydrothermal events could have altered the characteristics of the primary pyrochlore and further concentrated the U. The higher concentrations of dolomite in the halo N ocher ore support the interpretation that a carbonatitic magma assimilated phlogopitites in this region.
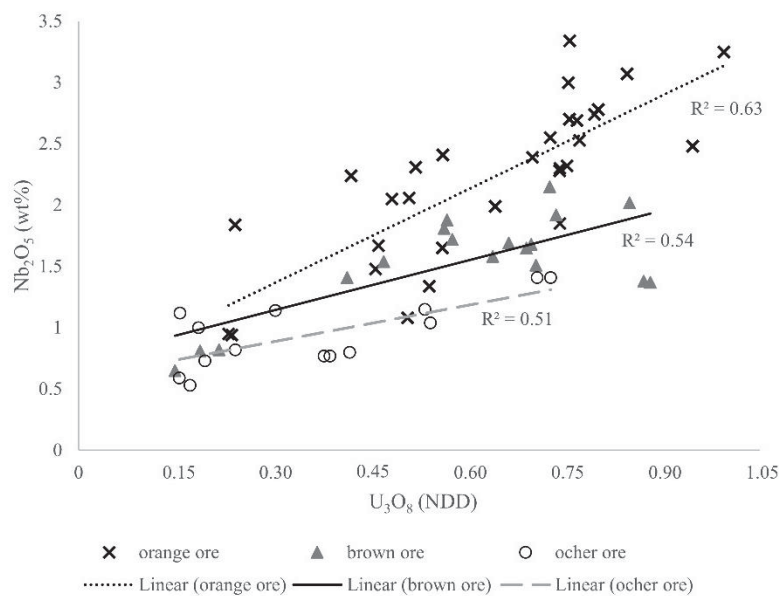
Fig.(A2) 6 - Scatter plot of the Nb_2O_5 vs U_3O_8 in the halo N region.

Influence of the ores from the core and transition halos on MR

The orange and brown ores of the transition halos have lower geometallurgical performance than the core ores (Fig. 7A). This study indicates three primary reasons for the loss of geometallurgical performance:

(1) The presence of contaminating minerals, such as clay minerals (e.g., kaolinite) and gibbsite, which occur on top of the orange ore and cause the phenomenon of slime coating, when fine particles cover the mineral of interest, impairing flotation (Yu et al., 2017). Apatite occurs in brown ore, whereas in the ocher ore, in addition to apatite, there are carbonates that consume acid, used to reduce the pH during pyrochlore flotation, making it impossible to stabilize the pH in the proper range (Bulatovic, 2010). These minerals also release calcium ions, impairing the interaction of the flotation collector with pyrochlore (Gibson, 2016). Vermiculite also occurs in the ocher ore and impairs the pyrochlore flotation process as it competes with it in the adsorption of the collector.

(2) The presence of other niobium-bearing minerals besides pyrochlore. Currently, the mineral beneficiation process is suitable for concentrating pyrochlore; however, niobium can occur in other minerals that do not respond to the flotation process similarly, such as goethite and anatase (LCT-USP, 2016).

(3) Texture aspects also interfere in the flotation process as the mineral processing adopted does not perform well when the pyrochlore is not well formed and in grains with adequate size. This is the case when there is an association of pyrochlore microcrystals with other minerals, e.g., with goethite and gorceixite in the core orange ore (LCT-USP, 2019).
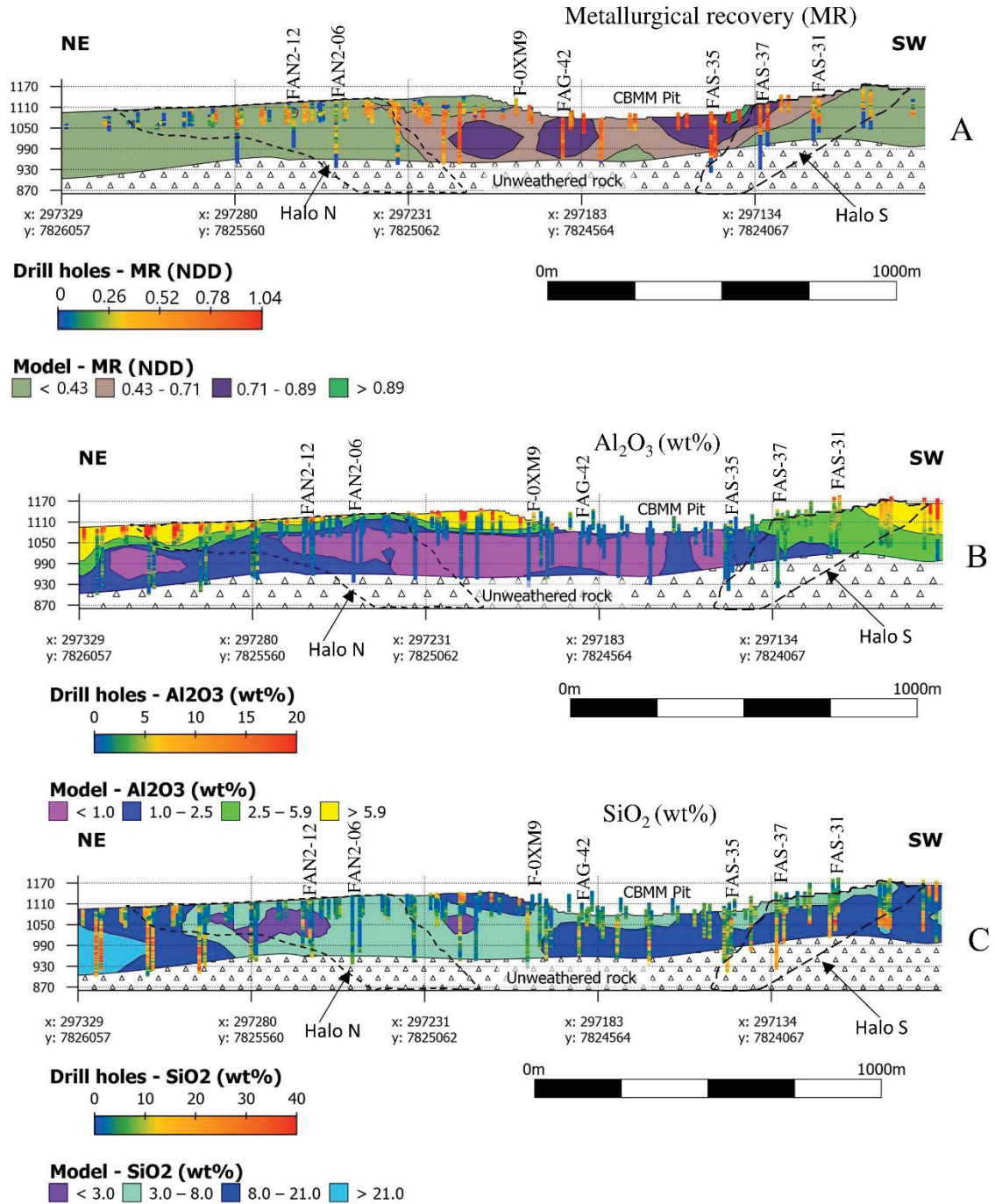
Fig.(A2) 7 - MR and chemical NE–SW sections through the Araxá Complex. (A) MR section. (B) Al_2O_3 section. (C) SiO_2 section.

The ocher ore generally occurs below the brown ore, even though a direct transition from orange to ocher may occur (Fig. 1C). The pyrochlore in the ocher ore from the core, halo S, and halo N regions was not concentrated during the flotation test (Fig. 5A). This may have occurred due to the following reasons: (a) high presence of contaminants, such as vermiculite, and particularly dolomite, which partially solubilizes in the acid pulp necessary for pyrochlore flotation; (b) the presence of vermiculite that

impairs flotation because it has similar behavior to pyrochlore in flotation; (c) the main Nb mineral is hydroxycalciopyrochlore and not hydrokenopyrochlore.

Although the brown ore from the core region contains similar proportions of hydroxycalciopyrochlore and hydrokenopyrochlore, the geometallurgical performance of this ore in the flotation test recovered an average of 0.84 NDD of the pyrochlore present in the sample (Table 3). This suggests that hydroxycalciopyrochlore was also being recovered with the flotation procedure adopted.

Thus, the ocher ore from the three regions is more likely to not have a good recovery due to the presence of deleterious minerals. Bearing in mind that dolomite and vermiculite are the primary Mg-bearing minerals detected by XRD (Table 2), the impact of MgO contents above 0.8% on MR is clear, which, on a laboratory scale, does not occur for CaO contents.

Some samples characterized as ocher ore, primarily from the halo S, do not contain dolomite (Appendix 1) but have high concentrations of vermiculite in some cases above 30%. This suggests that vermiculite can also impair the pyrochlore concentration process, as the pyrochlores present in these samples did not float. The poor performance was attributed to the fact that vermiculite has the ideal isoelectric point at pH 2.9 (Padilla-Ortega et al., 2013), significantly similar to the ideal pH range for the isoelectric point of pyrochlore, which is between 2.7 and 3.0 (Gibson, 2016; Gibson et al., 2021; Ni and Liu, 2013; Oliveira et al., 2001). As the pyrochlore concentration process is performed by flotation with cationic amine collectors under acidic pulp conditions (Gibson et al. 2015a), vermiculite and pyrochlore compete for collector adsorption as the two minerals are superficially electronegative.

According to Gibson et al. (2015a) and Bulatovic (2010), in some cases, carbonates must first be removed with a gangue reverse flotation step to achieve and maintain a stable pulp pH. This carbonate flotation process could enable the use of the pyrochlore in the ocher ore; however, if the vermiculite impairs the pyrochlore flotation, enabling a process to remove the silicates before the pyrochlore flotation would be necessary. Prior removal of silicates is practiced in the Catalão operation using an ether-amine and starch collector to depress the pyrochlore (Gibson, 2016). The process of direct flotation of pyrochlore would also be an alternative, as evaluated by Gibson et al. (2015a), where carbonate rock tailings samples were floated with benzohydroxamic acid as a collector and sodium hexametaphosphate as a modifying agent; however, this process has not yet been made feasible on an industrial scale.

The core brown ore showed an average MR of 0.84 NDD, similar to the core orange ore 0.87 NDD (Table 3). The recovery of most samples of halo S brown ore exceeded 0.52 NDD; however, another portion did not generate pyrochlore concentrate (Fig. 5B). Although XRD analysis of these samples did not detect the presence of any MgO minerals, samples that do not recover pyrochlore contain MgO concentrations between 0.8% and 2.0%. This small amount of MgO in the ore would probably be enough to inhibit the pyrochlore flotation.

Most samples of the halo N brown ore showed metallurgical recoveries between 0.13 and 0.52 NDD (Fig. 5B). The impact of the presence of contaminants in the ore usually presents another profile of MR, such as, for example, caused by small concentrations of kaolinite or gibbsite in the orange ore, which are sufficient to prevent pyrochlore flotation and MR be equal to zero.

Apatite is the main Ca-bearing mineral in the brown ore of the three regions (Fig. 4B). Despite the presence of Ca, in geometallurgical laboratory tests with the core and halo S ores, there was no impairment in the recovery of pyrochlore (Fig. 5B), suggesting that, on the laboratory scale, apatite does not interfere with the flotation of pyrochlore. Thus, the low MR of the samples of the brown halo N ore is more likely to be associated with the presence of Nb in some other mineral than hydrokenopyrochlore and hydroxycalciopyrochlore or with some textural problem in these ore minerals, affecting their releases during flotation, as already observed in the LCT-USP report (2019). This is confirmed because no contaminating minerals were detected in the XRD of this ore.

Although apatite did not harm the pyrochlore flotation process on a laboratory scale, feeding the beneficiation plant with an ore containing small amounts of apatite harms the pyrochlore flotation process. The reason for this production loss is still unclear; however, there is a possibility that apatite is being solubilized during the industrial process, enriching the water with Ca^{2+} and making it difficult to obtain the optimal pH for pyrochlore flotation. A similar observation was made by Gibson (2016), where Niobec pyrochlore ore samples were subjected to direct flotation. Gibson noticed that when the scale of the test went up to the pilot level, the process of direct flotation of pyrochlore suffered instability due to the high amounts of calcium dissolved in the water, the recirculation of the water, and the dissolution of the microcrystalline calcite, factors that depressed the pyrochlore flotation. One of the probable reasons for the apatite from the brown ore of Araxá not being solubilized during the laboratory test would be the longer exposure time of the apatite in an acidic pH environment during the industrial process.

Fig. 7 was generated by the implicit numerical modeling of the variables MR (Fig. 7A), Al_2O_3 (Fig. 7B), and SiO_2 (Fig. 7C), using the database of all CBMM drill-hole samples. MR above 0.43 NDD was concentrated in the central region of the NE–SW profile (Fig. 7A). In the halo N and S regions, the MR is generally below 0.43 NDD. This same region has SiO_2 (Fig. 7C) and Al_2O_3 (Fig. 7B) values lower than those in the halo S and core regions, indicating low concentrations of clay minerals in the halo N ores. It is important to remember the good correlation between Nb_2O_5 and U in the three types of halo N ores shown in Fig. 6. This good correlation indicates that the pyrochlore in this region could be enriched in U, which can generate physicochemical conditions that influence the flotation process and problems for the refining of the concentrate. Another possibility for the good correlation of Nb_2O_5 contents with U would be the association of pyrochlore with some U-bearing minerals. In this case, this association could influence its release, harming the flotation process with the reduction of recovered pyrochlore.

The core orange ore presents metallurgical recoveries above 0.52 NDD, showing that the flotation process for this ore is adequate.

Part of the flotation results for halo S orange ore is above 0.52 NDD, with values significantly close to those obtained with the core orange ore. The results are below 0.52 NDD elsewhere. MR values below 0.52 NDD are from FAS-31 drill-hole samples (Fig. 7B), far from the core, having higher Al_2O_3 content (Fig. 7A). The high concentration of Al_2O_3 would be associated with the presence of gorceixite/goyazite (Fig. 4B) and, perhaps, clay minerals (not detected in XRD analyses). These minerals would originate from the weathering of illite, dickite, vermiculite, and apatite in the ocher and brown ores. According to Gibson et al. (2015), amine and collectors for pyrochlore

flotation are sensitive to the presence of clay minerals. Although the Araxá operation also concentrates niobium from ultrafine particles, it is common to remove the fraction smaller than 15 μm before flotation, in a desliming operation. As it is likely that the loss of geometallurgical performance of the halo S orange ore, mainly those farthest from the core, is associated with the presence of clay minerals, an alternative to increasing recovery would be the use of dispersants and desliming agents.

The MR of the halo N orange ore shows the same range of values observed in the brown ore from the same region, below 0.52 NDD in all tests (Fig. 5C). The similarity between the geometallurgical behavior of the orange and brown ores suggests that, if the problem of low recovery of these ores is associated with the presence of some other Nb mineral, this mineral would most likely have been generated during the carbonatitic magma intrusion process or by hydrothermalism, but not by weathering. In this sense, Braga and Biondi (2022) observed that there would be a formation of Nb-goethite from the incorporation by goethite of Nb released by the weathering of pyrochlore. In addition, characterization studies carried out at the technological characterization laboratory at the University of São Paulo (LCT-USP, 2016), demonstrated the occurrence of Nb in the structure of anatase, Nb+Fe+Ti+Si oxide, Fe oxide +Nb+Ti+Mn+Al, and Nb-bearing goethite; however, none of the samples studied by the LCT-USP is from the halo N region. It may be that in the halo N ore, there is some other mineral containing Nb that has not yet been identified, such as, for example, uranopyrochlore or another mineral that contains U, as indicated by the good correlation observed between U_3O_8 and Nb_2O_5 (Fig. 6).

2.2.5 Conclusions

The Araxá Complex is a geological unit containing the largest known niobium deposit in the word, presenting resources in saprolitic and regolithic ores, formed by the weathering of phlogopitites, carbonatites, and magnetite-apatitites existing in the Complex core. Historically, niobium ore mining occurred in the orange ore formed by the weathering of the phlogopithitic breccia, characterized by Nb_2O_5 contents above 0.5% and CaO and MgO contents below 2%. Due to the distinct behavior during the geometallurgical testing of the niobium ores of the Complex, it was observed that there are saprolites and regoliths mineralized in niobium whose geometallurgical properties are inferior to those of the core ores. This new type of ore forms a transition halo that surrounds the main Nb-mineralized body located at the core of the Complex. The regions where these ores occur were called halo N and halo S. The transition halo ores present MR generally below 0.65 NDD.

XRF analyses showed that variations in the contents of U vs PbO, Al_2O_3 vs SiO_2 and SrO vs TiO_2 indicate compositional differences in the three types of ores (ocher, brown, and orange) of the halos S and N, reflecting different compositions of the rocks that gave rise to these ores. Furthermore, minerals such as vermiculite, anatase, dikite, illite, and dolomite were significant to justify the formation of transition halos of Nb mineralization.

Uranium proved to be suitable for classifying the halo N ore as this region has U_3O_8 values generally above 0.3 NDD, unlike the core and halo S ores, with concentrations generally lower than 0.15 NDD. Furthermore, the contents of Nb_2O_5 and U_3O_8 are positively correlated, indicating that uranium may be present in the pyrochlore structure or even associated with it in the form of another mineral, such as

uraninite, which could affect the pyrochlore flotation yield of the ore from this region or also change the characteristics of the pyrochlore concentrate. Additionally, the halo N ocher ore showed the highest dolomite content among the ocher ores of the three regions. These pieces of evidence suggest that some magmatic events, probably a carbonatitic intrusion associated with hydrothermal events, were responsible for generating the U anomaly of the halo N region.

Halo S ores have higher contents of Al_2O_3, SiO_2, and TiO_2. The vermiculite and anatase contents of the ocher ore from this region are higher than those of the ocher ores from the other regions. This suggests that the halo S ocher ore may have originated from the simultaneous assimilation of the mica-schists of the Ibia group and the phlogopites from the Complex core during the intrusion of the carbonatites surrounding the core of the Complex.

The geometallurgical test of the core, halo N, and halo S ocher ores did not produce pyrochlore concentrate, most likely because of the presence of dolomite and vermiculite, two minerals that impair pyrochlore concentration by flotation. We realized that the presence of MgO contents above 0.8% in the ore would be sufficient to inhibit the current pyrochlore flotation process. The main minerals with MgO detected by XRD are dolomite and vermiculite. Dolomite interferes with the Nb flotation process when it releases Ca and Mg ions, which makes it impossible to stabilize the appropriate pH range (2.7–3.0) for pyrochlore flotation. Vermiculite, however, has an ideal isoelectric point at pH 2.9, similar to the ideal pH range for the isoelectric point of pyrochlore, causing it to compete with pyrochlore in the adsorption of the collector, impairing the MR of pyrochlore.

The halo N orange and brown ores showed low geometallurgical performance, probably due to the presence of other Nb-bearing minerals than pyrochlore, such as, for example, Nb-goethite, anatase, or some (Nb, U)-bearing mineral, as suggested by the good correlation observed between U_3O_8 and Nb_2O_5. Alternatively, the poor MR would be a consequence of some morphological or textural aspect involving the pyrochlore of this region that would influence, for example, the degree of release of these minerals as no contaminating mineral was detected that justifies the low geometallurgical performance of this ore.

Part of the halo S brown and orange ore samples showed metallurgical recoveries above 0.65 NDD, and another part had MR below 0.65 NDD. The good metallurgical recoveries observed in the brown ore indicate that the hydroxycalciopyrochlore was also floated, the process being suitable not only for the flotation of the hydrokenopyrochlore, predominant in the orange ore. In the halo S brown ore, samples that recovered below 0.65 NDD have MgO content ranging from 0.8% to 2%, and the presence of low concentrations of vermiculite or dolomite may be responsible for the poor recovery results. In the halo S orange ore, the samples that had low metallurgical performance were collected at locations further away from the core, where the Al_2O_3 contents are higher. This indicates that contaminating clay minerals, such as kaolinite, or the presence of gibbsite, would be responsible for the low Nb recoveries during flotation.

Resultados e discussão

Declaration of competing interests: The authors have no conflicts of interest to declare.

References

Almeida, F.F.M., 1967, Origem e evolução da Plataforma Brasileira: Boletim da Divisão de Geologia e Mineralogia (DNPM), v.241, p.36.

Almeida, F.F.M., 1983, Relações tectônicas das rochas alcalinas mesozóicas da Região Meridional da Plataforma Sul-Americana: Revista Brasileira de Geociências, v.13, p.139-158.

Azzone, R. G., Ruberti, E., 2010, Evolução composicional dos filossilicatos no perfil intempérico do Complexo ultramáfico Alcalino-carbonatítico de Catalão I (GO): Geologia USP - Série Científica, v.10, p.23-43.

Braga Junior, J.M., and Biondi, J.C., 2022, Geology, geochemistry and mineralogy of regolith and saprolite ore with Nb, P, Ba, REEs (+ Fe) in mineral deposits from the Araxá alkali carbonatite Complex, Minas Gerais state, Brazil: Economic Geology, submitted, unpublished, 81p.

Bulatovic, S., 2010, Flotation of niobium - Handbook of Flotation Reagents - Chemistry, Theory and Practice: Elsevier B.V, v.2, p.111-125.

da Silva Lima, L., Alvarenga, R.A., de Souza Amaral, T., Nolli, P.D.T.G., & Dewulf, J., 2022, Life cycle assessment of ferroniobium and niobium oxides: Quantifying the reduction of environmental impacts as a result of production process improvements: Journal of Cleaner Production, v.348, 131327.

Traversa, G., Gomes, C. B., Brotzu, P., Buraglini, N., Morbidelli, L., Principato, M. S., and Ruberti, E., 2001, Petrography and mineral chemistry of carbonatites and mica-rich rocks from the Araxá Complex (Alto Paranaíba Province, Brazil): Anais da Academia Brasileira de Ciências, v.73, p.71-98.

Gibson, S.A., Thompson, R.N., Leonardo, O.H., Dickin, A.P., Mitchell, J.G., 1995, The Late Cretaceous Impact of the Trindade Mantle Plume - Evidence from Large-volume, Mafic, Potassic Magmatism in SE Brazil: Journal of Petrology, v.36, p.189-229.

Gibson, C.E., Kelebe, S., Aghamirian, M., Yu, B., 2015a, Flotation of pyrochlore from low grade carbonatite gravity tailings with benzohydroxamic acid: Minerals Engineering, v.71, p.97-104.

Gibson, C.E., Kelebek, S., and Aghamirian, M., 2015b, Niobium oxide mineral flotation: A review of relevant literature and the current state of industrial operations: International Journal of Mineral Processing, v.137, p.82-97.

Gibson, C.E., 2016, The Flotation of Niobium Oxide Minerals from Carbonatite Ores. Doctoral dissertation, 334P.

Gibson, C.E., Kelebek, S., Aghamirian, M., 2021, Pyrochlore flotation from silicate gangue minerals - Amine adsorption mechanisms and th effect of modifying reagents: Minerals Engineering, v.171, 107100.

Gomes, C.B., Ruperti, E., and Morbidelli, L., 1990. Carbonatite Complexes from Brazil: a review: Journal of South American Earth Sciences, v.3, p.51-63.

Grossi-Sad, J.H., Torres, N., 1971, Geologia e recursos minerais do Distrito do Barreiro, Araxá, Minas Gerais: Relatório DNPM/GEOSOL, Unpublished, 35p.

Huang, H., Wang, K.X., Cuney, M., Pan, J.Y., Bonnetti, C., Liu, X.D., and Zhong, F.J., 2022. Mesozoic magmatic and hydrothermal uranium mineralization in the Huayangchuan carbonatite-hosted U-Nb-polymetallic deposit, North Qinling Orogen (Central China) - Evidence from uraninite chemical and isotopic compositions: Ore Geology Reviews, v.146, 104958.

Issa Filho, A., Riffel, B.F., Sousa, C.A.F., 2001, Some aspects of the mineralogy of CBMM niobium deposit and mining and pyrochlore ore processing – Araxá, MG – Brazil. In: International Symposium on Niobium. Proceedings. Orlando. Patherson, 15p.

LCT–USP, 2016, Caracterização mineralógica em amostras de minério de nióbio – Minerais portadores de nióbio no Complexo alcalino de Araxá: Internal, unpublished report of the LCT–USP, 21p.

LCT–USP, 2019, Caracterização mineralógica em amostras de minério de nióbio – Produtos de moagem e finos naturais: Internal, unpublished report of the LCT–USP, 43p.

Morbidelli, L., Gomes, C.B., Beccaluva, L., Brotzu, P., Conte, A.M., Ruberti, E., and Traversa, G., 1995, Mineralogical, petrological, and geochemical aspects of alkaline and alkaline-carbonatite associations from Brazil: Earth-Science Reviews, v.39, p.135-168.

Ni, X., Liu, Q., 2013, Adsorption behaviour of sodium hexametaphosphate on pyrochlore and calcite: Canadian Metallurgical Quarterly, v.52:4, p.473-478.

Oliveira, T.F., Saraiva, S.M., Oliveira, A.P.A., Telhado, A., Nard, R., 2001, Investigation on the effect of collector, activator, and depressant on the selective flotation of pyrochlore and barite: Conference Proceeding - VISHMMT, XVIII ENTMME, Rio de Janeiro, Brazil.

Padilla, O.E., Leyva, R.R., Mendoza, B.J., 2013, Role of electrostatic interactions in the adsorption of cadmium (II) from aqueous solution onto vermiculite: Applied Clay Science, v.88, p.10-17.

Ribeiro, C.C., Brod, J.A., Junqueira, T.C., Gaspar, J.C., Palmieri, M., Cordeiro, P., and Gomide, C.S., 2014. Potencial e controles metalogenéticos de ETR, Ti e Nb em províncias alcalino-carbonatíticas brasileiras: Metalogenia das Províncias Tectônicas do Brasil, p.559-589.

Sonoki, I.K., Garda, G.M., 1988, Idades K / Ar de rochas alcalinas do Brasil Meridional e Paraguai Oriental – Compilação e adaptação às novas constantes de decaimento: Boletim IG – USP, Série Científica, v.19, p.63-85.

Ulbrich, H.H.G.J., and Gomes, C.B., 1981, Alkaline rocks from continental Brazil: Earth-Science Reviews, v.17, p.135-154.

Yu, Y., Ma, L., Cao, M., Liu, Q., 2017, Slime coatings in froth flotation - A review: Minerals Engineering, v.114, p.26-36.

APPENDIX 1 - Powder XRD from F-0XM9, F-5XIJ3, FAN2-06, FAS-37, FAS-31, and FAN2-12 drill-hole core samples.

Click here to access/download
Supplementary files (e-component)
Appendix A_ok.pdf

3   CONSIDERAÇÕES FINAIS

No Complexo Alcalino-Carbonatítico Araxá os minérios são saprolitos e regolitos formados pelo intemperismo de flogopititos e magnetita-apatititos existentes no núcleo do Complexo, e de carbonatitos que constituem um anel externo que envolve o núcleo. Com base na variação brusca das concentrações de MgO e de CaO, considera-se que existem três tipos de minério: o minério ocre, com teores de MgO e CaO maiores que 2,0%, o marrom com teores de MgO menores que 2,0%, e o laranja, com teores de MgO e de CaO menores que 2,0%.

A região do núcleo do Complexo contém minério polimetálico, com Nb, P, Ba, Ti, Fe e, localmente, com OTR. O intemperismo dos carbonatitos do anel externo gerou saprolitos e regolitos com P, eventualmente com OTR. Os principais minerais de minério de Nb são, hidrokenopirocloro e hidroxicalciopirocloro, o fluorcalcio pirocloro e o hidroxikenopirocloro ocorrendo localmente e em menores concentrações. No minério laranja parte do pirocloro é destruído e o Nb fica adsorvido à goethita. Há uma correlação proporcional e direta entre as concentrações de Nb e de Fe, ou seja, as concentrações de pirocloro aumentam quando as de magnetita também aumentam, apesar da magnetita não ser o único mineral portador de ferro no Complexo.

A apatita ocorre nos minérios ocre e marrom como fluorapatita, fluorapatita carbonatada e hidroxiapatita, ao passo que no minério laranja a apatita foi destruída pelo intemperismo e o P liga-se ao Ba e ao Al cristalizando gorceixita. As maiores concentrações de apatita, formando depósitos que foram e são lavrados, ocorrem em minérios formados sobre os carbonatitos do anel externo.

No centro do Complexo a barita ocorre nos três tipos de minério, gerada pela concentração residual da BaO da norsethita dos carbonatitos e pela ligação de Ba com enxofre liberado pela destruição intempérica da pirita e pelas emanações sulfurosas que provavelmente ocorreram. Porém, devido ao enxofre existir no sistema de intemperismo em menor concentração que o Ba, os minérios laranja e marrom contêm um excesso de Ba que deve existir como gorceixita e hidrokenopirocloro. Os minérios formados sobre o anel externo de carbonatito contêm baixas concentrações de barita devido às baixas concentrações de BaO e de enxofre nas rochas e nos minérios e a perda de enxofre durante o intemperismo.

Os OTR leves (Ce, La, Nd e Pr) concentram-se na monazita. A monazita presente nos minérios ocre e marrom seria majoritariamente de origem primária, no minério laranja haveria formação de monazita autigênica, com OTR provindos da destruição da apatita, se confundindo com a rabdofanita. Aparentemente esses minerais existem igualmente na região do núcleo do Complexo e na do anel de carbonatito.

Os mapas das superfícies dos topos dos minérios ocre, marrom e laranja mostram que os corpos mineralizados são estratiformes e grosseiramente horizontais. Saprolitos e regolitos com essa geometria indicam que as linhas de fluxo da água meteórica que os gerou migram da superfície para baixo e infletem para a horizontal. Esse processo de intemperismo lixivia as substâncias móveis, principalmente K_2O, CaO, MgO e SiO_2, e as retira do sistema de intemperismo lateral, horizontal e radialmente. Desse modo, as concentrações dos minerais e minério dependem igualmente de suas concentrações nas rochas que são intemperizadas e da

Referências

acumulação causada pelo enriquecimento residual que ocorre da superfície para baixo. Ocorrendo de cima para baixo, conforme os minerais concentram-se são, também, deslocados lateralmente, o que faz com que minerais típicos do núcleo do Complexo, originados pelo intemperismo de flogopititos e magnetita-apatititos, concentrem-se em regiões onde o substrato é carbonatítico, e vice-versa no caso dos OTR.

O intemperismo das rochas gera saprolitos e regolitos com volumes menores que os das rochas originais. Considerando que uma coluna de 100 m de espessura de flogopititos e magnetita-apatititos seja intemperizada, a coluna de minérios formada ao final do intemperismo será de 33 m de minério laranja, 9 m de minério marrom e 4 m e minério ocre. Se 100 m de carbonatitos forem intemperizados a coluna de minério formada será de 35 m e minério laranja, 7 m e minério marrom e 10 m de minério ocre. Silte argiloso e argilas, sedimentados em lagos de cratera constituem camadas com espessuras entre zero e 150 m que recobrem o regolito laranja e, localmente, também recobriram laterita e tufos vulcânicos intemperizados.

Na região do núcleo do Complexo, para formar o minério ocre houve ganho relativo de cerca de 50% de P_2O_5 e de Nb_2O_5, e perdas de 45% de MgO, 80% de K_2O, e 60% de LOI. Para formar o minério marrom houve ganhos relativos da ordem de 600% de Al_2O_3 e 500% de P_2O_5, e MgO, CaO e K_2O foram todos lixiviados. A formação do minério laranja envolveu o aumento da concentração relativa de enxofre em 100%, de 50% de Fe_2O_3, 45% de MnO, 50 a 100% de Nb_2O_5 e 70 a 100% de BaO, e perda de 50 a 100% de P_2O_5.

Na região do anel carbonatítico externo, para formar o minério ocre houve ganho relativo de 80% de SiO_2, 50% de P_2O_5, 70% de LOI, e 45% de BaO e lixiviação de enxofre. Ocorreram perdas de CaO, MgO e K_2O da ordem de 60%, 70% e 60% respectivamente. Para formar o minério marrom houve ganho de até 140% de P_2O_5, 50% a 250% de Nb_2O_5, e de 60% a 6,080% de BaO, a depender do local do Complexo. De 90 a 100% do enxofre da pirita das rochas, CaO, MgO e K_2O foram lixiviados. A formação o regolito laranja concentrou BaO entre 25% e 160%, lixiviou 50% a 80% do P_2O_5 e quase todo ($\approx$ 100%) SiO_2, CaO, MgO e K_2O. A quase inexistência de barita nos minérios formados sobre os carbonatitos se deve aos teores absolutos baixos de BaO (<3.0%) e de enxofre (<1.6 %) e a perda de enxofre durante o intemperismo.

Sobre o corpo mineralizado com minério laranja há uma cobertura descontínua de sedimentos argilosos que pode atingir 140 m de espessura. Esses sedimentos provavelmente acumularam-se no fundo de lagos de cratera que existiram intermitentemente após a formação do Complexo. Hoje estão sobre o corpo mineralizado com minério laranja, adaptados às mudanças de relevo que ocorreram na superfície conforme a espessura do corpo mineralizado aumentou de modo heterogêneo. A formação de bauxita silicosa envolveu ganhos muito elevados de substâncias móveis como SiO_2, K_2O e o BaO, o que sugere que se tenha formado por sedimentação em lago de cratera, e não por intemperismo do minério laranja.

O Complexo Araxá é uma unidade geológica única, pois contém o maior depósito de nióbio conhecido, apresentando recursos em minérios saprolíticos e regolíticos, formados pelo intemperismo de flogopititos e apatita-magnetititos existentes no núcleo do Complexo. Historicamente a lavra do minério de nióbio tem ocorrido no minério laranja formado pelo intemperismo da rocha do núcleo, caracterizado pelos teores de Nb_2O_5 > 0,5% e de CaO e MgO abaixo de 2%. Devido ao comportamento distinto durante o teste geometalurgico dos minérios de nióbio do

Complexo, percebeu-se que há saprolitos e regolitos mineralizados em nióbio cujas propriedades geometalúrgicas são inferiores às dos minérios do núcleo. Esse novo tipo de minério forma um halo de transição que envolve o principal corpo mineralizado com Nb, situado no núcleo do Complexo. Os minérios contidos nesse halo correspondem a aproximadamente 35% das reservas de Nb do depósito, tendo, portanto, grande importância econômica. As regiões onde esses minérios ocorrem foram denominadas de halos de transição N e halo S. Os minérios do halo de transição apresentam recuperação metalúrgica normalmente abaixo de 50%.

Análises com XRF mostraram que variações dos conteúdos de U vs PbO, Al_2O_3 vs SiO_2 e SrO vs TiO_2 indicam diferenças composicionais nos três tipos de minérios (ocre, marrom e laranja) do halo S e halo N, refletindo composições distinta das rochas que deram origem a esses minérios. Além disso, minerais como a vermiculita, anatásio, dikita, illita e dolomita foram importantes para construir o raciocíno sobre a formação dos halos de transição da mineralização de Nb.

O urânio se mostrou adequado para classificar o minério do halo N, uma vez que essa região apresenta valores de U_3O_8 normalmente acima de 0.3 NDD, diferentemente dos minérios do núcleo e halo S, com concentrações normalmente menores do que 0.15 NDD. Além disso, os conteúdos de Nb_2O_5 e U_3O_8 se correlacionam positivamente, indicando que o urânio possa estar presente na estrutura do pirocloro ou mesmo associado a ele na forma de outro mineral, como a uraninita, o que poderia afetar o rendimento da flotação do pirocloro do minério dessa região ou também mudar as características do concentrado de pirocloro gerado, como por exemplo elevar o conteúdo de U no concentrado final de pirocloro. Adicionalmente, o minério ocre do halo N foi o que apresentou maior conteúdo de dolomita dentre os minérios ocres das três regiões. Essas evidências sugerem que alguns eventos magmáticos, provavelmente uma intrusão carbonatítica associada a eventos hidrotermais, tenham sido responsáveis por gerar a anomalia de U da região do halo N.

Os minérios do halo S apresentaram conteúdos mais elevados de Al_2O_3, SiO_2 e TiO_2. Os conteúdos de vermiculita e anatásio do minério ocre dessa região são superiores aos dos minérios ocre das outras regiões. Isso sugere que o minério ocre do halo S possa ter se originado pela assimilação simultânea dos mica-xitos do grupo Ibia e da brecha flogopitítica do núcleo do Complexo durante a intrusão dos carbonatitos que circundam o núcleo flogopititico. Uma outra hipótese seria uma concentração supergenica diferenciada desses elementos sobre as rochas que compõe o anel carbonatítico em relação as rochas do núcleo flogopitítico.

O minério ocre do núcleo, do halo N e do S não produziu concentrado de pirocloro após o teste geometalúrgico, muito provavelmente por causa da presença de dolomita e vermiculita, dois minerais que prejudicam a concentração do pirocloro por flotação. Foi percebido que a presença de conteúdos de MgO acima de 0,8% no minério seria suficiente para inibir o processo atual de flotação do pirocloro. Os principais minerais contendo MgO detectados pela DRX são a dolomita e a vermiculita. A dolomita atrapalha o processo de flotação do Nb pois libera íons de Ca e Mg, o que impossibilita a estabilização da faixa adequada de pH (2,7 – 3,0) para flotação do pirocloro; a vermiculita, em contrapartida, apresenta ponto isoelétrico ideal em pH 2,9, muito similar à faixa de pH ideal para o ponto isoelétrico do pirocloro, fazendo com que ela concorra com pirocloro na adsorção do coletor, prejudicando a recuperação metalúrgica do pirocloro.

Os minérios laranja e marrom do halo N apresentaram baixo desempenho geometalúrgico provavelmente em função da presença de outros minerais portadores de Nb que não o pirocloro, como por exemplo a goethita, o anatásio, ou algum outro mineral contendo U, por causa da boa correlação observada entre U e Nb_2O_5. Alternativamente, a recuperação metalúrgica abaixo do esperado seria consequência de algum aspecto morfológico ou textural envolvendo o pirocloro dessa região que influenciaria, por exemplo, no grau de liberação desses minerais, já que não foi detectado nenhum mineral contaminante que justifique o baixo desempenho geometalúrgico desse minério.

Parte das amostras dos minérios marrom e laranja do Halo S apresentou recuperações metalúrgicas acima de 50%, enquanto outra parte apresentou uma recuperação metalúrgica abaixo desse valor. As boas recuperações metalúrgicas observadas no minério marrom sugerem que o hidroxicalciopirocloro também esteja sendo flutuado, o que indica que o teste de bancada considerado é adequado para flutuar não somente o hidrokenopirocloro, que é predominante no minério laranja.

No minério marrom do Halo S, as amostras que apresentaram recuperações abaixo de 50% possuem conteúdo de MgO variando de 0,8% a 2%, e a presença de baixas concentrações de vermiculita ou dolomita pode ser responsável pelos resultados ruins nos testes de flotação. Já no minério laranja do Halo S, as amostras que tiveram baixo desempenho metalúrgico foram coletadas em locais mais afastados do núcleo, onde os teores de Al_2O_3 são mais elevados. Essa elevação dos conteúdos de Al_2O_3 pode estar associada à presença de caulinita e gibbsta, como é comum, prejudicando a recuperação de piricloro. No entanto, esses minerais não foram identificados nas análises de DRX, o que pode ter ocorrido devido ao limite de detecção da análise ou a algum problema de interpretação dos difratogramas.

Dando continuidade aos estudos, serão produzidos outros dois artigos. Um artigo sobre a mineralogia dos principais minerais de minério do Complexo Araxá, interpretado com base em análises de microssonda (LA-ICP-MS), realizadas na UNESP de Rio Claro. E um outro artigo sobre processamento mineral com base nas caracterizações tecnológicas realizadas no laboratório de caracterização tecnológica da USP. Esses artigos serão concluídos em 2023 no programa de Pós-Graduação em geologia da UFPR.

REFERÊNCIAS

ALMEIDA, F. F. M. Origem e evolução da Plataforma Brasileira: **Boletim da Divisão de Geologia e Mineralogia (DNPM)**, v.241, p.36, 1967.

ALMEIDA, F. F. M. Relações tectônicas das rochas alcalinas mesozóicas da Região Meridional da Plataforma Sul-Americana: **Revista Brasileira de Geociências**, v. 13, p. 139-158, 1983.

AMARAL, C. et al. Potassiun-argon ages of alkaline rocks from Southern Brazil: **Geochimica et Cosmochimica Acta**, v. 31, p. 117-142, 1967.

AZZONE, R. G.; RUBERTI, E. Evolução composicional dos filossilicatos no perfil intempérico do Complexo Ultramáfico Alcalino-carbonatítico de Catalão I (GO): **Geologia USP - Série Científica**, v. 10, p. 23-43, 2010.

BARBOSA, O.; BRAUN, O. P. G.; DYER, R. C.; CUNHA, C. A. B. R. Geologia da região do Triângulo Mineiro. Rio de Janeiro: **Boletim 136 do DNPM/DFPM**, 140p, 1970.

BIONDI, J. C. Depósitos de minerais metálicos de filiação magmafica, **CBMM- T. A. Queiroz Ed**., S. Paulo, 602p, 1986.

BRAGA JUNIOR, J. M.; BIONDI, J. C. Geology, geochemistry and mineralogy of regolith and saprolite ore with Nb, P, Ba, REEs (+ Fe) in mineral deposits from the Araxá alkali carbonatite Complex, Minas Gerais state, Brazil: **Economic Geology**, submetido, 81p, 2022.

BROD, J.A.; et al. Geologia e mineralizações dos Complexos alcalino-carbonatíticos da Província Ígnea do Alto Paranaíba. **In: Congresso Brasileiro de Geologia**, Araxá, Minas Gerais, v.42, p.1-29, 2004.

BULATOVIC, S. Flotation of niobium - Handbook of Flotation Reagents - Chemistry, Theory and Practice: **Elsevier B.V**., v. 2, p. 111-125, 2010.

CHEN, W.; HONGHUI, H.; BAI, T.; JIANG, S. Geochemistry of Monazite within Carbonatite related REE Deposits: **MDPI Resources**, v. 6, (51); doi:10.3390/resources6040051, 2017.

CLAY, A. N.; ACKROYD, B. A preliminary economic assessment in the form of an independent technical report on MBAC FERTILIZER CORPORATION (MBAC) Araxá Project located in Minas Gerais State, Brazil, as amended, **prepared by VENMYN RAND (PTY) LIMITED (VENMYN)**, 112p., Internet, 2012.

DA SILVA LIMA, L.; ALVARENGA, R. A.; DE SOUZA AMARAL, T.; NOLLI, P. D. T. G.; DEWULF, J. Life cycle assessment of ferroniobium and niobium oxides: Quantifying the reduction of environmental impacts as a result of production process improvements: **Journal of Cleaner Production**, v. 348, 131327, 2022.
Folha Araxá, Mapa Geológico da Folha Araxá - SE.23-Y-C-VI Escala 1:100.000, **CODEMIG (Companhia para o Desenvolvimento de Minas Gerais)**, 2015.

Referências

GIBSON, S. A.; THOMPSON, R. N.; LEONARDO, O. H.; DICKIN, A. P.; MITCHELL, J. G. The Late Cretaceous Impact of the Trindade Mantle Plume - Evidence from Large-volume, Mafic, Potassic Magmatism in SE Brazil: **Journal of Petrology**, v. 36, p. 189-229, 1995.

GIBSON, C. E.; KELEBE, S.; AGHAMIRIAN, M.; YU, B. Flotation of pyrochlore from low grade carbonatite gravity tailings with benzohydroxamic acid: **Minerals Engineering**, v. 71, p. 97-104, 2015a.

GIBSON, C. E.; KELEBEK, S.; and AGHAMIRIAN, M. Niobium oxide mineral flotation: A review of relevant literature and the current state of industrial operations: **International Journal of Mineral Processing**, v. 137, p. 82-97, 2015b.
GIBSON, C. E., The Flotation of Niobium Oxide Minerals from Carbonatite Ores. **Doctoral thesis**, 334p, 2016,

GIBSON, C. E.; KELEBEK, S.; AGHAMIRIAN, M. Pyrochlore flotation from silicate gangue minerals - Amine adsorption mechanisms and the effect of modifying reagents: **Minerals Engineering**, v. 171, 107100, 2021.

GOMES, C. B.; RUPERTI, E.; MORBIDELLI, L. Carbonatite Complexes from Brazil: a review: **Journal of South American Earth Sciences**, v. 3, p. 51-63, 1990.

GOMES, C. B.; COMIN-CHIARAMONTI, P. Magmatismo Alcalino Continental da Região Meridional da Plataforma Brasileira. **Editora EDUSP**, 595p, 2017.

GRANT, J. A. The Isocon Diagram - A Simple Solution to Gresens' Equation for Metasomatic Alteration: **Economic Geology**, v. 81, p. 1976-1982, 1986.

GRASSO, C. B. Geologia e geometalurgia dos minérios de fosfato na base do manto de intemperismo da mina do Barreiro, Araxá: **Tese de doutorado n° 126, Universidade de Brasília, Instituto de Geociências**, 261p, 2015.

GRESEN, R. L. Composition-volume relationships of metasomatism: **Chemical Geology**, v. 2, p. 47-55, 1967.

GROSSI-SAD, J. H.; TORRES, N. Geologia e recursos minerais do Distrito do Barreiro, Araxá, Minas Gerais: **Relatório DNPM/GEOSOL, não publicado**, 35p, 1971.

HUANG, H.; et al. Mesozoic magmatic and hydrothermal uranium mineralization in the Huayangchuan carbonatite-hosted U-Nb-polymetallic deposit, North Qinling Orogen (Central China) - Evidence from uraninite chemical and isotopic compositions: **Ore Geology Reviews**, v.146, 104958, 2022.

ISSA FILHO, A.; LIMA, P. R. A. S.; Souza, O. M. Aspectos da geologia do Complexo Carbonatítico do Barreiro, Araxá, Minas Gerais, Brasil. **In: Complexos carbonatíticos do Brasil – Geologia. Brasilia, CBMM**, 1984.

Referências

ISSA FILHO, A.; RIFFEL, B. F.; SOUSA, C. A. F. Some aspects of the mineralogy of CBMM niobium deposit and mining and pyrochlore ore processing – Araxá, MG – Brazil. **In: International Symposium on Niobium. Proceedings.** Orlando. Patherson, 15p, 2001.

LCT–USP. Caracterização em produtos de processamento de minérios de Terras Raras: **Relatório interno da CBMM**, não publicado, 35p, 2016.

LCT–USP. Caracterização mineralógica em amostras de minério de nióbio – Minerais portadores de nióbio no Complexo alcalino de Araxá: **Relatório interno da CBMM**, não publicado, 21p, 2016.

LCT–USP. Caracterização mineralógica em amostras de minério de nióbio – Produtos de moagem e finos naturais: **Relatório interno da CBMM**, não publicado, 43p, 2019.

MARIANO, A. N.; MARIANO Jr. A. Overview of REE Deposits and Mines in the World and in Brazil: **Palestra com texto não publicado**, 67 slides, 2012.

MARSH, J. S. Relationships between transform directions and alkaline igneous rock lineaments in Africa and South America. **Earth Planet. Sci. Letters**, v. 18, p. 317-323, 1973.

MIYAWAKI, R.; et al. Hydroxykenopyrochlore, $(A,Ce,Ba)_2(Nb,Ti)_2O_6(OH,F)$, A new member of the pyrochlore group from Araxá, Minas Gerais, Brazil: **The Canadian Mineralogist**, v. 59, p. 589-601 DOI: 10.3749/canmin.2000094, 2021.

MORAES, L. C.; et al. Análises geométrica do alojamento de magmas no entorno do Complexo Alcalino-Carbonatítico do Barreiro, Araxá, Minas Gerais, por meio da atitude espacial de fraturas e diques. I**n: IV Simpósio de vulcanismo e ambientes associados**, Foz do Iguaçu-PR, Anais, CD-Rom, 2008.

MORBIDELLI, L.; et al. Mineralogical, petrological, and geochemical aspects of Alkaline and Alkaline-carbonatite associations from Brazil: **Earth-Science Reviews**, v. 39, p.135-168, 1995.

NI, X.; LIU, Q. Adsorption behaviour of sodium hexametaphosphate on pyrochlore and calcite: **Canadian Metallurgical Quarterly**, v. 52:4, p. 473-478, 2013.

OLIVEIRA, S. M. B.; IMBERNON, R. A. L. Weathering alteration and related REE concentration in the Catalão Carbonatite Complex, central Brazil: **Journal of South American Earth Sciences**, v. 11 (4), p. 379-388, 1998.

OLIVEIRA, T. F.; et al. Investigation on the effect of collector, activator, and depressant on the selective flotation of pyrochlore and barite: **Conference Proceeding - VISHMMT, XVIII ENTMME**, Rio de Janeiro, Brazil, 2001.

PADILLA, O. E.; LEYVA, R. R.; MENDOZA, B. J. Role of electrostatic interactions in the adsorption of cadmium (II) from aqueous solution onto vermiculite: **Applied Clay Science**, v. 88, p. 10-17, 2013.

Referências

RAPOSO, D. B. Caracterização do aquífero associado ao Complexo Alcalino Carbonatítico do Barreiro, oeste de Minas Gerais: **Dissertação de mestrado, Universidade de Campinas**. 126p, 2011.

RIBEIRO, C. C.; et al. Potencial e controles metalogenéticos de ETR, Ti e Nb em Províncias Alcalino-carbonatíticas brasileiras: **Metalogenia das Províncias Tectônicas do Brasil**, p. 559-589, 2014.

SANTOS, J. J. A.; CONCEIÇÃO, H.; LEANDRO, M. V. S.; ROSA, M. L. S. Formation of monazite-(Ce, La) by fluid-apatite interaction: The Floresta Azul Alkaline Complex, Bahia, Brazil: **Brazilian Journal of Geology**, v. 48(4), p.721-733, 2018.

SEER, H. J.; DARDENNE, M. A.; FONSECA, M. A. O Grupo Ibiá na sinforma de Araxá: um terreno tectonoestratigráfico ligado à evolução de arcos magmáticos. **In.: SIMPÓSIO DE GEOLOGIA DO CENTROOESTE**, 7, 1999, Brasília.

SEER, H. J.; DARDENNE, M. A.; PIMENTEL, M. M.; FONSECA, M. A.; MORAES, L. C. O grupo Ibiá na sinforma de Araxá: um terreno tectono-estratigráfico ligado à evolução de arcos magmáticos: **Revista Brasileira de Geociências**, v. 30(4), p. 737-744, 2000.

SEER, H. J.; MORAES, L. C.; SILVA, C. H. Mapa Geológico da Folha Araxá - SE.23-Y-C-VI, Escala 1:100.000, **CODEMIG**, 2015.

SILVA, C. H.; SIMÕES, L. S. A.; DAMÁZIO, W. L.; FERREIRA, S. N.; LUVIZOTTO, G. L. O Grupo Canastra em sua área-tipo, região de Tapira, sudoeste do estado de Minas Gerais: **Revista do Instituto de Geociências – USP, Série Científica**., v. 12(2), p. 8-98, 2012.

SONOKI, I. K.; GARDA, G. M. Idades K / Ar de rochas alcalinas do Brasil Meridional e Paraguai Oriental – Compilação e adaptação às novas constantes de decaimento: **Boletim IG – USP, Série Científica**, v. 19, p. 63-85, 1988.

TOLEDO, M. C. M.; LENHARO, S. R. L.; FERRARI, V. C.; FONTAN, F.; DE PERCEVAL, P.; LEROY, G. The compositional evolution of apatite in the weathering profile of the Catalão I alkaline-carbonatitic Complex, Goias, Brazil: **The Canadian Mineralogist**, v. 42, p. 1139-1158, 2004.

TRAVERSA, G.; et al. Petrography and mineral chemistry of carbonatites and mica-rich rocks from the Araxá Complex (Alto Paranaíba Province, Brazil): **Anais da Academia Brasileira de Ciências**, v. 73, p. 71-98, 2001.

ULBRICH, H. H. G. J.; GOMES, C. B. Alkaline rocks from continental Brazil: **Earth-Science Reviews**, v. 17, p. 135-154, 1981.

VALERIANO, C. M.; et al. A evolução tectônica da Faixa Brasília. **In: Mantesso-Neto V**., Bartorelli A., Carneiro C. D.R., Brito-Neves B.B (Eds.) Geologia do Continente Sul-Americano: Evolução da Obra de Fernando Flávio Marques De Almeida, São Paulo, Ed. Beca, p. 575-592, 2004.

Referências

VIANA, H. S.; DAVIS, E. G.; BEATO, D. C.; CABRAL, J. L. Projeto Araxá/Barreiro: Estudo Geoambiental do Barreiro. Belo Horizonte. **COMIG/CPRM**, 118p, 1998.

YU, Y.; MA, L.; CAO, M.; LIU, Q. Slime coatings in froth flotation - A review: **Minerals Engineering**, v. 114, p. 26-36, 2017.